Int J Cardiovasc Imaging (2019) 35:2249–2309
https://doi.org/10.1007/s10554-019-01687-6

MEETING ABSTRACTS

ESCR Abstracts

Published online: 21 October 2019

A rare case of metastatic carcinoid tumor to the heart

C. Cicciò[1], A. Cecchetto[2], J. Doraku[1], E. Dalla Chiara[1], C. Dugo[1], M. Salgarello[1], E. Barbieri[1], G. Carbognin[1]; [1]Verona/IT, [2]Padua/IT

Purpose The frequency of heart metastases is rare in patients with known malignancies, with increase risk on account histological type of primitive tumour and metastatic disease burden.
Cardiac involvement from carcinoid is observed in about 50% of patients with carcinoid syndrome, typically with involvement of the right side of the heart and in patients with liver metastasis.
To underline the pivotal role of multimodality imaging approach for the diagnosis, we presents a rare case of carcinoid metastasis at the heart from ileal neuroendocrine tumor without evidence of liver metastasis or signs or symptoms for carcinoid syndrome.
Methods & Materials A 78-year-old man was referred to Cardiology Department at our Hospital for transthoracic echocardiography (TTE) ultrasound for evaluation of suspect myocardial antero-septal wall mass with increase of up-take at 18F-Choline PET-CT, performed during follow-up of prostate cancer, surgically treated 2-years before.
Cardiac Magnetic Resonance (CMR) and MDCT were respectively performed for mass characterization and for primary tumor detection; 18F-FDG PET-CT and 68 Ga-DOTA-TATE PET/CT were performed to support the diagnosis of gastro-intestinal carcinoid tumor with lymph node involvement and solitary myocardial metastasis.

Results CMR confirm antero-septal myocardial solid mass with huge necrotic central portion, with inhomogeneous hyperintense signal at T2-STIR and T1-weighted sequences; increase signal intensity was detected during material contrast administration along peripheral portion. No pericardial effusion was observed. MDCT detected nodular thickening at terminal ileum with lymph-nodes enlargement, dealing with carcinoid tumor with involvement of loco-regional lymph-node. No liver metastasis was detected. 68 Ga-DOTA-TATE PET/CT and 18F-FDG PET-CT was subsequently performed for non invasive confirmation of diagnosis and showed high tracer uptake of 68G-labeled somatostatin analogues at ileal polipoid lesion, enlarged lymph-node and also at myocardial mass with not significant up-take of 18F-FDG tracer at PET-CT at both sides; all these findings confirmed the hypothesis of myocardial metastasis from carcinoid tumor with primary ileal localization. On account high-risk for abdominal and also cardiac surgery, patient was submitted to somatostatin analogue drug therapy (octeotide).
Conclusion CMR has a crucial role for advanced tissue characterization of myocardial mass; functional imaging (PET-CT) complements anatomic imaging (MDCT) with wall body approach

and is usually used to confirm diagnosis before surgery and for imaging staging or restaging carcinoid tumors.

References 1. Pandya U, Pellikka P, Enriquez-Sarano M, et al. Metastatic carcinoid tumourto the heart: echocardiographic-pathologic study of 11 patients. J Am Coll Cardiol 2002;40:1328.
2. Baxi AJ1, Chintapalli K1, Katkar A Multimodality Imaging Findings in Carcinoid Tumors: A Head-to-Toe Spectrum Radiographics. 2017 Mar-Apr;37(2):516-536.

Cardiac high-pitch CT angiography in the preoperative diagnostics of neonates with congenital heart disease: Radiation dose optimization by omitting test bolus or bolus tracking

P. Schindler, H.-G. Kehl, W. Heindel, C. Schülke; Münster/DE

Purpose Cardiac CT angiography (CTA) is increasingly established in the pre- and postoperative diagnostics of neonates with congenital heart disease (CHD). The aim of the study was to further optimize the radiation dose by omitting the test bolus or bolus tracking scan, which can have a relevant share of radiation exposure, especially in newborns.

Methods & Materials The retrospective study included twenty-five neonates with CHD who received a CTA from 2008 to 2018. The examination was performed as a high-pitch CTA (pitch, 3.4, 80 kV) with manual contrast administration (1.5 ml/kg body weight, flow rate about 1 ml/s) and fixed scan delay depending on the respective heart defect. Diagnosis, adverse events, radiation dose parameters, objective (noise, contrast-to-noise ratio (CNR)) and subjective (4-point Likert scale) image quality as well as diagnostic accuracy compared with intraoperative findings were recorded.

Results All examinations were diagnostically evaluable without adverse events. The median CT dose index volume was 0.5 (range 0.15–0.94), the median dose-length product was 8 (range 3–17). The estimation of the effective dose by Monte Carlo simulation showed with 0.66 mSv (range 0.25–1.4 mSv) lower median dose levels than previously published in comparable groups. All examinations achieved a very good image quality score of 1.2 ± 0.4 with only minimal image noise and CNR of 16.1 ± 7.0. Cardiac anatomy revealed no new diagnoses or significant differences in the subsequent cardiac surgery.

Conclusion Cardiac high-pitch CTA of neonates with CHD can be performed safely and dose-reducing without additional test bolus or bolus tracking scan. With very good image quality, it provides a detailed insight into the cardiac anatomy and thus enables a differentiated, non-invasive therapy planning and control.

Computed tomography angiography validation of peri-coronary adipose tissue measurements in different no-plaque coronary arteries and tube voltages

R. Ma, D. Ties, G. J. Pelgrim, R. van Dijk, M. van Assen, G. Sidorenkov, P. van der Harst, R. Vliegenthart; Groningen/NL

Purpose To compare the peri-coronary adipose tissue mean attenuation ($PCAT_{MA}$) among three main coronary arteries in CCTA obtained at different tube voltages in patients without coronary plaque.

Methods & Materials In this retrospective study, $PCAT_{MA}$ was measured on CCTA in 192 patients suspected of coronary artery disease, but without coronary plaque on CCTA, scanned between 2015 and 2017. $PCAT_{MA}$ was performed semi-automatically around the proximal segment of three main coronary arteries on curved planar reformats. Repeated measures ANOVA was used to compare $PCAT_{MA}$ between the coronary arteries; paired *t* test was used to compare the $PCAT_{MA}$ between pairs of the coronary arteries. The Kruskal–Wallis test was used for the $PCAT_{MA}$ comparison of different kV groups.

Results $PCAT_{MA}$ of LAD, LCX and RCA were -92.4 ± 11.6 HU, -88.4 ± 9.9 HU, and -90.2 ± 11.4 HU, respectively ($p < 0.001$). When comparing the arteries using pairwise tests, all showed significant difference in $PCAT_{MA}$: LAD and RCA ($p = 0.009$), LCX and RCA ($p = 0.033$), LAD and LCX ($p < 0.001$). The $PCAT_{MA}$ of the 70 kVp, 80 kVp, 90 kVp, and above 100 kVp groups were -95.6 ± 9.6 HU, -90.2 ± 11.5 HU, -87.3 ± 9.9 HU, and -81.2 ± 7.1 HU, respectively ($p < 0.001$).

Conclusion $PCAT_{MA}$ of the main coronary arteries in patients without coronary plaque shows slight differences. There is an important effect of CCTA tube voltage on reference $PCAT_{MA}$ values.

Differences in the CT findings between vulnerable plaque and culprit lesion in acute coronary syndrome

S. M. Yoo[1], D. S. Ryu[2]; [1]Bundang/KR, [2]Gangreung/KR

Purpose CT findings of vulnerable (rupture-prone) plaque of acute coronary syndrome (ACS) have been regarded as similar to those of the culprit lesion. However, this hypothesis may not be accurate if considering potential changes in the vulnerable plaque during episode of ACS.

Methods & Materials We retrospectively evaluated coronary CT angiography of 25 patients with ACS who had vulnerable (n = 10) or culprit plaques (n = 15). We analyzed CT features including positive remodeling (PR), low attenuation plaque (LAP), the napkin ring sign (NRS), degree of stenosis (normal, < 50%, 50–99%, 100%), and myocardial hypoperfusion in the left ventricle.

Results There was no difference in the prevalence of PR, NRS, or LAP between the vulnerable and culprit plaques. In contrast, majority (80%, 8/10) of vulnerable plaques had normal or < 50% stenosis while total occlusion was only identified in 46.7% (7/15) patients of culprit plaque ($p = 0.037$). In all patients with occlusion, myocardial hypoperfusion was demonstrated in the corresponding artery territory on CT and TIMI flow score decreased due to thrombosis on coronary angiography.

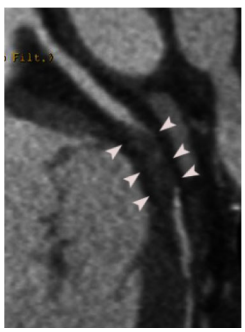

Fig. 1a 75-year-old male patient with non-ST elevated myocardial infarction. A. Total occlusion with mainly non-calcified plaque (arrowheads) with positive remodeling is noted at the distal circumflex coronary artery on a curved MPR

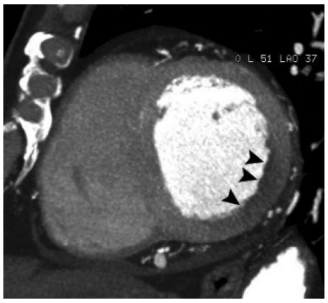

Fig. 1b Myocardial hypoperfusion (arrowheads) is demonstrated in the lateral wall of left ventricle on a short axis CT image. Emergent coronary angiography confirms the CT findings

Conclusion CT features of vulnerable and culprit plaques differ in cases with thrombotic occlusion reflecting dynamic changes related to the episode of ACS.

References Motoyama S, et al. Multislice computed tomographic characteristics of coronary lesions in acute coronary syndromes. J Am Coll Cardiol 2007;50:319-326. Motoyama S, et al. Computed tomographic angiography characteristics of atherosclerotic plaques subsequently resulting in acute coronary syndrome. J Am Coll Cardiol 2009;54:49-57.

Cardiac magnetic resonance imaging with parametric mapping in long-term ultra-marathon runners

M. Barczuk-Falecka[1], Ł. Małek[1], K. Werys[2], A. Czajkowska[1], A. Mróz[1], K. Witek[1], W. Bakalarski[1], D. Nowicki[1], D. Roik[1], M. Brzewski[1]; [1]Warsaw/PL, [2]Oxford/UK

Purpose There is a direct reverse dose–effect relationship between the amount of physical activity and cardiovascular risk. It is unknown whether this is true for extreme, persistent endurance training. The aim of the study was to assess structural changes of the heart in long-time ultra-marathon runners with special focus on myocardial fibrosis using parametric mapping.

Methods & Materials We studied a group of 30 healthy, male ultra-marathon runners (mean age 40.9 ± 6.6 years, median 9 years of running with frequent competitions) and 10 matched controls not engaged in any regular activities. All of them underwent cardiovascular magnetic resonance (CMR) with 3T scanner including T1-mapping, late gadolinium enhancement (LGE) and extracellular volume (ECV) quantification.

Results Athletes demonstrated significantly larger heart chambers and left ventricular (LV) mass. LV systolic function was unchanged. 73.3% of athletes fulfilled volumetric criteria for dilated cardiomyopathy or arrhythmogenic right ventricular cardiomyopathy. Non-ischemic, small volume LGE was found in 8 athletes and in 1 control (27% vs. 10%, p = 0.40). It was localised at insertion points (5 athletes, 1 control) or in the septum or infero-lateral wall (3 athletes). Athletes with insertion point LGE had higher right ventricular end-diastolic volume index in comparison to athletes without LGE (p = 0.04), which suggests its relation to volume overload. There were no differences between athletes and non-athletes in terms of ECV values (26.1% vs. 25%, p = 0.29).

Conclusion Ultra-marathon runner's hearts demonstrate a high degree of structural remodelling, but there is no significant increase in focal or diffuse myocardial fibrosis.

Anomalous pulmonary venous return (TAPVR): A pictorial review

O. Karapanagiotou[1], S. Katsilouli[1], S. Kampanarou[2], M. Kanakis[1], D. Bobos[1], N. Giannopoulos[1], T. Syrigou[1], I. Mastorakou[1]; [1]Athens/GR, [2]Kallithea/GR

Purpose Anomalous pulmonary venous return or connection is a congenital cardiac abnormality and can be either total or partial.

In *Total Anomalous Pulmonary Venous Return (TAPVR)*, all four pulmonary veins are malpositioned and make anomalous connections to the systemic venous circulation. It is a rare abnormality, accounting for 1–3% of all cardiac congenital abnormalities. It is a fatal condition unless there is a left-to-right shunt. Even so, surgical redirection must be performed within the first few weeks of life.

There are four variants Supracardiac Cardiac Intradiaphragmatic Mixed

In *Partial Anomalous Pulmonary Venous Return (PAPVR)* some but, not all pulmonary veins drain to the left atrium. A less severe condition than TAPVD, it can be diagnosed later in life usually as a cause of secondary pulmonary hypertension.

The purpose of this pictorial presentation is to familiarize radiologists with these entities through: reviewing the embryological development of the system of pulmonary veins so as to explain the different types of developmental abnormalities discussing the CTA protocols used to obtain the optimal imaging result.

TAPVR Type I—supracardiac

Methods & Materials 15 patients with either TAPVR or PAPVR diagnosed with ultrasound, were referred in our department for a computed tomography angiogram before surgery during the past 24 months. All of them but one, were newborn children, aged between 2 and 5 days. All types of TAPVR were detected. The only adult, aged 50 years, presented with severe arterial pulmonary hypertension and the diagnosis of the underlying disease was PAPVR. The purpose of CTA was the complete investigation of the vascular anatomy, especially in areas difficult for ultrasound access. In addition, 3D reconstruction provided valuable information about the relationship of various vessels.

Results Images from all different types of anomalous pulmonary venous return will be uploaded and explained so as radiologists get familiar with this pathological entity.

Conclusion Anomalous pulmonary venous return is a rare congenital abnormality. In order that radiologists get familiar with this entity, the embryogenesis and after birth appearance will be fully explained. The optimal CTA imaging protocols will be given and each type will be fully illustrated.

References Douglas Y et al. Normal and abnormal development of pulmonary veins: State of the art and correlation with clinical entities Int J of Cardiology 2011;147(1):13-24 Dillman et al. Imaging of the pulmonary veins developmental anomalies AJR 2009;192:1272-1285 Porres DV. Learning from the pulmonary veins Radiographics 2013;33(4) Hassani C & Saremi F. Comprehensive cross-sectional imaging of the pulmonary veins Radiographics 2017;37(7):1928-1954.

Diagnostic performance and radiation doses of non-gated coronary artery calcium scoring with standard and low-dose chest CT in comparison to gated calcium scoring CT

K. Zhuravlev, V. E. Sinitsyn, A. Spektor; Moscow/RU

Purpose Calcification of the coronary arteries is a quite common characteristic finding at chest CT and is a recognized marker of coronary atherosclerosis. The number of chest CTs is growing annually including due to lung cancer screening. A lot of patients who performed chest CT examinations are eligible for calcium score screening. The purpose of this study was to compare the correlations between the gated and non-gated coronary artery calcium score (CACS) values obtained with standard and with low-dose chest CT. The difference in patients' radiation dose were also evaluated.

Methods & Materials The study included 425 patients who for the period of November 2017 and June 2018 underwent non-gated chest CT and gated calcium scoring CT. Patients with a history of coronary revascularization or with pacemakers were excluded from the study. ECG-gated cardiac CT for CACS was performed with every eligible patient. CACS was calculated using conventional methods/scores (Agatston, Volume, Mass). Differences and correlations between gated and non-gated CACS values as well as correlation coefficients of standard-dose and low-dose CT groups were evaluated. Statistical analysis was performed with and without "zero" values of CACS. The radiation dose was estimated separately for non-gated chest CTs and for gated CACS CTs and compared with each other.

Results The study comprised 398 patients. The standard CT protocol was used in 202 cases, and the low-dose one in 196 cases. The value of CACS = 0 was found in 109 patients (27%). The mean Agatston values of CACS were 395 $\pm$ 583 for gated CACS and 384 $\pm$ 602 for non-gated CACS ($p = 0.41$). The correlation between CACS obtained with gated and non-gated CT was high even when "zero" values of CACS were excluded (Agatston: $r = 0.975$; Volume: $r = 0.977$; Mass: $r = 0.976$). There were no significant difference between correlation coefficients calculated separately for standard-dose and low-dose CT groups (r: 0.97 vs. 0.979, $p = 0.065$). The chest CT radiation dose was significantly less than in combination with the gated CACS (2 ± 0.6 vs. 3.5 ± 0.7 mSv; $p < 0.001$). Moreover, the radiation dose in low-dose chest CT was significantly less compared to the radiation dose obtained by the calcium scoring (0.9 ± 0.3 vs. 1.4 ± 0.2 mSv; $p < 0.001$).

Conclusion The study shows that the calcium score obtained from non-gated standard-dose or low-dose chest CTs is comparable to gated calcium score with a high advantage in low-dose CT in terms of patients radiation dose. These results could be used for combined screening of lung cancer and coronary atherosclerosis.

Artificial intelligence based automatic segmentation of the myocardium in late enhancement MRI

T. Gassenmaier, J. Heidenreich, T. A. Bley, T. Wech; Würzburg/DE

Purpose To develop and evaluate an artificial intelligence based semantic segmentation technique for an improved efficiency of the cumbersome post-processing in late enhancement (LE) imaging.

Methods & Materials A convolutional neural network for semantic segmentation of endo- and epicardial borders was pre-trained using 100.248 cardiac cine MR images from the public Kaggle second annual data-science-bowl-database [1], and labels obtained using the method presented in [2]. Transfer learning was then used to qualify the network for the segmentation of left-ventricular images with LE contrast in short axis. LE images and manual segmentation labels from 216 patients with history of acute myocardial infarction of our local database were used for this purpose ($\sim$ 2.200 images in total).

The obtained network was then applied to the LE image stacks of 26 patients with history of acute myocardial infarction which were not part of the training dataset, and the obtained segments were compared to the segments obtained manually by an experienced operator using the Sørensen–Dice coefficient.

Results The application of the neural network resulted in meaningful segmentation results for all 26 patients. The obtained Dice score was 0.76 ± 0.06. A trend towards slightly lower Dice scores for basal and apical images was apparent with respect to mid-ventricular slices. Figures 1 and 2 exemplarily show a comparison of the manual and the AI based segmentation for a high (Figure 1) and a low (Figure 2) Dice score, respectively.

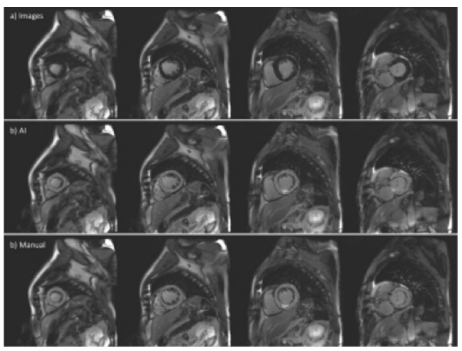

Figure 1 a original LE images, b AI based segmentation, c manual segmentation. Dice score of 0.87

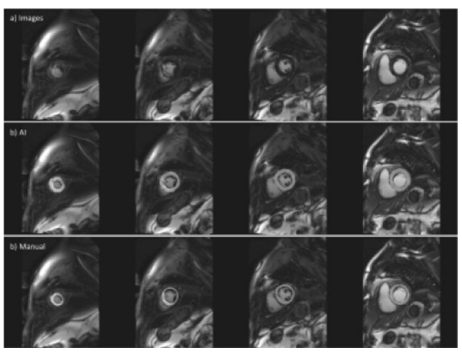

Figure 2 a original LE images, b AI based segmentation, c manual segmentation. AI segmentation tended to produce larger segments than manual segmentation, resulting in a Dice score of 0.68

Conclusion Artificial intelligence based segmentation promises a breakthrough improvement of the efficiency in LE diagnostics. For technical reasons we fixed the matrix size of all images to 192 × 192 in our study. This significantly accelerated the training process for the presented proof-of-principle, however, it also required a reduction of the resolution of the images (and labels) in almost all cases. A repetition of the training at full resolution might also improve the accuracy of the segmentation. Furthermore, the inclusion of more training data will undoubtedly lead to a higher overall dice score, especially for the rather heterogeneous peripheral slices orientations.

References [1] Kaggle. Data Science Bowl Cardiac Challenge Data. https://www.kaggle.com/c/second-annual-data-science-bowl/data.
[2] Bai et al., JCMR 20:65 (2018).

The clinical utility of early postoperative cardiac multidetector computed tomography after coronary artery bypass grafting

D. K. Kang, J. S. Sun, T. H. Kim, T. Ha; Suwon/KR

Purpose We evaluated the clinical utility of early postoperative cardiac computed tomography (CT) for evaluating left ventricular (LV) function and predicting the prognosis in patients who had undergone coronary artery bypass grafting (CABG).

Methods & Materials Of 205 patients who underwent CABG from March 2011 to December 2014, 136 underwent early postoperative cardiac CT (within 30 days after CABG). The LV myocardium was assessed using the 16-segment model of the American Heart Association. The LV function was evaluated using a semi-automated LV endocardial and epicardial contour detection technique based on threshold-based blood volumes. The baseline and postoperative follow-up echocardiographic findings, major adverse cardiac events (MACEs), and death were recorded for follow-up period (mean 5.8 ± 1.1 years). Functional cardiac CT parameters were compared with echocardiographic measurements. The associations between the cardiac CT findings and both functional recovery and prognosis were evaluated by logistic regression analysis.

Results On baseline echocardiography, 28% (n = 38) of the patients had LV systolic dysfunction; this decreased to 23% (n = 31) on early postoperative echocardiography and 9% (n = 12) on long-term follow-up echocardiography. Postoperative cardiac CT showed regional wall motion abnormalities in 62 patients (46%), myocardial hypoenhancement in 73 patients (54%), and myocardial thinning in 26 patients (19%). The left ventricular ejection fraction (LVEF) and wall motion score index (WMSI) measured by cardiac CT correlated well with the early postoperative echocardiographic assessment ($r = 0.7500$, $p < 0.0001$ and $r = 0.9382$, $p < 0.0001$, respectively). LVEF and WMSI measured with early postoperative echocardiography (OR 0.9631, $p = 0.0240$ and OR 5.3598, $p = 0.0032$, respectively) and cardiac CT (OR 0.9619, $p = 0.0097$ and OR 17.2347, $p < 0.0001$, respectively) predicted MACEs, but only WMSI measured by cardiac CT predicted all-cause death (OR 10.6017, $p = 0.0035$).

Conclusion In CABG patients, LVEF and WMSI, measured with early postoperative cardiac CT, were comparable with echocardiography and predicted the development of MACEs and all-cause death.

References 1. Kaniewska M, Schuetz GM, Willun S, Schlattmann P, Dewey M. Noninvasive evaluation of global and regional left ventricular function using computed tomography and magnetic resonance imaging: a meta-analysis. Eur Radiol. 2017;27(4):1640-1659.
2. Awan MA, Khan Au, Siddiqi TA, Hussain A, Rabbi F, Tasneem H. Early effects of coronary artery bypass grafting on left ventricular regional wall motion abnormalities. J Coll Physicians Surg Pak. 2007;17(1):3-7.
3. Swaminathan M, Morris RW, De Meyts DD, Podgoreanu MV, Jollis JG, Grocott HP, Milano CA, Newman MF, Mathew JP. Deterioration of regional wall motion immediately after coronary artery bypass graft surgery is associated with long-term major adverse cardiac events. Anesthesiology. 2007;107(5):739-745.

Segmental approach and evaluation of Cardiac Morphology in Congenital Heart Disease

M. Sakanyan; Yerevan/AM

Purpose Segmental approach and evaluation of Cardiac Morphology in Congenital Heart Disease.

Methods & Materials Multiplanar reconstructions of images obtained with computed tomography or magnetic resonance imaging are particularly useful for evaluating congenital hearth disease.

The segmental approach, which is widely used in the imaging work-up of congenital hearth disease, consists of a three-step evaluation of the cardiac anatomy.

Results: Step 1.

The determination of visceroatrial situs refers to the position of the atria in relation to the nearly anatomy (including the stomach, liver, spleen, bronchi).

There are three different anatomic configuration Situs solitus (normal) Situs inversus (congenital condition, in which the major visceral organs are reversed or mirrored from their normal positions) Situs ambiguous (also known as heterotaxy, is a rare congenital defect in which the major visceral organs are distributed abnormally within the chest and abdomen).

Step 2

Evaluate left or right orientation of the ventricular loop and position of the ventricles and identify on the basis of their internal morphologic features.

Step 3

Determination of the position of the great vessels and any abnormalities.

Abnormalities in the origin of the great vessels, or conotruncal anomlies, are predominantly of three types: D-transposition (dextro-transposition) L- transposition (levotransposition) D-malposition with double outlet right ventricle.

Next determine relationships between the atria and ventricles as well as the ventricles and great vessels:

There are two levels: Atriventricular (concordant, discordant, ambiguous, double inlet, absence of right or left connection) ventriculolateral (concordant, discordant, double outlet).

Last determine any associated abnormalities of the cardiac, chambers, septa, outflow tract and great vessels.

Conclusion By executing these steps sequentially during image review, the radiologist can achieve a more accurate interpretation.

Cardiac remodelling in elite cyclists of a U23 Worldtour team

O. Ghekiere[1], B. Vande Berg[2], J. Bogaert[3], M. D. K. Lefebvre[1], M. D. L. Herbots[1], D. Hansen[1], M. D. M. Claeys[3], M. P. D. R. Willems[3], H. Heidbuchel[4], M. P. D. A. La Gerche[5], M. D. G. Claessen[3]; [1]Hasselt/BE, [2]Leuven, BE/BE, [3]Leuven/BE, [4]Antwerp/BE, [5]Melbourne/AU

Purpose To establish in elite athletes right (RV) and left ventricular (LV) volumetric, myocardial strain and tissue characteristics obtained by cardiac magnetic resonance (CMR) and to compare them to age-matched healthy controls.

Methods & Materials Forty-two elite male cyclists of U23 Worldtour team (mean age 19 ± 1 year)underwent CMR on a 1.5T system, as part of the Pro@Heart study. Results were compared to 15 healthy controls (mean age 21 ± 0 year). Global volumetric and functional parameters included (indexed) LV/RV end-diastolic (EDV, EDVi), end-systolic (ESV, ESVi) and ejection fraction (LVEF/RVEF). A non-rigid elastic algorithm was used to calculate global LV and RV myocardial strain. Native and post-contrast T1 mapping with extracellular volume (ECV) calculation was performed in septal and lateral LV wall on a 4-chamber view. Data were analyzed with a nonparametric Mann–Whitney U test.

Results Compared to controls, cyclists showed lower heart rates, i.e., 55 ± 8 vs. 73 ± 13 bpm ($p < 0.001$) and higher VO2max values, i.e., 65 ± 6 vs. 40 ± 5 ml/min/kg ($p < 0.001$). Cardiac volumes were significantly higher in cyclists, i.e., LVEDVi 128 ± 12 vs. 96 ± 8 ml/m^2; LVESVi 55 ± 10 vs. 40 ± 7 ml/m^2; RVEDVi 144 ± 18 vs. 108 ± 12 ml/m^2; RVESVi 71 ± 13 vs. 52 ± 8 ml/m^2 (all p values < 0.001). LVEF and RVEF, however, were not statistically different between groups (52 ± 5 vs. 48 ± 5%). Cyclists presented a higher LV mass, i.e., 79 ± 9 vs. 59 ± 8 g/m^2 ($p < 0.001$). Myocardial T1 values were lower in cyclists, i.e. septal: 980 ± 24 vs. 1030 ± 30 ms, ($p < 0.001$), lateral: 965 ± 26 vs. 997 ± 29 ms ($p = 0.001$). ECV-values in athletes were lower in LV septum, i.e., 22.9 ± 2.0 vs. 25.1 ± 1.5% ($p < 0.001$), but not in LV lateral wall: 22.1 ± 2.4 vs. 22.9 ± 2.6%. RV longitudinal peak systolic strain was higher in controls: − 16.2 ± 3.2 vs. − 13.8 ± 2.9% ($p = 0.02$), while no significant differences were found in global LV strain values between groups.

Conclusion Young, elite cyclists show physiological cardiac remodeling with increased ventricular volumes and myocardial mass. As revealed by CMR myocardial tissue characterization, physiological remodeling involves the myocyte compartment with smaller ECV values than age-matched controls. Endurance training is associated with greater RV than LV remodeling as evidenced by greater RV volumes and lower strain values at rest.

References none.

Cardiac MR Imaging of Hypertrophic Cardiomyopathy: what radiologists need to know

M. Rodriguez Alvarez, C. Saborido Avila, L. Trillo Fandiño, P. Pazos, J. M. Vieito Fuentes; Vigo/ES

Purpose Resume in a practical guide the paper of CMRI in HCM: technical aspects, phenotypes and risk stratification and what the radiologist should reflect in his report to allow taking clinical decisions.

-We also searched PubMed for clinical trials that investigated the prognostic utility of LGE and T1 mapping in risk stratification of HCM patients and correlate it with our experience.

We review CMR studies of HCM patients performed at our institution for collecting data.

Methods & Materials Resume and update in a practical guide for radiological use, the paper MRI in hypertrophic myocardiopathy.

Results Cine-CMRI demonstrate clearly the typical HCM phenotypes and also wall motion and the turbulence jet across the LVOT, crypts and anomalous papilar muscles associated.

Perfusion CMRI at rest shows the close relationship between perfusion decrease and wall thickness.

The presence of fibrosis is evaluated with LGE-CMRI and its extent has been associated with clinical markers of SCD risk. We describe different patterns of LGE CMRI also demonstrates the coexistence of myocardial hypertrophy and thinning in burn-out phase as well as impairment of systolic function.

T1 mapping provides information about the extracellular volume fraction (ECV) also correlated with clinical markers of SCD risk.

Diferential diagnosis from phenocopies is also updated

The radiological report should reflect: ventricular function and morphology (phenotype, papillary muscles anomalíes…) myocardial thickness, outflow tract área and pressure gradient if SAM is present, mitral valve morphology and function, left atrium size, perfusion defects, myocardial enhancement pattern and percentage of enhanced myocardium, and T1 and ECV values if mapping techniques are available.

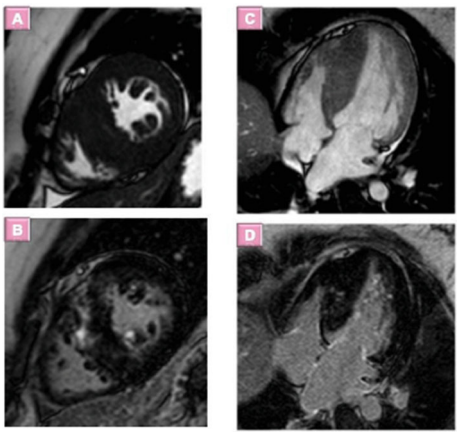

Asymmetric diffuse septal HCM. images show diffuse hypertrophy and delayed enhancement of the thickened septal myocardium.

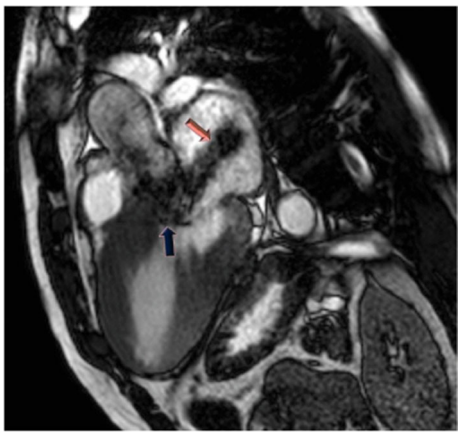

Septal hypertrophy and SAM, signal-void jet flow into the LVOT(blue arrow), Mitral regurgitation (pink arrow) directed to posterior wall of an enlarged left atrium.

Disease	Morphologic appearance	LGE pattern	Other
HCM	Many phenotypes; LV predilection. Spiral pattern of Hypertrophy valvular disease and	Mesocardial usually in area of major hypertrophy	Elongated mitral valve/SAM Myocardial crypts,anomalies papillary muscles,apical-basal muscle bundle Supernormal LVEF Hypocontractility
Athletic heart	Ratio of diastolic wall thickness to LV end diastolic volume corrected to body surface will have a value <0.15 mm /m2 /mL	None	Hypertension history; aortic stenosis
Secondary Hypertrophy	LV circumferential thickening inferior to 15 mm	None	Hypertension history; aortic stenosis
Amyloidosis	Diffuse involvement; valvular thickening; papillary muscle thickening	Biventricular circumferential subendocardial enhancement (zebra pattern) Null myocardial signal pattern 2 or 3	Systolic disfunction pericardial effusion Not spared atrial walls and septum
Anderson-Fabry disease	symmetric involvement	Inferolateral LV wall with mesocardial distribution	X-linked disorder
Sarcoidosis	Preferential involvement of basal septum, in chronic phase: granulation zones become thin and are interspersed with normal zones	transmural in chronic state Subendocardial at RVside of septum	T2-weighted hypersignal in active granulation zone

Differentiating HCM MR imaging Features from Those of Phenocopies.

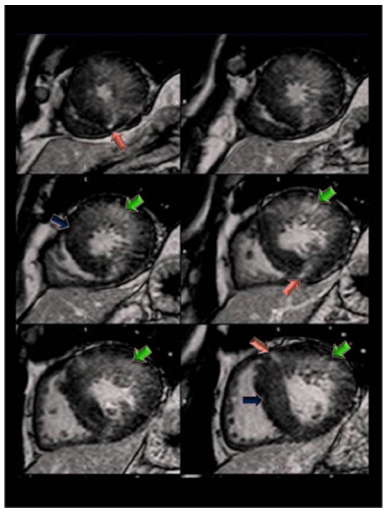

Concentric HCM. Short-axis LGE images show different patterns of enhancemente reflecting conspicuity of LGE due to different types of fibrosis.

Conclusion Cardiac MR imaging is useful for making a diagnosis of HCM and identifying the phenotypes of HCM, can also contribute to risk stratification because of its accurate measurement of LVH, detection of "high-risk" phenotypes, and identification of myocardial fibrosis.

have an updated guide that resumes: protocol, MRI findings and how to perform the radiological report of the disease, is very useful for clinical decision-making allowing a faster and more accurate diagnosis with better approach to the risk stratification of SCD.

References Ameya Jagdish Bax et all, Hypertrophic Cardiomyopathy from A to Z: Genetics, Pathophysiology, Imaging, and Management. RadioGraphics 2016; 36:335–354. Barry J. Maron and Martin S. Maron. LGE Means Better Selection of HCM Patients for Primary Prevention Implantable Defibrillators. JACC: Cardiovascular Imaging.Volume 9, Issue 12, December 2016 Jan Bogaert, MD Iacopo Olivotto, MD. MR Imaging in Hypertrophic Cardiomyopathy: From Magnet to Bedside. Radiology:vo, l273:N2—November 2014. etc….

Assessment of Right Ventricular Strain and Dyssynchrony in Patients with Precapillary Pulmonary Hypertension predicts Mortality. Cardiac Magnetic Resonance Feature-Tracking Study

A. Kallifatidis[1], S.-A. Mouratoglou[1], C. A. Kouskouras[2], C. Feloukidis[1], D. Farmakis[1], G. Sianos[1], S. Finitsis[1], H. Karvounis[1], G. Giannakoulas[1]; [1]Thessaloniki/GR, [2]Thessaloniki, GR/GR

Purpose/Objectives Right ventricular (RV) mechanical dyssynchrony has been described in the assessment of the non-uniform contractile function of the RV in patients with precapillary pulmonary hypertension (pPH). However, little is known on its impact on survival in patients with pPH. The aim of our study is to reveal the prognostic value of RV dyssychrony in this category of patients measured by CMR Feature-Tracking.

Methods & Materials Consecutive adult patients with pPH underwent CMR (AVANTO Siemens 1.5T) for the evaluation of biventricular volumes, and strain analysis. Time to peak strain was calculated as the time interval needed to achieve the maximum of the strain, over the whole cardiac cycle. All analyses were performed

using a CVI42 platform version 5.6.6. The collected RV strain indices included peak global longitudinal strain measured at the 4-chamber images along with respective time-to-peak metrics (Figure 1). All patients were followed up and time to death was recorded.

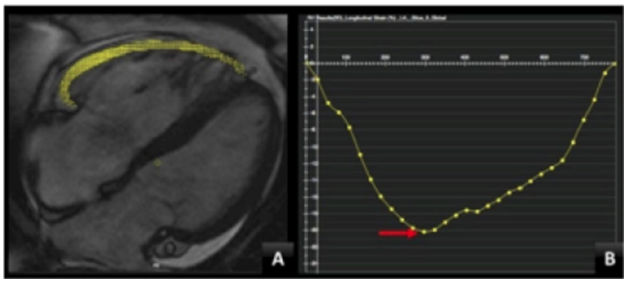

Figure 1 .

Results Our study included 39 patients with pPH (27 women, age 53.9 ± 16.9 years). Over a median follow-up of 51.3 months (IQR 16.8–68.7 months) 7 patients died. Univariate Cox proportional hazard analysis showed that time to peak RV strain was a significant predictor of survival. In Cox proportional hazard analysis, time to peak RV strain was significantly related to death (HR 0.981, 95% CI 0.966–0.995). ROC curve analysis showed that the optimal cut-off value of time to peak RV strain which predicted death was 333.1 ms (AUC 0.808, 95% CI 0.657–0.959). Kaplan–Meier survival analysis showed that time to peak RV strain $\leq$ 333.1 ms was associated with a sevenfold increased risk for clinical failure (Figure 2).

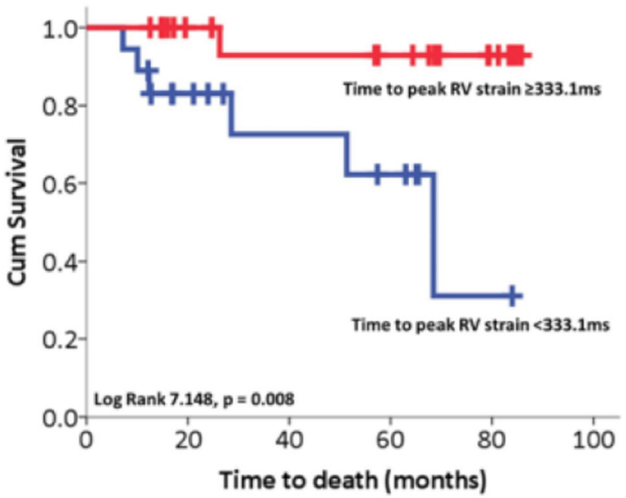

Figure 2 .

Conclusion RV mechanical dyssynchrony as expressed by time to peak RV longitudinal strain is a predictor of mortality in pPH.

Pre-TAVI MDCT assessment: dos and don'ts

F. Paciolla, G. Rovere, B. Merlino, L. Natale, R. Marano, R. Manfredi; Rome/IT

Purpose To show how to assess the morphology and measurements of aortic root, aorta and peripheral arteries before transcatheter aortic valve implantation (TAVI).

Methods & Materials Over the last 10 years, the development of transcatheter aortic valve implantation (TAVI) allowed a practicable way to treat severe aortic stenosis. The pre-procedural imaging with MDCT is required to determine the appropriate approach and the proper device; it implies the assessment of the morphology of the aortic valve, the aortic root, a global study of the anatomy of the aorta and peripheral arteries. MDCT provides detailed information on the cardiac anatomy and 3D volumetric data sets allow unlimited plane reconstructions, playing an important role in pre-procedural screening and procedural planning, minimizing post procedural complications.

Results We present and discuss CT findings in patients with severe aortic stenosis, candidates to undergo TAVI procedures. We show how to assess the morphology of the aortic valve (bicuspid or tricuspid shape), the presence of aortic valve calcification (quantification and localization, both in the valve and the sinotubular junction), aortic valve annular dimension (fundamental for appropriate selection of prosthesis size), as well as dimensions of the sinus of Valsalva, sinotubular junction and ascending aorta (especially in patients undergoing a self-expandable device implantation). Furthermore, correct techniques to assess the distance of coronary ostia from the annular plane (which is important to guarantee patency of the coronary arteries during implantation) and course and diameters of aorta and peripheral arteries (fundamental to plan the procedural strategy).

Conclusion MDCT takes a leading role in pre-TAVI assessment as it furnishes a global evaluation of the anatomy prior to the procedure. An appropriate post processing protocol is also essential to select the most appropriate approach and help avoiding possible post-procedural complications.

References: Alkadhi H, Leschka S, Trindade PT et al. (2010) Cardiac CT for the differentiation of bicuspid and tricuspid aortic valves: comparison with echocardiography and surgery. Am J Roentgenol 195:900–908 Kapadia SR, Schoenhagen P, Stewart W et al. (2010) Imaging for transcatheter valve procedures. Curr Probl Cardiol 35:228–276.

Can myocardial T1 mapping reveal concealed cardiomyopathy in sickle cell disease before MGE T2* mapping changes?

R. T. M. Khafagy[1], A. El Sayed[1], S. Khalil[1], B. M. R. M. A. Habib[1], G. Samir[1], D. F. Haroun[1], S. W. Tantawy[1], F. R. M. Elkafrawy[2], S. Nabil[1], A. Elmogy[1], A. Salama[1], M. Shaaban[3], A. S. Ibrahim[1]; [1]Cairo/EG, [2]Alexandria/EG, [3]Aswan/EG

Purpose To investigate the role of cardiac MRI using advanced techniques as, T1 mapping and basic function and volume analysis in assessment of early myocardial fibrosis in young Sickle cell disease (SCD) patients in absence of cardiac siderosis.

Methods & Materials With institutional review board approval and informed consent, a prospective pilot study was conducted including 20 patients with SCD (median age 13.5 years, range 7–21 years old). Inclusion criteria included patients with SCD receiving regular blood transfusions, treatment with iron chelation therapy, and referral for cardiac MRI assessment of cardiomyopathic changes and myocardial iron overload. Only cases with normal cardiac iron overload were included. Hematocrit level was measured for each patient within 24 h prior to the MRI examination.

Patients with any of the following conditions were excluded from the study: myocardial siderosis(n = 2),claustrophobia(n = 1), impaired renal function(n = 1) or any general MRI contraindication.
Cardiac MRI at 1.5T included short axis cine steady-state free-precession images, for left ventricular function assessment, and T2* images using a cardiac-gated segmented multi-gradient-echo (MGE) sequence, with 8 equally spaced echoes, 2.5 ms apart, for myocardial iron assessment. Mid septal T2* values were calculated for each patient.
Assessment of myocardial fibrosis was performed using late gadolinium-based contrast material enhancement (LGE) and modified Look-Locker inversion recovery (MOLLI)–based T1mapping. MOLLI sequence was performed before and 10 min after administration of 0.3 mmol of gadolinium-based contrast per kilogram of body weight. Mid septal T1 values were calculated for each patient.
Results All candidates showed elevated native T1 average values (mean 1156 ± 79 ms) and extracellular volume (ECV) average values (mean 37 ± 5.3%) indicating underlying diffuse interstitial fibrosis. T2* values were normal in all included patients (mean 26.3 ± 7.6 ms/normal being > 20 ms) thus excluding myocardial siderosis. All patients showed preserved normal EF% (mean 59.5 ± 5.1%) with decreased end diastolic volumes (mean 85.6 ± 26.4 ml) suggesting restrictive cardiomyopathic changes. No evidence of myocardial wall enhancement in LGE images.
We recognize the limitations of our study, including absence of a control group, however we found it not ethical to perform contrast enhanced procedure in asymptomatic children.

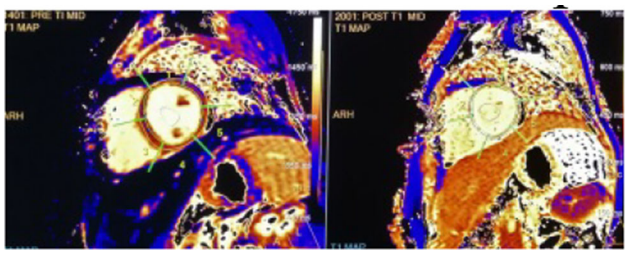

Native (left) and post contrast (right)T1 colored maps, average native T1 value = 1071 ± 46 ms, average ECV value = 38.4%.

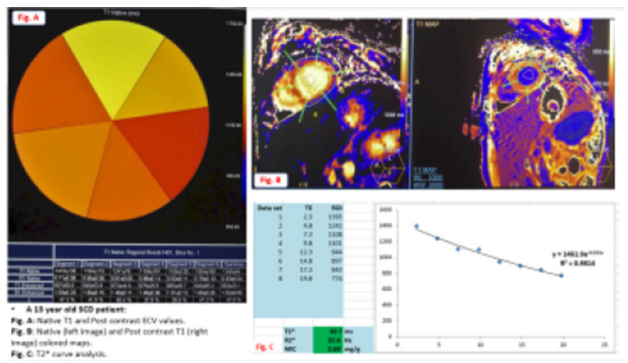

Another example to a SCD patient's data analysis.
Conclusion Myocardial T1 mapping can reveal concealed cardiomyopathy in SCD patients before T2* mapping changes, so it is recommended to be integrated in the follow up protocol of SCD. Further research should investigate the possibility of modifying current treatment protocols, including adding anti-fibrotic therapies, for these patients even in the absence myocardial siderosis.

Aortic valve dysfunction and aortopathy according to the presence or absence of raphe in patients with bicuspid aortic valve disease

S. M. Ko; Seoul/KR

Purpose/Objectives This study was to investigate the association between bicuspid aortic valve (BAV) morphologic findings (raphe vs. nonraphe) and the degree of valve dysfunction and presence of aortopathy in Korean patients.
Methods & Materials This study cohort included 281 subjects (206 men, age 52.3 ± 14.5 years) who underwent both cardiac computed tomography (CCT) and transthoracic echocardiography (TTE) from 2008 to 2016. BAVs were classified according to the presence or absence of a raphe based on CCT and intraoperative findings. Aortic valve function was divided into normal, regurgitation, or stenosis using TTE. The dimensions of the sinus of Valsalva and proximal ascending aorta were measured by CCT. The ascending thoracic aorta was assigned to one of four main anatomical types depending on whether the segment of the vessel exclusively or predominantly involved in dilatation Association between the presence of raphe and the risk of significant (moderate and severe) aortic valve dysfunction and aortopathy was analyzed.
Results Of the 281 patients 168 (59.8%) had BAV with raphe, whereas 113 (40.2%) had BAV without raphe. The prevalence of aortic valve (136 [81%] vs. 84 [74.3%], p = .188) and ascending aorta operation (62 [36.9%] vs. 51 [45.1%], p = .169) were not significantly different between BAVs with raphe and without raphe. BAVs without raphe had a significantly higher prevalence of aortic stenosis, (80 [70.8%] vs. 72 [42.9%], p < .001), but lower prevalence of aortic regurgitation (13 [11.5%] vs. 134 [49.4%], p < .001) compared with BAVs with raphe. Types of BAV aortopathy were significantly different (p = .001) between BAVs with raphe (48 [28.6%] normal, 37 [22%] tubular, 23 [13.7%] root, and 60 [35.7%] combined) and without raphe (23 [20.4%] normal, 49 [43.3%] tubular, 7 [6.2%] root, and 34 [30.1%] combined). Raphe was associated with aortic stenosis and regurgitation on simple (p < .001) but only associated with aortic regurgitation (p < .001) on multiple logistic regression analysis.
Conclusion The presence of raphe was associated with a higher prevalence of significant aortic regurgitation, lower prevalence of stenosis, and higher prevalence of tubular type of aortopathy. The prevalence of aortic valve and aortic surgery was not different according to presence or absence of raphe. Raphe was independently associated with aortic regurgitation. Presence or absence of raphe is associated with types of aortic valvular dysfunction and aortopathy in patients with BAV.

Imaging in aortic emergencies—tips and tricks

R. E. Birla Coroiu[1], R. Manea[2]; [1]Covasna/RO, [2]Brasov/RO

Purpose The term "acute aortic syndrome" (AAS) include acute aortic dissection (AAD), intramural hematoma (IMH), penetrating atherosclerotic ulcer (PAU) and in fewer cases aortocaval (ACF) or aortoenteric fistula (AEF).
To identify the key CT findings of these entities and to make a checklist of the radiological characteristics differentiating them.

Methods & Materials As AAS has a high associated mortality and morbidity rate, early diagnosis and management is necessary.
MDCT is the modality of choice in emergency department for imaging AAS.
Precontrast image acquisition is essential for diagnosis of IMH and intrapericardial rupture. In case of renal disfunction or iodine-contrast allergy MRI is an alternative.
Transesophageal echocardiography at the bedside remain a widely available and portable option.
Results AAD results from separation of the aortic wall layers enabling blood to create a false and a true lumen. Accordingly the key imaging finding are the the intimal flap and the double lumen. A checklist of imaging features is helpful for radiologist to differentiate true from false lumen, such as the beak sign and cobweb and the higher density of the true compared to the false lumen.
On precontrast CT, IMH appears as high density crescent-shaped thickening of the aortic wall, which does not enhance on post contrast images. One way to differentiate IMH from a thrombosed false lumen of aortic dissection is that IMH maintains a constant circumferential relationship with the aortic wall.
PAU is caused when an atherosclerotic lesion ulcerates and penetrates the intima allowing contained hematoma formation within the media. Since "time is Brain" the intra/retroperitoneal hematoma seen on precontrast CT is important for "saving time to surgery planning".
ACF and AEF are rare and devastating spontaneous complications of abdominal aortic aneurysm (AAA), occurring when the aneurysm erodes into the inferior vena cava or retroperitoneal enteric segment (duodenum). The clinical features can be atypical (fainting, abdominal pain, hematemesis and hematochezia) leading to delay in diagnosis. Contrast-enhanced CT identifies the presence of mural thrombus that may obstruct the fistula and volume rendering reconstructions helps radiologist-surgeon team for better treatment. Because of its fatal nature early diagnosis and prompt treatment is recommended, therefore the radiologist holds the key of preoperative diagnosis.

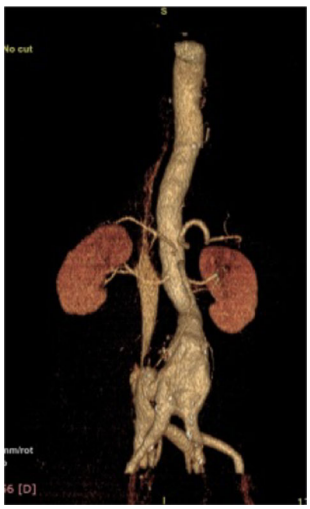

Anterior view of contrast enhanced CT with VR reconstruction of an aortocaval fistula (ACF) of a patient with acute aortic syndrome (AAS)

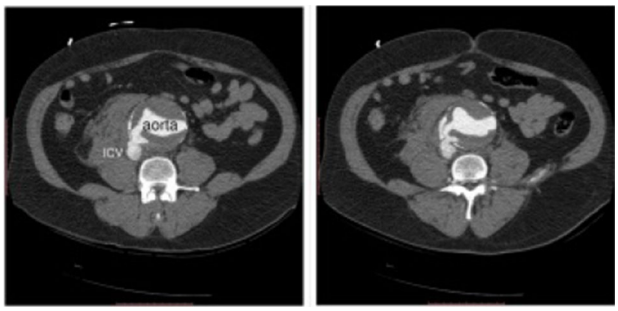

Axial views of contrast enhanced CT pointing the fistula of the aorta into inferior cava vein

Coronal view of contrast enhanced CT of a patient with acute aortic syndrome (AAS)—aneurysm of the infrarenal aorta complicated with aortocaval fistula

Coronal view of contrast enhanced CT of the patient with aortocaval fistula presenting a partially thrombosed aneurysm.
Conclusion Acute aortic syndrome should include ACF and AEF which have "silent" development and acute onset—proper imaging analysis and radiologist-surgeon collaboration is essential for a better treatment outcome.
Specific imaging findings help the radiologist to reach an accurate diagnosis and identify life-threatening complications of AAS.

Impact of contrast media on flow measurements and signal-to-noise ratio in a conventional and compressed sensing 4D flow prototypes

N. Ring[1], N. Jin[2], R. S. Strecker[3], K.-F. Kreitner[1], C. Düber[1], T. Emrich[1]; [1]Mainz/DE, [2]Cleveland/US, [3]Frankfurt am Main/DE

Purpose/Objectives 4D Flow is an emerging imaging technique for flow visualization and quantification. Its applicability to analyze complex hemodynamic properties without invasive testing and ionizing radiation promises a great future in cardiovascular imaging. Compressed Sensing (CS) is a new method to accelerate MRI acquisitions by randomly undersampling k-space data and recovering image quality through iterative reconstruction. Contrast media (CM) can increase SNR in regular 4D flow sequences. Nevertheless, washout effects of CM can degrade image quality. The aim of this study was to compare SNR and flow measurements between native and post-contrast scans using a CS 4D flow prototype in comparison to a conventional GRAPPA accelerated 4D flow prototype.
Methods & Materials CS and conventional 4D flow were acquired on 20 volunteers pre and post CM injection on a 3-Tesla MRI Scanner in sagittal orientation to cover the whole heart. CS 4D flow was acquired with rate-7.7 acceleration, and the conventional 4D flow was acquired with rate-3 GRAPPA. Flow measurements were performed at three different locations (proximal ascending aorta, aortic arch, and descending aorta). SNR was measured in a region of interest in the ascending aorta in two end-diastolic magnitude images using the following equation: $SNR = (\text{mean}(S1 + S2))/(SD(S1-S2) \times \sqrt{2})$.
Results There were no statistically significant differences between contrast and non-contrast conventional and CS flow measurements regarding total volume, maximum mean velocity and net flow (e.g. total volume for conventional and CS 4D flow: $p = 0.107$ resp. $p = 0.256$). Signal increased in all conventional and CS measurements after contrast injection. In 15.8% of conventional and 31.6% of CS flow studies, the amount of noise post CM increased in a way that the SNR of the post contrast flow studies was lower than in the pre contrast study (Figure).

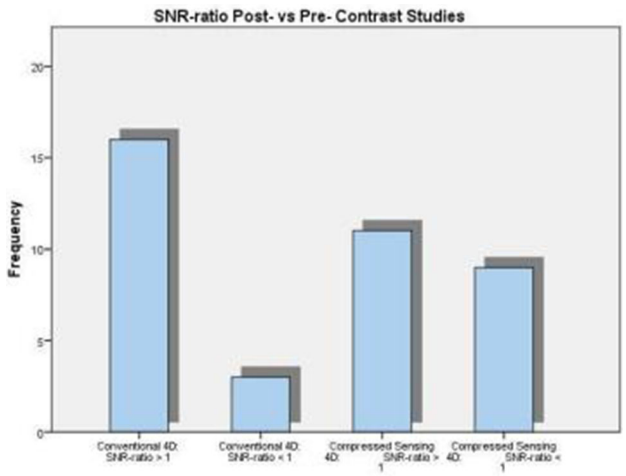

SNR-ratio post vs. pre contrast.
Conclusion 4D measurements can be performed before and after contrast media injection without relevant changes in quantitative flow measurements. In comparison to conventional 4D flow, SNR from post contrast CS flow studies seems to be more affected by gadolinium wash-out effects.

Flow mediated dilation of posterior tibial artery in geriatric population—a pilot study

M. Kotecki, J. Obiała, A. Skoczylas, I. Sudoł-Szopińska, T. Targowski, A. Nowicki, R. Olszewski; Warsaw/PL

Purpose Cardiovascular diseases are the leading cause of death in the modern world, especially among older population. However, there is still a lack of stratification strategies assessing the cardiovascular risk in geriatric populations. Novel noninvasive method which focuses on flow meditated dilation (FMD) indirectly shows the function of endothelium.
The aim of this study was assessment of FMD in left posterior tibial artery and carotid arterial stiffness, intima media thickness (IMT) of carotid arteries, carotid and femoral plaques in geriatric population.
Methods & Materials Patients were enrolled from the Department of Geriatrics, National Institute of Geriatrics, Rheumatology and Rehabilitation, Warsaw, Poland. Every patient has filled a short questionnaire regarding their basic- and personal data. More sufficient data were obtained after patient hospitalization.
The ultrasound examination was performed with the use of Samsung RS-80A with Prestige.
Prior to the study all patients have been fasting for at least 6 h, ceased smoking, alcohol and caffeine consumption for at least 12 h.
Directly before the study the patients were lying on the supine position in dark, quiet and temperature stable examination rooms for 10 min. The study was divided into 2 stages:
Pre-FMD: After the 10 min of rest cuff was placed on the studied leg approximately 20 cm over the medial malleolus. Then, the cuff was inflated to the pressure up to 100 mm Hg above systolic pressure for 5 min. During this period the assessment of plaque burden in carotid and femoral arteries were made.
FMD: after the 5 min the cuff was released causing hyperemia. The diameter of posterior tibial artery was recorded.
Results 33 patients were recruited for the study (28 woman, mean age 77.3 ± 7.86). Maximal IMT of left carotid artery was higher (1.11 vs. 0.91 mm; $p = 0.03$) and FMD was lower (9.3 vs. 14.1%; $p = 0.04$) among patients diagnosed with lung diseases, while no significant correlation with cardiovascular diseases has been found. The presence of plaques in left common femoral artery lead to lower diameter of posterior tibial artery (1.65 vs. 2.03 mm; $p = 0.02$). Finally, FMD correlated with left IMT thickness ($p = 0.01$; $r = -0.490$).
Conclusion Performed study revealed association between IMT, FMD and pulmonary disorders in geriatric population, while there was no significant correlation with cardiovascular diseases. Our cohort will be followed-up, further investigations are necessary to understand this phenomenon.

Twin-beam dual-energy CT for diagnosis of pulmonary embolism: First clinical results

B. M. W. Petritsch, A. Weng, P. Pannenbecker, S. Veldhoen, T. A. Bley, A. Kosmala; Würzburg/DE

Purpose To compare image quality and radiation dose of a new technical dual-energy approach using a split-filter design versus standard CTA at a single-source CT scanner in patients with suspected pulmonary embolism.
Methods & Materials This prospective study was approved by the institutional review board. Computed tomography pulmonary angiography (CTPA) was performed with two protocols at the same 128-row CT system (SOMATOM Edge, Siemens Healthineers). Group 1 (n = 22) received standard single-energy CTPA (automatic tube voltage selection), group 2 (n = 17) received a dual-energy

CTPA using a split-filter (Twin-Beam $_{50}$Sn & $_{120}$Au, fixed tube voltage 120 kV; Figure 1). The measured CT attenuation in the pulmonary artery (PA) and calculated signal-to-noise ratio (SNR) and contrast-to-noise ratio (CNR) were compared. Subjective image quality of standard CTPA and calculated iodine maps was assessed (five-point scale: 1 = excellent; 2 = good; 3 = moderate; 4 = fair; 5 = non-diagnostic). The DLP was reported, and the effective radiation dose was estimated.

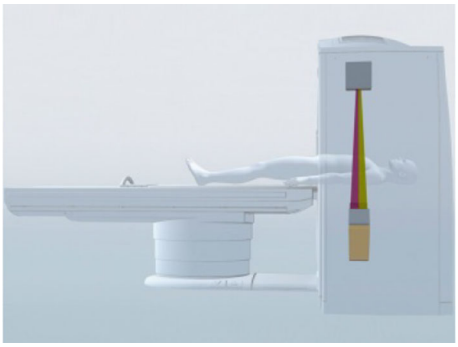

Figure 1 An Sn/Au split-filter allows for dual-energy acquisition at single source CT systems

Results The PA attenuation was higher in the standard CTPA (447 ± 146 HU) compared to the dual-energy cohort (329 ± 127 HU) ($p < 0.05$). In contrast, SNR (17.0 ± 4.6 vs. 23.6 ± 6.0) and CNR (14.8 ± 4.6 vs. 19.3 ± 6.3) were both higher in the dual-energy group ($p < 0.05$). Subjective image quality (median) of CTPA was rated excellent (= 1) in group 1, and good (= 2) in group 2. In the dual-energy cohort four iodine maps were of non-diagnostic quality (= 5; Figure 2), possibly due to breathing artifacts. Mean DLP (138.6 ± 61.4 mGy*cm/182.1 ± 85.2 mGy*cm) and effective radiation (2.49 ± 1.10 mSv/3.28 ± 1.53 mSv) dose were similar in both groups (p = n.s).

Figure 2 VRT shows zebra crossing artifacts. Iodine map was rated as non-diagnostic (= 5) in this case

Conclusion Twin-Beam Dual-Energy CT scanners are an alternative to dual-source or dual-layer CT scanners and offer the possibility to gain dual-energy information from a single-source single-layer CT system when pulmonary embolism is suspected (Figure 3). The new technique provides higher SNR and CNR than standard CT, while the effective radiation dose of Twin-Beam scans is similar to standard CT.

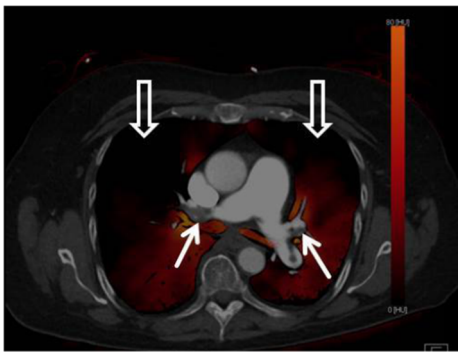

Figure 3 Twin-beam dual-energy CT reveals pulmonary embolism (arrows) and visualizes the corresponding peripheral perfusion defects (open arrows)

References

Dual-energy CT quantitative imaging: a comparison study between twin-beam and dual-source CT scanners. Med. Phys. 44 (1), January 2017.

Initial Results of a Single-Source Dual-Energy Computed. Tomography Technique Using a Split-Filter. Investigative Radiology 51, Number 8, August 2016.

Comparison of image quality and radiation dose between split-filter dual-energy images and single-energy images in single-source abdominal CT. European Radiology (2018) 28:3405–3412.

Dual-energy CT for acute pulmonary embolism: How do image quality and iodine map appearance depend on contrast injection protocol?

A. Kosmala, P. Gruschwitz, A. Weng, T. A. Bley, B. M. W. Petritsch; Würzburg/DE

Purpose To compare four contrast material injection protocols for dual-energy (DE) computed tomography pulmonary angiography (CTPA) in patients with suspected acute pulmonary embolism (PE) with regard to quality of the DE iodine map and absolute pulmonary blood volume (PBV) values as well as image quality of the pulmonary angiography.

Methods & Materials One reader retrospectively evaluated four different groups of contrast agent injection protocols consisting of 60 patients each: group 1: 60 ml@5 ml/s; group 2: 50 ml@5 ml/s; group 3: 50 ml@4 ml/s; group 4: 40 ml@3 ml/s. All examinations were performed on a 3rd generation dual-source CT with otherwise identical settings. Patients with pathologies hampering DE-data evaluation were excluded. Subjective image quality of CTPA and iodine maps (five-point scale: 1 = excellent; 5 = non-diagnostic), total PBV, attenuation in the pulmonary artery (PA) with calculated contrast-to-noise ratio (CNR) were compared.

Results Overall, data from 165 patients was included (groups 1-4 [n]: 40, 41, 43, 41). Mean subjective quality of iodine maps was rated significantly lower in group 4 (2.0 ± 0.7) compared to groups 1-3 (Figure 1; p < .001, respectively; 1: 1.3 ± 0.5; 2: 1.3 ± 0.5; 3: 1.4 ± 0.7), while the other groups showed no significant differences. Mean subjective quality of CTPA datasets was high for all groups (1: 1.1 ± 0.4; 2: 1.3 ± 0.6; 3: 1.2 ± 0.5; 4: 1.5 ± 0.7). Mean total PBV was significantly higher for groups 1 and 2 (34.0 ± 8.9 and 34.4 ± 11.9) vs. groups 3 and 4 (24.9 ± 6.4 and 19.3 ± 5.5) (p < .001). Group 1 presented with highest mean attenuation (428,7 ± 112.1 vs. groups 2-4: 332.8 ± 146.0, 352.7 ± 109.1,

298.5 ± 89.1; p < .001) and CNR in the PA (25.2 ± 7.3 vs. groups 2-4: 19.0 ± 7.2, 21.5 ± 8.0; 16.6 ± 5.8; p < .001). There was no significant DLP-difference between groups.

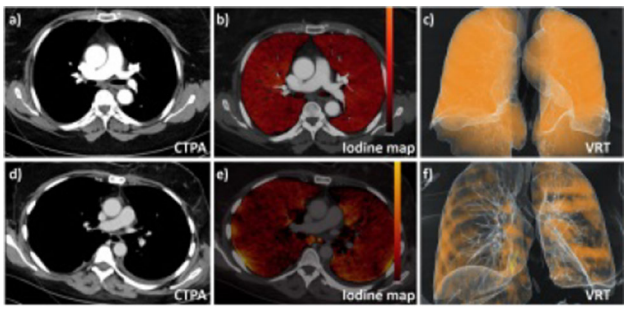

Fig. 1 CTPA image, iodine map and iodine map VRT in two healthy patients at identical window settings: a–c group 1, high volume of contrast medium (60 ml), high flow (5 ml/s). d–f group 4, low volume of contrast medium (40 ml), low flow (3 ml/s)

Conclusion DE CT for acute PE provides high subjective CTPA image quality irrespective of contrast injection protocol, with only slightly inferior subjective quality for low flow rates (group 4). The low-volume/low-flow protocol (group 4) resulted in inferior DE-specific data (iodine map, PBV), while the moderate-volume/moderate–flow protocol (group 3) showed acceptable iodine map quality, but poor PBV values.

Consequently, calculation of high quality iodine maps requires comparatively high volumes of contrast medium injected at high flow rates, while CTPA image quality is a more robust parameter and similarly high among contrast protocols.

References Kang, MJ "*Dual-energy CT: clinical applications in various pulmonary diseases*." Radiographics. 2010May;30(3):685-98. Petritsch, B "*Diagnosis of Pulmonary Artery Embolism: Comparison of Single-Source CT and 3rd Generation Dual-Source CT using a Dual-Energy Protocol Regarding Image Quality and Radiation Dose.*" Rofo. 2017Jun;189(6):527-536.

The role of computed tomography in preoperative planning for septal myectomy in hypertrophic cardiomyopathy

M. Tregubova, K. Rudenko, S. Fedkiv; Kiev/UA

Purpose Hypertrophic cardiomyopathy (HCM) is the most common genetic cardiomyopathy. Septal myectomy (SM) is the preferred approach for medication-refractory obstructive HCM. To assess the anatomical features of the structure of the left ventricle and mitral valve, and single-step assessment of coronary arteries patency and anatomy, when performing preoperative planning, we used computed tomography (CT).

Methods & Materials From April 2016 to April 2019, we reviewed studies of 198 patients who underwent preoperative CT scans prior to SM. Gated cardiac CT was performed in order to delineate the left ventricular (LV) myocardium, to assess the distribution of hypertrophy and the presence of crypts. Also, special attention was paid to the anatomy of the mitral valve and subvalvular apparatus. Patency of the coronary arteries was rated by Coronary Artery Disease—Reporting and Data System (CAD-RADS).

Results Mean patient age was 47 ± 18 years, 42% were male. All the patients had symptomatic medication-refractory obstructive HCM. Mean maximal LV wall thickness was 19 mm (range 16-33). Preoperative mean peak LV outflow tract gradient was 80 mm Hg (range 52–100). Mean postoperative LV outflow tract gradient was 15 mm Hg (range 10-20). Mean LV mass index was 152 ± 43 g/m^2. 39 patients had myocardial crypts, 4 of which where in the surgical resection area.

179 patients had patent coronary arteries (CAD-RADS 0). 7 patients had coronary artery stenosis—CAD-RADS 2. 8 patients had coronary artery stenosis—CAD-RADS 2. 2 patients had coronary artery stenosis—CAD-RADS 3. 2 patients had coronary artery stenosis—CAD-RADS 4. One patient had the anomalous origin of the left circumflex coronary artery from the right sinus of Valsalva. 12 patients had myocardial bridging.

190 patients had systolic anterior motion of the mitral valve. 56 patients had thickened secondary chordae of the mitral valve anterior leaflet.

Actual surgical resection volume was 6.1 ± 1.1 cm^3. In-hospital mortality was 0,5%.

Conclusion Gated cardiac CT can be a valuable addition to preoperative planning of patients with obstructive hypertrophic cardiomyopathy.

Association of global myocardial strains with the severity of pulmonary hypertension: A cardiac magnetic resonance cine realtime feature tracking study

V. Nizhnikava, G. Reiter, U. Reiter, G. Kovacs, C. Reiter, C. Kräuter, H. Olschewski, M. Fuchsjäger; Graz/AT

Purpose/Objectives Pulmonary hypertension (PH) is associated with left (LV) and right ventricular (RV) functional and myocardial alterations, which are related to progression and prognosis of disease. Cardiac magnetic resonance (MR) feature-tracking is increasingly used for assessment of myocardial strains, allowing evaluation of myocardial dysfunction additionally to volumetric functional parameters from cine-imaging. The aim of the current study was to analyze global LV and RV strain parameters derived from cine-realtime feature-tracking in PH and to investigate their associations with presence and severity of PH.

Methods & Materials 40 subjects with known or suspected PH underwent right heart catheterization (RHC) and 3T cardiac MR (Skyra, Siemens, Germany) within 1 ± 3 days. PH was confirmed in 28 patients by RHC (mPAP = 43 ± 11 mmHg in PH; mPAP = 15 ± 3 mmHg in non-PH). Global radial (GRS), circumferential (GCS) and longitudinal (GLS) LV and RV strains and strain rates (GRS_{rate}, GCS_{rate}, GLS_{rate} respectively) were analyzed from cine-realtime free-breathing short-axis and four-chamber series using cvi42 software (Circle, Canada). LV and RV volumetric function parameters were evaluated by dedicated software (Argus, Siemens, Germany). Group differences were compared by t test; relations between parameters were investigated by correlation and regression analysis. $p < 0.05$ was considered to be statistically significant.

Results Among LV strain parameters, diastolic LV-GRS_{rate} (r = 0.57) and diastolic LV-GCS_{rate} (r = − 0.46) showed significant correlations with mPAP. In parallel, numerous RV strain parameters demonstrated significant correlations with mPAP: RV-GRS (r = − 0.34), systolic RV-GRS_{rate} (r = − 0.36), RV-GCS (r = 0.30), and RV-GLS (r = 0.74). From these parameters, diastolic LV-GRS_{rate} (− 1.8 ± 0.7/s in PH vs. − 2.8 ± 0.8/s non-PH, p = 0.0001), diastolic LV-GCS_{rate} (1.0 ± 0.4/s in PH vs. 1.5 ± 0.4/s non-PH, p = 0.0031), and RV-GLS (− 14 ± 4% in PH vs. − 21 ± 2% non-PH, $p < 0.0001$) differed between PH and non-PH as well. Linear regressions of diastolic LV-GRS_{rate}, diastolic LV-GCS_{rate}, and RV-

GLS on mPAP are given in Figure 1. Besides their correlations with mPAP, these parameters demonstrated correlations with various volumetric function parameters. LV ejection fraction was the strongest LV predictor for LV strain rates ($r = -0.65$ for diastolic LV-GRS_{rate}, and $r = 0.51$ for diastolic LV-GCS_{rate}), RV ejection fraction for RV-GLS ($r = -0.63$). With the respective ejection fractions as covariates, partial correlations of all strain parameters with mPAP remained significant ($r = 0.58$, -0.46, and 0.56 for diastolic LV-GRS_{rate}, diastolic LV-GCS_{rate}, and RV-GLS respectively).

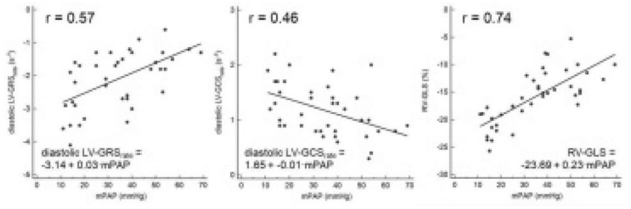

Figure 1 Linear regressions of diastolic LV-GRSrate, diastolic LV-GCSrate and RV-GLS on mPAP together with the correlation coefficients r

Conclusion Cine-realtime feature-tracking derived diastolic LV-GRS_{rate}, diastolic LV-GCS_{rate} and RV-GLS differ between PH and non-PH subjects and correlate with mPAP even after correction of dependencies on volumetric function parameters.

Incidence and quantification of coronary artery and aortic valve calcifications on non-gated unenhanced CT chest in middle aged adults

V. Majcher, R. Bakewell, S. Karia, J. Babar, M. T. A. Wetscherek; Cambridge/UK

Purpose Coronary artery disease is the single biggest cause of cardiac morbidity and mortality, while calcific aortic stenosis is the third-leading cause of cardiovascular disease. The increasing number of CT chest examinations presents an opportunity to screen a large number of individuals for coronary and aortic valve disease. The Agatston method for quantification of coronary artery calcification (CAC) on ECG-gated CT scans has been validated and more recently, a visual approach has been proposed for the quantification of CAC on nonECG-gated studies. The aim of our study was to evaluate the incidence of coronary artery and aortic valve calcifications on non-ECG gated, unenhanced CT chest examination and to quantify this calcification using the visual and Agatston scores.
Methods & Materials We retrospectively evaluated 120 non-ECG-gated unenhanced CT chest examinations performed using volumetric acquisitions with slice thickness of 1 mm of 120 patients between the ages of 40-69 years. Visual scores were determined by two observers blinded to the Agatston score and using the Ordinal method by assigning a value of 0, 1, 2 or 3 for no calcification, mild (< 1/3rd of artery affected), moderate (up to 2/3rds affected) and severe (> 2/3rds affected), to each of the four coronary arteries. The final score represented the sum of the per-vessel values and was categorised as mild (< 4), moderate (4–8) and severe (> 8) disease. Using the Agatston score, four severity groups were defined, 0: no identifiable disease, 1–100: mild, 101–400: moderate and > 400: severe disease.
Results 63 patients (53%) had coronary artery and/or aortic valve calcification with 42 (35%) showing mild, 12 (10%) moderate and 6 (5%) severe coronary artery calcification on visual assessment. A high degree of correlation was found between the severity of coronary artery calcification assessed by the visual scoring method and by the Agatston score. 85% of severity rankings were in the same category when the two calcium quantification methods were compared with accuracy of 85%, 67% and 100% in the mild, moderate and severe coronary artery calcium severity categories respectively.
Conclusion Visual quantification of coronary artery and aortic valve calcification on unenhanced CT chest demonstrates good correlation with Agatston score. High incidence of calcification was found on these CT studies performed for various indications with many patients having no documented history of aortic or coronary artery disease. Given the increasing importance of preventive medicine, our result encourages routine reporting and quantification of coronary artery and aortic valve calcifications on non-ECG-gated CT chest examinations.

Assessment of left ventricular flow in hypertrophic cardiomypathy by 4D-flow MRI

O. Y. Dariy, E. Glazkova, S. Aleksandrova, V. Makarenko; Moscow/RU

Purpose The purpose of our study was to assess phase-contrast MRI in the evaluation of left ventricular (LV) 3D hemodynamics changes in various phenotypes of hypertrophic cardiomyopathy (HCM).
Methods & Materials We performed 15 cardiac magnetic resonance imaging (CMR): in 11 patients with HCM (48 ± 13 years), including (n = 3) apical phenotype; (n = 4) diffuse-septal and (n = 4) focal-basal phenotype. 4 CMR of healthy controls (43 ± 12 years). All patients underwent the standart CMR protocol with an additional phase-contrast sequence of the LV area (4D flow (field strength = 1.5T, resolution = 2.2–4.0 × 2.2-4.0 × 2.5–3.2 mm(3); venc = 80–100 cm/s; TE/TR/FA = 3.36 ms/79.95 ms/15°) for the in vivo assessment of 3D blood flow velocities with full coverage of the LV. Postprocessing carried out in 4D FLOW (Siemens).
Results Data were obtained on the geometry and dynamics of vortex diastolic flows in the LV of all group patients. HCM demonstrated significantly increase in the distance to the center of the vortex and decrease in the normalized area, decrease peak velocity of the vortex ($P < 0.005$) compared to controls. The diffuse-septal HCM phenotype was characterized by a minimal vortex peak velocity; the apical one—the maximum vortex sphericity index. For patients with a focal-basal HCM phenotype- the maximum changes in blood flow were determined in late diastole (absence of vortexes).
Conclusion Phase-contrast MRI allows identifying and assessing the general trends in the LV vortical flow in HCM. Quantitative analysis of hemodynamic data can be used to characterize the LV blood flow remodeling of various HCM phenotypes.

Balloon pulmonary angioplasty improves right atrial reservoir and conduit functions in patients with chronic thromboembolic pulmonary hypertension

Y. Yamasaki, T. Kamitani, K. Sagiyama, T. Hida, Y. Matsuura, Y. Murayama, K. Hosokawa, K. Abe, H. Yabuuchi; Fukuoka/JP

Purpose Right atrial (RA) reservoir and passive conduit functions contributes to maintain right ventricular (RV) function. Recently, these functions were reported to be independent predictors of clinical worsening in patients with pulmonary arterial hypertension. However, the impacts of balloon pulmonary angioplasty (BPA) on RA functions remains unclear in patients with inoperable chronic thromboembolic pulmonary hypertension (CTEPH). This study investigated the effects of BPA on RA functions in those patients using cardiac magnetic resonance imaging (CMRI).
Methods & Materials CMRI and RV catheterization were conducted before BPA sessions and at the follow-up periods in 20 CTEPH patients.

RA maximum volume, minimum volume and ejection fraction (EF) were measured. Reservoir (RA longitudinal strain [RA-LS] and RA longitudinal strain rate [RA-LSR]), conduit (RA early LS rate), and active (RA late LS rate) phases were assessed using feature tracking software. RV catheterization provided right atrial pressure, pulmonary artery pressure (PAP), pulmonary capillary wedge pressure (PCWP), and cardiac output. Consequently, pulmonary vascular resistance (PVR) was calculated.

Results BPA significantly reduced mean PAP levels (40.0 ± 10.9 vs. 24.4 ± 4.2 mmHg; $p < 0.001$). Following BPA, RAEF, RA-LS and early LS rate were significantly increased (EF: 43 ± 9% vs. 51 ± 10%, $p < 0.01$, LS: 34.6 ± 15.5% vs. 54.2 ± 22.6%, $p < 0.001$, LSR: 7.0 ± 2.9% vs. 10.9 ± 4.5%, $p < 0.001$ and early LS rate: − 2.4 ± 2.3% vs. − 5.1 ± 4.2%, $p < 0.05$), whereas there was no significant change in RA late LS rate. Among RA functional parameters, conduit function is correlated with pulmonary hemodynamic parameters, such as mean PAP, PVR and CI the best.

Conclusion In inoperable CPEPH, BPA improved not only RAEF but also RA reservoir and conduit function. The assessment of RA function using cardiac MRI could be useful to evaluate BPA effect.

References 1. Querejeta Roca G, et al. Right Atrial Function in Pulmonary Arterial Hypertension. Circulation Cardiovascular imaging. 2015. 2. Aoki T, et al. Comprehensive evaluation of the effectiveness and safety of balloon pulmonary angioplasty for inoperable chronic thrombo-embolic pulmonary hypertension: long-term effects and procedure-related complications. Eur Heart J. 2017. 3. Kawakubo M, et al. Clinical usefulness of right ventricular 3D area strain in the assessment of treatment effects of balloon pulmonary angioplasty in chronic thromboembolic pulmonary hypertension: comparison with 2D feature-tracking MRI. Eur Radiol. 2019.

Workforce in academic cardiovascular radiology: is the future bright? Preliminary results and global perspective of academic involvement at the level of core radiology training

M. Arzanauskaite[1], S. C. Shelmerdine[2], J. M. D. Choa[3], D. F. Haroun[4], E. Estades[5], E. Terrazas[6], S. Türk[7], M. Serra[8], B. Bold[9], F. Vernuccio[10]; [1]Liverpool/UK, [2]London/UK, [3]Philippines/PH, [4]Cairo/EG, [5]Wilmington/US, [6]Distrito federal/MX, [7]Izmir/TR, [8]BUENOS AIRES/AR, [9]Bangkok/TH, [10]Palermo/IT

Purpose/Objectives To assess the involvement in research and teaching of radiology trainees who are interested in cardiovascular imaging and to identify the challenges they encounter.

Methods & Materials We distributed an online survey worldwide using social media and radiology societies that agreed to share it by the time of abstract submission. Factors affecting research and teaching during training were covered. Responses from trainees with interest in cardiovascular imaging were obtained. Data were then analysed with appropriate statistics.

Results A total of 116 trainees and fellows with an interest in cardiovascular imaging were assessed (68 (59%) males; 77 (66%) participants have been trained in European countries). 79/116 (68%) of trainees are involved in research, yet only 45/116 (39%) reported formally allocated research time; 37/45(82%) of them reported ≤ 5 h per week.

Only 42/116 (36%) are involved in teaching activities. 47/116(41%) reported to have formally allocated teaching time, of those the majority (45/47(96%)) had ≤ 5 h per week.

Of the participants without such opportunities, 69/71(97%) would like to have protected time for research, and 65/79 (81%) would like to have protected time for teaching. Trainees agree that research (69/116, 59%) and teaching (83/116, 72%) contribute to improving their clinical competency.

Although there were no statistically significant differences in article publications between women and men, a significantly higher number of women (15/45, 31%) consider their gender as a challenge in academic opportunities compared to men (5/68, 7%) ($p = 0.0062$).

The most important perceived barriers limiting involvement of residents in research activities were time constraints (79/116, 68%) and lack of mentorship (59/116, 51%).

The majority (99/116, 85%) presented at conferences without statistically significant difference between the trainees with and without allocated time (38/45, 84% vs 61/71, 86% $p = 1$). No statistically significant difference was seen in first author publications between the trainees with and without allocated time either (20/45 vs. 26/71, $P = 0.4$).

After completion of training, the majority (83/116, 72%) would like to work in an academic setting – combined, public or private.

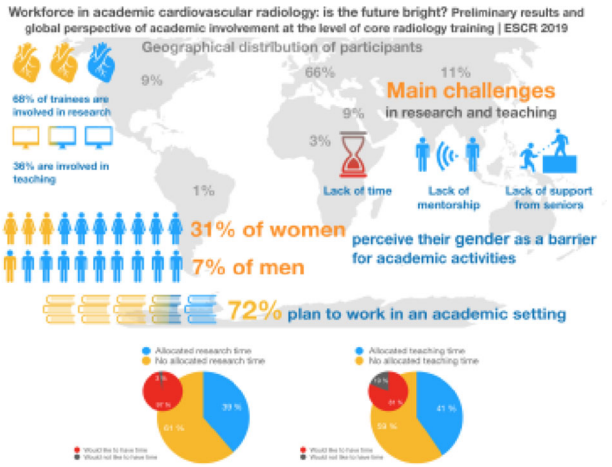

Figure 1 .

Conclusion Although the majority of trainees interested in cardiovascular imaging are research-active and plan to work in an academic setting, most do not have protected academic time. Time constraints and lack of mentorship are the main barriers to academic activities. There is a significant perceived gender barrier for women in academic opportunities. Institutions and societies seeking to develop radiology should focus on providing protected time and mentorship. Having protected academic time could potentially lessen burnout.

Strain evaluation in patients with bicuspid aortic valve insufficiency: can the direction of the regurgitation jet influence diastolic function?

G. Cundari[1], N. Galea[1], G. Pambianchi[2], L. Marchitelli[1], I. Carbone[1], C. Catalano[1], M. Francone[1]; [1]Rome/IT, [2]Fermo, FM/IT

Purpose Bicuspid aortic valve (BAV) is one of the most frequent congenital cardiac malformation (prevalence 1-2%). Many other aortic and cardiac disorders can affect patients with BAV, such as valvular insufficiency.

We analysed patients with BAV insufficiency with Cardiovascular Magnetic Resonance (CMR), in order to examine the regurgitation jet direction and determine if the jet impact on the anterior mitral leaflet can affect the diastolic function.

Methods & Materials We retrospectively studied a group of 24 patients with BAV and aortic valve insufficiency. In 12 of them, jet regurgitation was oriented to the mitral valve (MV group) during diastole, while in the other 12, the jet had another direction (NMV group). We analysed their ventricular volumes and diastolic function using a 3T scanner. The CMR protocol included long axis and short axis breath-hold cine-Steady State free precession sequences. We evaluated the strain rate and the peak diastolic velocity (radial, circumferential and longitudinal), in order to identify deformability alterations of myocardial fibres.
Results We found a reduction in mean circumferential peak diastolic velocity (125.85 deg/s ± 40% in NMV group vs. 50.15 deg/s ± 12% in MV group, p value < 0.01), in mean longitudinal peak diastolic velocity (56.01 mm/s ± 30% in NMV group vs. 34.39 mm/s ± 4% in MV group, p value < 0.01) and in mean radial peak diastolic velocity (43.97 mm/s ± 9.14% vs. 33.8 mm/s ± 0.4%, p value < 0.05). We also found a statistically significant decrease in circumferential strain rate (1.22/s ± 27.8% vs. 0.95/s ± 14.7%, p value < 0.05) and longitudinal strain rate (1.01/s ± 22% vs. 0.81/ ± 5.54%, p value < 0.05). No significant differences have been found in the comparison of ventricular volumes between the two groups.
Conclusion Regurgitation jet direction can hinder MV opening during diastole, causing a slowdown in peak diastolic velocity (radial and circumferential) and in myocardial diastolic strain rate.

Ticagrelor to reduce myocardial injury in patients with high-risk coronary artery plaque

A. Moss[1], M. Dweck[1], M. Doris[1], J. Andrews[1], E. J. R. van Beek[1], L. Forsyth[1], R. Lee[1], S. Lewis[1], N. Mills[1], D. E. Newby[1], P. Adamson[2]; [1]Edinburgh/UK, [2]Christchurch/NZ

Purpose/Objectives: Background
High-risk coronary atherosclerotic plaque is associated with higher plasma troponin concentrations suggesting ongoing myocardial injury that may be a target for dual antiplatelet therapy.
Objectives
To determine whether ticagrelor reduces high-sensitivity troponin I concentrations in patients with established coronary artery disease and high-risk coronary plaque.

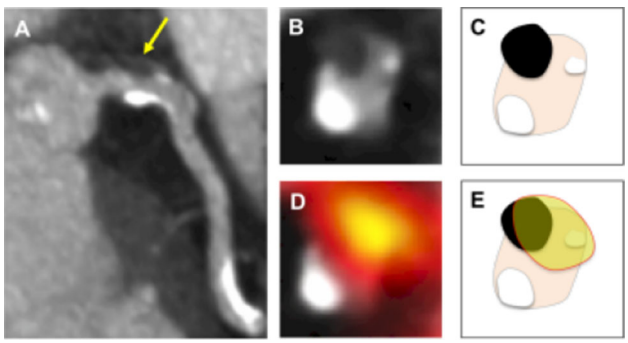

Coronary 18F-fluoride and thrombus
Methods & Materials: Methods
In a randomized double-blind placebo-controlled trial, patients with multivessel coronary artery disease underwent coronary 18F-fluoride positron emission tomography-computed tomography and measurement of high-sensitivity cardiac troponin I and were randomized (1:1) to ticagrelor 90 mg twice daily or matched placebo. The primary endpoint was troponin I concentration at 30 days in patients with increased coronary 18F-fluoride uptake.
Results: Results
In total, 202 patients were randomized and 191 met the pre-specified criteria for inclusion in the primary analysis. In patients with increased coronary 18F-fluoride uptake(n = 120/191) there was no evidence that ticagrelor had an effect on plasma troponin concentrations at 30 days (ratio of geometric means for ticagrelor vs. placebo 1.11, [95% confidence interval 0.90 to 1.36], p = 0.32). Over 1 year, ticagrelor had no effect on troponin concentrations in patients with increased coronary 18F-fluoride uptake(ratio of geometric means, 0.86, 95% confidence interval 0.63 to 1.17, p = 0.33).

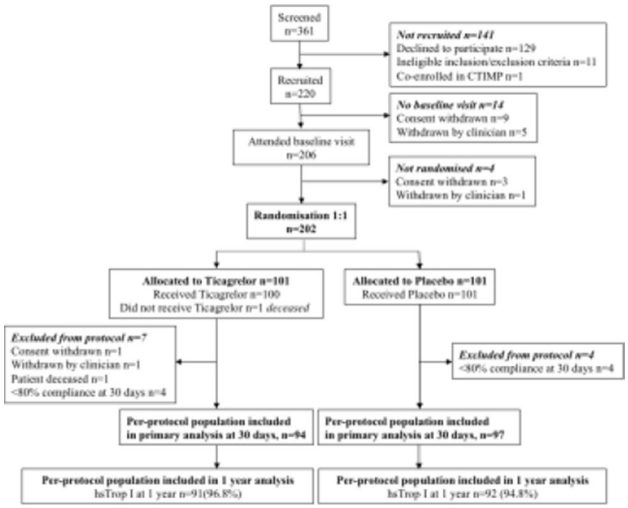

Consort diagram
Conclusion: Conclusions
Dual antiplatelet therapy with ticagrelor does not reduce plasma troponin concentrations in patients with high-risk coronary plaque, suggesting that subclinical plaque thrombosis does not contribute to ongoing myocardial injury in this setting.
Clinical Trials.gov Study ID: NCT02110303.

Coronary artery calcium scoring on gated and non-gated thoracic computed tomography

M. Williams[1], G. Roditi[2], E. J. R. van Beek[1], D. E. Newby[1]; [1]Edinburgh/UK, [2]Glasgow/UK

Purpose/Objectives Coronary artery calcification (CAC) can be identified on non-gated thoracic computed tomography (CT) performed for non-cardiac indications and this may provide additional information on cardiovascular risk.
Methods & Materials We identified patients who underwent gated CT as part of the SCOT-HEART (Scottish Computed Tomography of the Heart) trial who subsequently underwent non-gated thoracic CT for lung nodule follow-up. Demographic and imaging information was obtained from the SCOT-HEART database. Coronary artery calcium scoring (CACS) on gated non-contrast CT was performed using the Agatston method. Ordinal CACS was also performed on non-gated non-contrast thoracic CT. For this CAC was identified in the left main stem, left anterior descending, left circumflex and right coronary artery and was scored on a four-point scale (0, none; 1, mild;

2, moderate; 3, severe). Vessel scores were summed to give the total ordinal CACS and categorized into four groups (none, 0; mild, 1–4; moderate, 5–8; severe, 9–12). On non-gated non-contrast thoracic CT, CACS was performed using the Agatston method (n = 33).

Results The images of 67 patients were assessed (mean age 57 ± 10 years, 44 (66%) male). CAC was identified in 47 (70%) patients on gated CT. There was excellent correlation between gated Agatston CACS and ordinal CACS (r 0.91, $p < 0.001$). There was excellent correlation between gated and non-gated Agatston CACS (r 0.90, $p < 0.001$). Bland–Altman plots for gated and non-gated Agatston CACS showed a low bias of 17 AU, with good agreement (lower limit − 51, upper limit 86 AU). As CACS increased the spread of the difference between gated and non-gated Agatston CACS increased. Patients with mild, moderate and severe total ordinal CACS had median gated Agatston CACS of 47 [IQR 19, 122] AU, 430 [IQR 318, 738] AU and 1119 [IQR 926, 1683] AU, respectively. Diagnostic accuracy for the identification of CAC on non-gated compared to gated CT was excellent, with sensitivity 94%, specificity 85%, positive predictive value 94% and negative predictive value 85%.

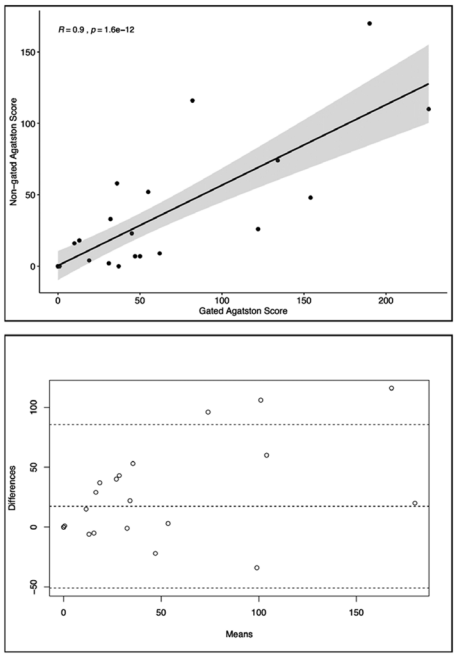

Scatter plot and Bland–Altman plot showing excellent correlation between gated and non-gated Agatston CACS

Conclusion CAC can be identified on non-gated non-contrast thoracic CT with good diagnostic accuracy and quantification compared to standard gated coronary calcium score CT.

Coronary artery calcium scoring based on high-pitch third-generation dual-source CT: Comparison between non-ECG triggered and ECG-triggered scanning

C. Xia, G. J. Pelgrim, M. Rook, M. Oudkerk, M. Vonder, R. Vliegenthart; Groningen/NL

Purpose/Objectives The purpose of this study was to validate non-electrocardiographically (ECG)-triggered low-dose chest CT for coronary artery calcium (CAC) scoring, by comparing with ECG-triggered cardiac CT.

Methods & Materials In total, 1000 participants from a population-based imaging study who underwent CT scanning using third-generation dual-source CT (Somatom Force, Siemens Healthineers, Germany) were included. An ECG-triggered cardiac acquisition (120 kVp, 64 mAs, pitch 3.2) was performed, immediately followed by a non-ECG-triggered chest acquisition (120 kVp, 20 mAs, pitch 3.0). Both cardiac and chest scans were reconstructed using CAC scoring setting (250 mm field of view, 3 mm slice thickness and 1.5 mm slice increment). Calcium scores were determined by Agatston's method using commercial software (CaScoring, Syngo Via, Siemens, Germany). Correlation in calcium scores between chest and cardiac scans was assessed using Kendall's tau-b (τb). Agreement between chest and cardiac scans in CAC detection (absent vs. present) and risk classification (strata: 0, 1–99, 100–399, ≥ 400) were assessed by Cohen's kappa.

Results There was a high correlation in calcium score between non-ECG triggered chest CT scans and cardiac CT scans (τb = 0.938, $p < 0.001$). Accuracy, sensitivity and specificity of non-ECG triggered chest CT in CAC detection were 97%, 96% and 99%, respectively compared to cardiac CT. Excellent agreement in CAC detection (kappa 0.95) and risk classification (weighted kappa 0.95) between non-ECG triggered chest CT scans and cardiac CT scans were found. There were 65 cases (6.5%) reclassified by non-ECG triggered chest CT based on the CAC risk strata, compared with cardiac CT. In 85% (55/65) of these cases, participants shifted one risk category downward and none of the participants shifted more than one risk category.

Conclusion For third-generation, dual-source CT in high-pitch setting, the agreement between non-ECG triggered chest CT and ECG-triggered cardiac CT with regards to CAC detection and risk classification was excellent.

USPIO-Enhanced magnetic resonance coronary angiography compared to computed tomography coronary angiography

M. Daghem[1], R. Ramaesh[1], G. Macnaught[2], M. Dweck[1], S. Semple[1], E. J. R. van Beek[1], D. E. Newby[1], M. Williams[1]; [1]Edinburgh/UK, [2]Glasgow/UK

Purpose Imaging of the coronary arteries by magnetic resonance imaging (MRI) can identify both anatomy (1) and the presence of coronary artery stenoses (2). Recent concerns regarding gadolinium has led to the investigation of alternatives for magnetic resonance coronary angiography (MRCA) including non-contrast imaging and contrast imaging with ultrasmall superparamagnetic particles of iron oxide (USPIO) (3).

This study assesses the image quality of USPIO-enhanced MRCA compared to computed tomography coronary angiography (CTCA).

Methods & Materials Eight patients underwent USPIO-enhanced MRCA using a 3 Tesla PET/MRI scanner (Biograph mMR, Siemens) and CTCA using a 128-multidetector computed tomography (CT) scanner (Biograph PET-mCT, Siemens). MRCA was performed using FLASH magnetic resonance angiography sequences with 3 to 4 mg/kg of intravenous ferumoxytol. Per segment image quality was rated on a 4-point scale (1 excellent, 2 mild reduction in image quality, 3 moderate reduction in image quality, 4 non-diagnostic with severe reduction in image quality or non-visualised segment) by two separate observers, blinded to other imaging. CTCA was taken as the gold standard for which segments were present.

Results The images of 99 segments in 7 patients were assessed. Diagnostic image quality was observed in 80% (79/99) of segments with USPIO-enhanced MRCA compared to 99% (98/99) of segments with CCTA. Excellent image quality was observed in 45% segments

with USPIO MRCA (45/99). Image quality was mildly reduced in 16% (16/99), moderately reduced in 18% (18/99) and severely reduced and non-diagnostic in 20% (20/99). Diagnostic image quality for USPIO MRCA was more frequent in proximal and mid segments compared to distal segments (90%, 44/49 vs. 70%, 35/50).

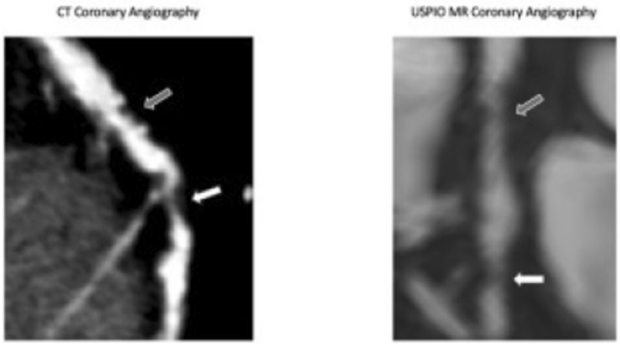

Left anterior descending artery stenosis

Conclusion USPIO-enhanced MRCA has a good image quality for the identification of vessel segments, particularly proximal segments. These protocols offer an alternative to gadolinium-based MRCA.

References 1)Gharib AM, Ho VB, Rosing DR et al.. Coronary artery anomalies and variants: technical feasibility of assessment with coronary MR angiography at 3 T. Radiology 2008;247(1):220–227.
2)Kim WY, Danias PG, Stuber M, Flamm SD, Plein S, Nagel E, et al. Coronary magnetic resonance angiography for the detection of coronary stenoses. N Engl J Med. 2001;345:1863–9. https://doi.org/10.1056/nejmoa010866.
3) Hope MD, Hope TA, Zhu C, et al. Vascular Imaging With Ferumoxytol as a Contrast Agent. AJR Am J Roentgenol 2015;205(3):W366–73.

First results of a population-based study into prevalence and severity of coronary calcification as determined by third-generation dual-source computed tomography

C. Xia, M. Rook, G. J. Pelgrim, J. N. van Bolhuis, P. M. van Ooijen, M. Vonder, M. Oudkerk, G. de Bock, P. van der Harst, R. Vliegenthart; Groningen/NL

Purpose The coronary artery calcium score (CACS) is a non-invasive imaging biomarker for the extent of coronary atherosclerosis and is a robust predictor for cardiovascular events. The purpose of this study is to establish a reference for CACS distribution in an unselected Dutch adult population, which can help to determine optimal cut-off values for cardiovascular risk classification in the future.

Methods & Materials The Imaging in Lifelines (ImaLife) study involves a subgroup of adult participants (age $\geq$ 45 years) from the population-based Lifelines cohort for a low-dose chest and cardiac CT examination. The ImaLife study was launched in August 2017 and is still on running. CT scanning was performed using third-generation dual-source CT (Somatom Force, Siemens Healthineers, Germany). We determined CACS according to Agatston's method, using commercial software (CaScoring, Syngo Via, Siemens, Germany).

Results So far, a total of 4142 participants have been recruited (mean age 54 years, range 45–82 years, 42.3% men). Prevalence of positive CACS was 39.7% in all participants, and 56.1% and 27.8% in men and women, respectively. In 45–49, 50–54, 55–59, 60–64 year age groups, prevalence of positive CACS were 37.5%, 50.6%, 62.5%, 76.7% in men and 14.3%, 21.4%, 34.3%, 42.9% in women. The median CACS in 45–49, 50–54, 55–59, 60–64 year age groups were 0, 1, 6, 22 in men and 0, 0, 0, 0 in women.

Conclusion The first results of the ImaLife study show the CACS distribution by age and gender in a middle-aged Dutch population. Compared with previous studies, CACS were lower in our cohort in both genders. The project is planned to be completed by early 2021. By then, reference of CACS for the Dutch population can be established.

Dual-Source Dual-Energy CT to Differentiate Healthy from Cardiomyopathic Myocardium via Myocardial Extracellular Volume Fraction Estimation

A. F. Abadia[1], V. Vingiani[1], S. S. Martin[2], M. van Assen[3], U. J. Schoepf[2]; [1]Charleston/US, [2]Charleston, SC/US, [3]Groningen/NL

Purpose/Objectives This study aimed to evaluate the feasibility of dual-energy CT (DECT)-based iodine quantification to estimate myocardial extracellular volume (ECV) fraction in patients with and without cardiomyopathy (CM), and assess its ability to distinguish healthy myocardial tissue from cardiomyopathic, with the goal of defining a threshold ECV value for disease detection.

Methods & Materials This study was approved by the institutional review board; informed consent was obtained. Ten healthy (i.e. free of heart-related disease) subjects and 60 patients (40 with ischemic CM and 20 with non-ischemic CM) were retrospectively selected (mean age 64.96 $\pm$ 12.85, 59 males and 11 females). Late iodine enhanced DECT imaging was performed 7 min after contrast material injection. Images were analyzed on a commercially available workstation and myocardial iodine maps were obtained using 3-material decomposition. ECV was estimated from hematocrit (HCT) levels and the iodine maps using the AHA 16-segment model of the left ventricle (apex excluded). Median ECV values are reported with their corresponding interquartile ranges. Receiver operating characteristic (ROC) curve analysis was performed, with corresponding area under the curve (AUC), along with Youden's index assessment, to establish a threshold for CM detection.

Results The ECV for ischemic CM, non-ischemic CM, and healthy myocardium were 36.92% (32.39–41.09), 38.34% (33.71–42.97), and 25.38% (22.94–27.31), respectively. Healthy myocardium showed significantly lower median ECV values compared to ischemic and non-ischemic CM ($p < 0.001$). From Youden's index analysis, an ECV > 29.48% would indicate the presence of CM (vs. healthy) in the myocardium (sensitivity = 90.3; specificity = 90.3); the AUC for this criterion was 0.950 ($p < 0.001$).

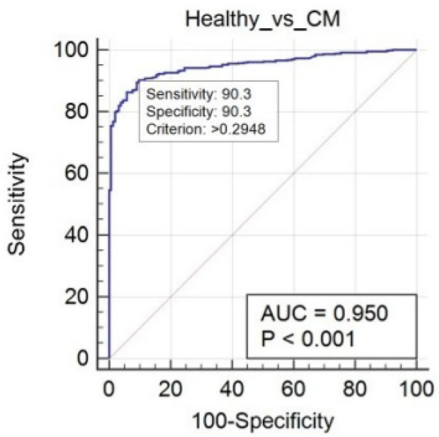

Results from ROC curve analysis (with corresponding AUC) and

Youden's index assessment to distinguish healthy myocardium ECVs from CM

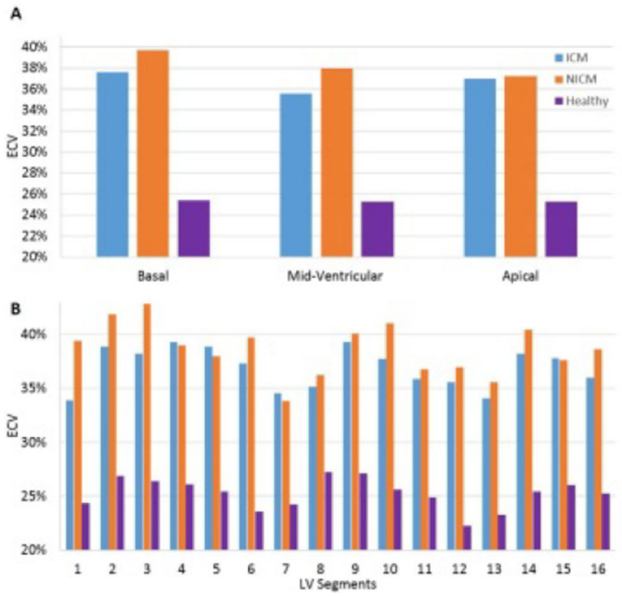

Results from a per-layer analysis (basal, mid-ventricular, apical) (A), and a per-segment analysis (B) of the median ECV values found across the entire study population.

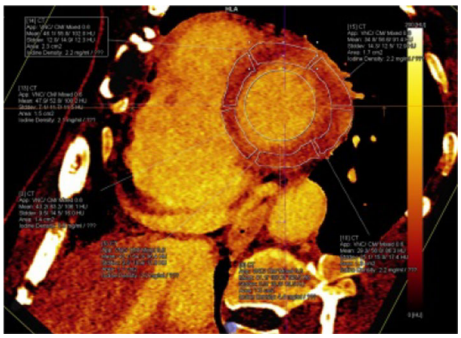

Example of iodine map obtained with delayed contrast-enhanced DECT acquisition and illustration of AHA LV segmentation.

Conclusion ECV measurements based on iodine maps obtained from DECT provide additional value for the characterization of the myocardium. The findings of this study led to the establishment of a promising threshold ECV value that could facilitate the differentiation between healthy and diseased myocardium, and highlight the potential of this DECT methodology to detect cardiomyopathic tissue.

Patient-tailored Coronary Artery Calcium Scoring Using a kVp-independent Reconstruction Kernel and an Automated Tube Voltage Selection

V. Vingiani, A. F. Abadia, S. S. Martin, U. J. Schoepf; Charleston/US

Purpose This study aimed to prospectively investigate an automated tube voltage selection (ATVS)-based coronary artery calcium scoring (CACS) protocol, using a software-based correction algorithm and a kVp-independent kernel, for the accurate assessment of Agatston calcium scoring.

Methods & Materials The institutional review board approved this prospective single-center study. Forty-two patients (60.2 ± 10.5 years, 40% male) underwent conventional clinical CACS at 120 kVp and an additional research CACS acquisition using an individualized tube voltage between 70 and 130 kVp based on the ATVS selection. Datasets of the additional CACS scans were reconstructed using a kVp-independent kernel that enables using the Agatston scoring without changing the weighting threshold of 130 HU, regardless of the original tube voltage chosen for image acquisition. Agatston scores and radiation dose estimates derived from the different ATVS-based CACS studies were compared with the standard acquisition at 120 kVp. Paired samples T test was used to assess the statistical differences between the two methodologies.

Results The median Agatston scores derived from the standard 120 kVp and the patient-tailored kVp-independent protocols were 41.55 (IQR 0–338.4) and 48.75 (IQR 0–381.3), respectively; there were no statistically significant differences observed ($p = 0.58$). We found an excellent correlation for Agatston scores derived from the two different protocols with a Pearson's correlation coefficient of $r = 0.99$. The dose-length-product was 30.3 ± 12.4 mGy × cm using the ATVS protocol and 32.2 ± 11.7 mGy × cm using the standard 120 kVp protocol, resulting in a significantly lower effective radiation dose (0.42 ± 0.17 mSv vs. 0.45 ± 0.16 mSv) ($p < 0.001$). Additionally, 90% of all patients were classified into the same risk categories (0, 1–10, 11–100, 101–400, or > 400) by the two different protocols.

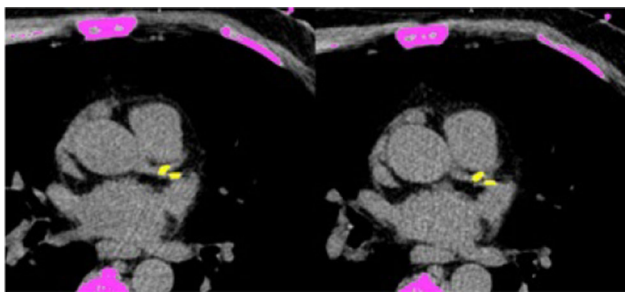

57-year-old man with a BMI of 24.2 kg/m2 who underwent CACS. Images were acquired using the standard 120 kVp (left image) and a 100 kVp (right image) protocol. The corresponding Agatston scores were 360.6 (120 kVp) and 367.3 (100 kVp).

Conclusion ATVS-based CACS using a kVp-independent kernel allows for a high accuracy of Agatston calcium scoring compared to the standard 120 kVp scanning. Additionally, radiation dose parameters were significantly reduced using the ATVS-based protocol.

Accuracy of Cardiac Magnetic Resonance T1 Mapping in Patients with Atrial Fibrillation

S. H. Hwang, J. Shim, J.-I. Choi, Y.-H. Kim, Y.-W. Oh, K.-N. Lee; Seoul/KR

Purpose/Objectives Atrial fibrillation (AF) related cardiomyopathy can be quantified by cardiac magnetic resonance (CMR) T1 mapping. However, irregular CMR data acquisition by AF itself may interrupt accurate CMR T1 mapping. Therefore, we evaluated accuracy of CMR T1 map with reference myocardium phantoms in patients with AF.

Methods & Materials This prospective study was approved by institutional review board. All patients gave written informed consent. All 46 patients with AF underwent CMR T1 mapping with non-contrast myocardium phantom (NCM phantom, T1 relaxation time of 1120 ms) and contrast myocardium phantom (CM phantom, T1 relaxation time of 330 ms), and were enrolled in this study. Absolute difference of T1 relaxation time (AdT1, in msec) of every phantom on CMR T1 map was calculated. All phantom T1 maps were divided to 1) accurate map (with AdT1 of $\leq$ 50 ms) and 2) error map (with AdT1 of $>$ 50 ms). Logistic regression analysis was used to investigate variables related to the error map.

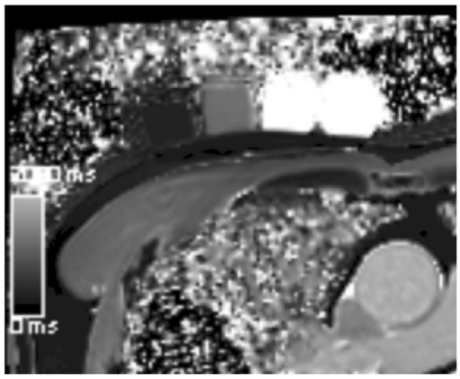

Cardiac magnetic resonance T1 mapping with the myocardium phantoms of different T1 relaxation time.

Results Of all 46 patients, 18 (39.1%) represented AF during CMR T1 mapping. Averages of AdT1 in NCM phantom and CM phantom were 112.8 $\pm$ 68.9 ms (range 0–280.0 ms) and 27.4 $\pm$ 17.3 ms (range 0–55.0 ms), respectively. Of all 92 phantom T1 maps, 52 (56.5%) and 40 (41.6%) were assigned to the accurate map and error map. Adjusting the rhythm status, the NCM phantom was independently associated with the error map (odds ratio 39.1, 98% confidence interval 9.9–153.7, $p < 0.001$).

Conclusion The non-contrast myocardium of high T1 relaxation time was inappropriate in the evaluation of the myocardial remodeling related to AF using CMR T1 mapping.

Prognostic value of dual-energy computed tomography-based iodine quantification versus conventional CT in acute pulmonary embolism: A propensity-match analysis

J. Hur, D. J. Im, Y. J. Suh, Y. J. Hong, H.-J. Lee, Y. J. Kim, K. Han, B. W. Choi; Seoul/KR

Purpose The prognostic value of dual-energy computed tomography (DECT) parameters has not been adequately addressed. The present study investigated whether quantitative DECT parameters have incremental risk stratification benefit over the CT ventricular diameter ratio in patients with acute pulmonary embolism (PE) using propensity score analysis.

Methods & Materials The propensity-matched study was conducted on 480 patients with acute PE who underwent CT pulmonary angiography (CTPA) or DECT pulmonary angiography (DE CT-PA). The primary endpoint was all cause death within 30 days. Cox proportional hazards regression model was used to identify associations between CT parameters and outcomes and to identify potential predictors. Concordance (C) statistics were used to compare the predictive prognosis between two groups.

Results The propensity-matched study population included 240 patients with acute PE in the CTPA group and 240 patients with acute PE in the DECT group. A total of 260 (54.1%) patients were men, and the mean age was 64.9 years (64.9 $\pm$ 13.5). In both groups (CTPA and DECT groups), VD ratio ($\geq$ 1) was associated with an increased risk of all cause death within 30 days (hazards ratio (HR): 3.707, $p < 0.001$ and 6.847, $p < 0.001$, respectively). However, C-statistics showed no statistically significant difference between the CTPA group and the DECT group for predicting death within 30 days (C-statistics: 0.756 vs. 0.832, $p = 0.097$).

Conclusion Quantitative measurement of lung perfusion defect volume by DECT had no added benefit over CT ventricular diameter ratio for predicting all-cause death within 30 days.

Automatic Segmentation of left and right atrium on long-axis cardiac MRI views using neural networks

C. Anastasopoulos[1], C. R. Rutigliano[1], S. Yang[1], A. Abdulkadir[2], T. Akinci D'antonoli[1], B. Stieltjes[1], A. W. Sauter[1], J. Bremerich[1], G. Sommer[1]; [1]Basel/CH, [2]Berne/CH

Purpose/Objectives Deep learning algorithms have proven valuable for cardiac MRI post-processing, especially for ventricle and atrial 3D-segmentations on SSFP stacks. The left and right atrium (LA and RA), however, are usually covered only in 2D and so their volumes are estimated from manual measurements on 4- and 2-chamber (4ch and 2ch) views using the biplane method of area & length. Although it tends to underestimate atrial volumes compared to the Simpson's method on short-axis stacks, it is still frequently used. To get around the time-consuming and error-prone task of manual segmentation, we trained neural networks in identifying atrial borders on a dataset of long-axis cines.

Methods & Materials Both 4ch and 2ch cines of 240 subjects with various cardiac diseases were retrospectively assessed. Segmentation was performed by three radiologists in training, with experience of 3, 3 and 1 year in cardiothoracic imaging, respectively. Images acquired before opening of the atrioventricular valves were visually chosen. Three masks were drawn on the resulting 2D-images: LA and RA on the 4ch- and LA on the 2ch-image, excluding the pulmonary veins. Neural networks were separately trained with 200 images for each mask. A 3D U-Net architecture with two spatial dimensions was implemented using NiftyNet. The inference was applied on 40 datasets. Overlap between ground-truth and prediction was quantitatively evaluated with relative difference (prediction minus ground-truth divided by ground-truth) and Dice-coefficient.

Results The location of the LA was correctly predicted in all 40 test cases in both views. The relative difference between predicted and ground-truth mask was small: median of 0.9% (25. and 75. quartiles: $-$ 2.0% and 4.6%) in 4ch and 0.7% (quartiles: $-$ 4.9% and 3.3%) in 2ch-view, with median Dice-coefficients of 95.8% and 94.8%, respectively. The location of the RA in 4ch was also correctly predicted in all 40 cases. The masks were slightly overestimated with relative differences of 5.7% (quartiles: 2.2% and 7.8%) and a median Dice-coefficient of 95.3%.

Conclusion We were able to demonstrate that both atria can be identified fully automatically on the long-axis views by 2D neural networks. The segmentation algorithms were trained on a relatively small dataset of 200 images each, but nevertheless segmented left and right atrium on long-axis views in all test cases reliably. Further steps

will include a similar training on phases of the atrium other than end-diastole, which could provide segmentations and volumetric calculations over the whole cardiac cycle.

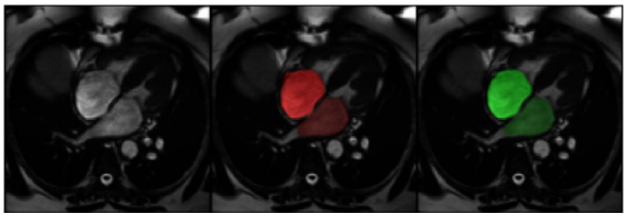

Example of atrial segmentation. Left: 4-chamber view in atrial end-diastole. Middle: manual segmentation of left and right atrium. Right: automatic segmentation with U-Net

Novel attempt to characterize the left atrium of patients with atrial fibrillation referred for catheter ablation using cine MRI

M. Pradella, S. Knecht, M. Moor, S. Osswald, M. Kühne, C. Sticherling, B. Stieltjes, J. Bremerich; Basel/CH

Purpose Anatomical and functional changes of the left atrium (LA) occur with the progression of atrial fibrillation (AF) which affects outcome of catheter ablation.
In this study, we evaluated a novel approach to characterize left atrial function based on cine magnetic resonance imaging (MRI) in patients undergoing catheter ablation.
Methods & Materials 44 patients referred for catheter ablation of AF were retrospectively analysed. All patients underwent preinterventional MRI on a 1.5T scanner (Magnetom, Siemens Healthineers, Germany). A steady-state free precision cine sequence in transversal orientation covering the whole heart (slice thickness 6 mm) was acquired. Temporal resolution was 40 ms.
First, the LA was segmented on each slice and time point using the freely-available Segment software version 2.2 R6435 (http://segment.heiberg.se, Figure 1). Pulmonary veins and appendage were excluded.
Second, an ellipsoid was fitted into the segmented contours of the LA using a custom-written algorithm (Matlab, Mathworks, USA, Figure 2). Thereby, main axis diameter, volume, surface area, sphericity and their respective rates (delta over time) were be evaluated. The beginning of the left atrial contraction phase was defined as pre-atrial contraction (V_pre, Fig. 3).
Minimum follow up was 12 months after the last procedure and a maximum of two ablations.

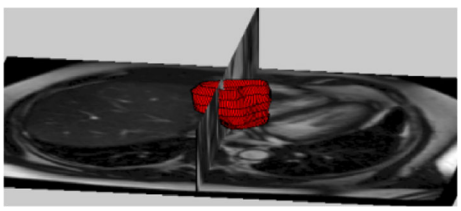

Figure 1 Contours of segmented LA

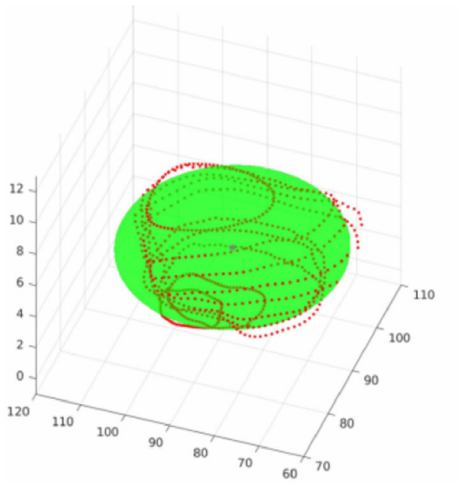

Figure 2 Fitted ellipsoid within point cloud of segmented LA

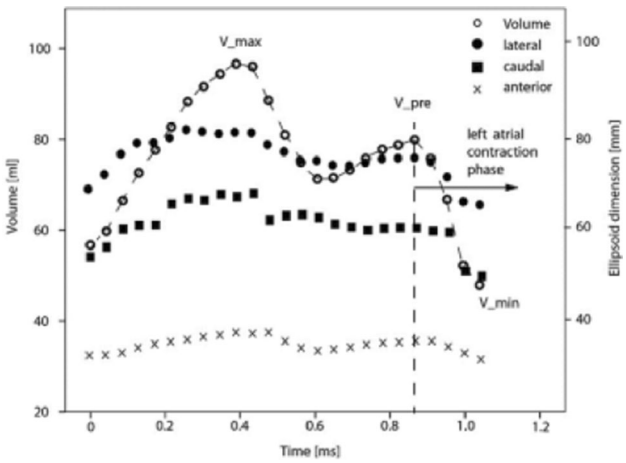

Figure 3 Plot of volume and main axis diameter of the ellipsoid over time with a distinct left atrial contraction phase in one patient

Results Baseline characteristics: mean age 64.3 ± 9.1 year, BMI 26.3 ± 3.8 kg/m^2 and 31.8% were females. There was a high correlation between segmentation volumes and volumes of the fitted ellipsoid (Pearson > 0.95, p < 0.001).
After a follow-up of 12 months, 12 out of 44 patients presented with recurrence of AF (27.3%). Patients with recurrence showed higher maximal und minimal indexed volumes (60.5 ± 8.2 vs. 51.4 ± 13.9 ml/m^2, p = 0.011 and 35.8 ± 11.7 vs. 29.2 ± 12.0 ml/m^2, p = 0.035 respectively), a larger lateral diameter (41.5 ± 3.2 mm vs. 37.4 ± 5.0 mm, p = 0.033) and greater surface area (110 ± 10 vs. 97 ± 22 cm^2, p = 0.025) at pre-atrial contraction.
Multivariable logistic regression (corrected for age, BMI and sex) revealed the lateral diameter at pre-atrial contraction (in mm) as the only independent predictor for AF recurrence (OR 1.331; 95% CI 1.048–1.690, p = 0.019).
Conclusion A fitted ellipsoid is a feasible and valuable substitute of the LA. Thereby, the lateral diameter at pre-atrial contraction is most likely representing the remodelling of the anterior and posterior walls

of the LA which could be a novel predictor for recurrence of AF after ablation.

The efficacy of iterative model-based reconstruction on coronary CT angiography for plaque quantification

J. Y. Yoo[1], E. J. Chun[2], J. M. Lee[3]; [1]Cheongju-si/KR, [2]Seongnam-Si/KR, [3]Seongnam-Si, Gyeonggi-Do, 463-707,Korea/KR

Purpose/Objectives To evaluate the efficacy of iterative model-based reconstruction (IMR) for assessment of plaque volume (*Pvol*) and burden (*Pbur*) on coronary CT angiography (CCTA) compared with intravascular ultrasound (IVUS) according to the plaque types.
Methods & Materials We prospectively enrolled 18 patients (64.1 ± 10.3 years, 15 males) with significant coronary artery disease who underwent CCTA and transferred to IVUS. CCTA images were reconstructed with filtered back projection (FBP), hybrid iterative reconstruction (iDose[4]) and IMR. Two independent observers assessed plaque types (calcified, mixed, non-calcified) and semi-automatically quantified *Pvol* and *Pbur* with commercially available software. We compared the *Pvol* and *Pbur* of CCTA datasets reconstructed with FBP, iDose[4] and IMR with those derived from IVUS using Spearman's rank correlation (r). We also evaluated whether these agreements are different depends on plaque types.
Results A total of 56 plaque lesions (27 calcified, 15 mixed and 14 non-calcified plaques) were analyzed. Inter-observer reproducibility of *Pvol* and *Pbur* using IMR were higher than those of iDOSE and FBP regardless of plaque types. As compared to IVUS, CCTA tends to underestimate *Pvol*, while overestimate *Pbur* through all reconstruction algorithms. When using IMR, the CCTA-IVUS agreement for *Pvol* and *Pbur* was increased than those using FBP or iDose[4]. According to plaque types, IMR significantly improves agreement with IVUS for *Pbur* in mixed plaque than FBP (r = 0.73 vs. 0.31) or iDose4 (r = 0.41), and also improves agreement in noncalcified plaque than FBP (r = 0.72 vs. 0.56) (all $p < 0.05$). While, calcified plaque quantification is all excellent regardless of reconstruction algorithm (IMR vs. iDose4 vs. FBP, r = 0.96 vs. 0.90 vs.0.86).
Conclusion Compared to FBP or iDose4, IMR can significantly improve agreement with IVUS for *Pbur* in noncalcified and mixed plaque.

Leaflet Thrombosis and Subvalvular Tissue Ingrowth After Transcatheter Aortic Valve Replacement: Computed Tomography Features

H. J. J. Koo, J. Choi, J.-W. Kang, D. H. Yang; Seoul/KR

Purpose/Objectives This study evaluated post-transcatheter aortic valve replacement (TAVR) findings such as leaflet thrombosis and structural valve degeneration using cardiac computed tomography (CT).
Methods & Materials 138 patients with post-TAVR CT scans were included. The median duration from the TAVR to CT scans was 17.5 (3–390.8) days. Post-TAVR CT findings such as subvalvular tissue ingrowth, hypoattenuating leaflet thickening (HALT), native valve thrombosis, and leaflet opening limitation were retrospectively reviewed. Clinical and CT findings were compared between patients with HALT and those without HALT. The relationships between the implant duration and echocardiography parameters or CT findings were compared. Logistic regression analysis was performed to determine the factors associated with the HALT.
Results HALT and leaflet motion limitation were found in 25 (18%) and 20 (14%) of the patients, respectively. Subvalvular tissue ingrowth was noted in 32 (23%) patients. The implant duration [odds ratio (OR), 1.5; $p < 0.001$], hypertension (OR, 0.2; $p = 0.03$), and subvalvular tissue ingrowth (OR, 4.9; $p = 0.003$) were associated with the HALT. Native valve thrombosis was detected in five (4%) patients. Subvalvular pannus was diagnosed in two patients. Transaortic peak velocity and peak pressure gradient ($r = 0.20$, $p = 0.02$) were increased relative to the implant duration. The implant durations were longer in patients with subvalvular tissue ingrowth ($p = 0.003$), HALT ($p = 0.01$) or leaflet motion limitation ($p = 0.006$) compared to the patients without those findings.
Conclusion Implant duration, hypertension, and subvalvular tissue ingrowth are associated with the presence of HALT. The implant durations were longer in patients with subvalvular tissue ingrowth, HALT or leaflet motion limitation.

Cardiac CT for the measurement of right ventricular volume and function in comparison with cardiac MRI: a meta-analysis

J. Y. Kim[1], Y. J. Suh[2], K. Han[2]; [1]Daegu/KR, [2]Seoul/KR

Purpose/Objectives To meta-analytically compare the accuracy of cardiac computed tomography (CT) in the assessment right ventricular (RV) volume and functional parameters with cardiac magnetic resonance imaging (CMRI).
Methods & Materials PubMed, EMBASE and Cochrane library were systematically searched for studies which compared CT with CMRI as standard reference in terms of measurement of RV volume and function; end-diastolic volume (EDV), end-systolic volume (ESV), stroke volume (SV), or ejection fraction (EF). Meta-analytic methods was utilized to determine the pooled bias (mean weighted difference), limits of agreement (LOA), and correlation coefficient (r) between CT and CMRI.
Results Nineteen studies (757 patients) that compared CT and CMRI for RV measurements were included. Pooed bias was 3.0 mL for EDV, 3.7 ml for ESV, − 0.39 ml for SV, and − 2.1% for EF. Pooled LOA was − 5.7 to 11.7 ml for EDV, − 3.9 to 11.3 ml for ESV, − 5.7 to 4.9 ml for SV, and − 6.5 to 2.3% for EF. Pooled correlation coefficients were strong for all RV parameters (r = 0.94, 95% confidence interval [CI] 0.9–0.96 for EDV; r = 0.93, 95% CI 0.9–0.96 for ESV; r = 0.89, 95% CI 0.82–0.93 for SV; and r = 0.87, 95% CI 0.82–0.93 for EF).
Conclusion CT is accurate for the measurement of RV volume and function parameters, with acceptable range of bias and LOA, and strong correlation with CMRI.

Prevalence and pattern of cardiac injury identified by late gadolinium-enhancement of cardiac magnetic resonance image in acute moderate to severe CO poisoning

W. Kwon, J. Lee; Wonju/KR

Purpose/Objectives Myocardial injury is a frequent consequence of moderate to severe carbon monoxide (CO) poisoning. In addition, long-term mortality is significantly higher in patients who experienced myocardial injury than patients without myocardial injury. No studies have investigated myocardial injury due to carbon monoxide

poisoning through cardiac magnetic resonance image (CMR). We want to know whether there are actually cardiac muscle changes identified by late gadolinium-enhancement (LGE) in CMR in acute phase after acute CO poisoning.
Methods & Materials This prospective observational study collected data from consecutive patients who were diagnosed with acute CO poisoning and myocardial injury, defined as elevated high-sensitivity TnI (hs-TnI) level above the upper limit, at the ED between August 2017 and February 2019. CMR was performed to evaluate cardiac muscle changes identified by LGE. Patients with coronary artery disease were excluded. We classified the location of myocardial injury into 4 categories (subepicardium, mesocardium, subendocardium, and transmural) and examined the distribution of injured myocardium.
Results Seventy-five patients were included. Fifteen patients (20.0%) had cardiac injury identified by LGE in CMR. The territory of left anterior descending artery (LAD) (7 patients, 46.7%) was the most common distribution in patients with positive LGE. Patients with LAD territory pattern all showed damage to the subendocardial area. In addition, mesocardium (6 patients, 40.0%) was second common site in patients with positive LGE and there was no transmural damage. Two patients with damage to the subepicardial area also showed in the RCA territory pattern. One patient had global damage distribution, defined as including distribution of all three coronary artery (LAD, left circumflex artery, and right coronary artery). Male sex was significantly more in the positive LGE group than in the negative LGE group ($p = 0.011$). Decreased initial mental status was significantly more in the positive LGE group than in the negative LGE group ($p = 0.006$).
Conclusion Cardiac injury identified by LGE of cardiac MRI was found in 15 patients (20.0%) in acute moderate to severe CO poisoning with elevated hs-TnI.

Deep learning-based automatic analysis of cardiovascular borders on frontal chest radiograph

C. Kim, G. Lee, H. S. Yong, N. Kim, J. Lee, E. J. Chun, D. H. Yang; Seoul/KR

Purpose/Objectives To develop and validate a deep learning-based automatic cardiovascular border (CB) analysis on frontal chest radiograph (CXR) for diagnosing cardiovascular disease quantitatively.
Methods & Materials Artificial intelligence (AI) based automatic CB drawing (CB-AI) algorithm was developed by using 1209 CXR and validated in 1182 CXR (one internal dataset 402 CXR; two external validation datasets 281 & 499 CXR). All subjects performed echocardiography and 49% have valvular heart disease. Using CBs drawn by experienced technician (CB-human) and AI (CB-AI), following cardiovascular indices of CXR were calculated: cardiothoracic (CT) ratio, cardiac area, and widths of aortic knob/pulmonary conus/left atrial appendage (LAA)/right lower CB/left lower CB/descending aorta. The absolute percentage measurement error (APE) was calculated between indices by CB-AI and CB-human. All cardiovascular indices on CXR were correlated with quantitative parameters (i.e. left ventricular [LV] dimension, LV volume, and LV ejection fraction) from the echocardiography.
Results The mean APEs of CT ratio between CB-AI and CB-human is very small in all datasets (2.3% from the internal dataset; 3.4% and 3.6% from the external dataset). The mean APEs were 10% or less in all widths of aortic knob, pulmonary conus, left lower CB, right upper CB, right lower CB, and descending aorta. The range of APE in the width of left atrial appendage was wide (7.5% for an internal dataset; 22.9% for an external dataset). There were significant differences in all CXR indices by CB-AI and CB-human between normal control and patients with valvular heart disease ($p < 0.05$). There were significant correlations between all the CXR indices by CB-AI and quantitative echocardiography parameters (r, -0.522 to 0.575, all $p < 0.05$).
Conclusion Deep learning-based automatic measurement algorithm for drawing cardiovascular borders on CXR is feasible. This CB-AI may be new analysis approach of CXR for diagnosing cardiovascular disease quantitatively. Further validation studies using various clinical scenario and population is required.

Cardiac manifestation of peripheral eosinophilia: Assessment with Cardiac MRI and MDCT

J. Y. Yoo[1], E. J. Chun[2], S. I. Choi[2], H. I. Choi[3]; [1]Cheongju-si/KR, [2]Seongnam-Si/KR, [3]Seoul/KR

Purpose This topic presents the various findings of cardiac manifestation in patients with peripheral eosinophilia according to various etiologies and follow-up images using cardiac MRI and MDCT.
Methods & Materials 1. Overview of the eosinophilic heart disease. 2. Etiology and pathophysiology of cardiac involvement with peripheral eosinophilia.
Results Various findings of eosinophilic heart diseases assessed by cardiac MRI including comprehensive review of multisystemic involvement hypereosinophilic syndrome,—Churg-Strauss syndrome,—Eosinophilic leukemia,—Parasite infection Progression of eosinophilic heart diseases using follow-up cardiac MRI according to eosinophil count Differential diagnosis for eosinophilic heart diseases from other cardiac involvement of systemic disease 6. The Potential role of cardiac MRI in patients with eosinophilic heart diseases.
Conclusion Cardiac MRI can demonstrate cardiac manifestation of eosinophilic infiltration including myocarditis, apical obliteration with restrictive pathophysiology or intracardiac thrombus, and can differentiated other infiltrative cardiac diseases. In addition, multidetector CT is helpful for assessment of multi-systemic involvement, besides the cardiac manifestation.
References Ogbogu, P. U., et al. (2007). "Cardiovascular manifestations of hypereosinophilic syndromes." Immunol Allergy Clin North Am 27(3): 457-475. ten Oever, J., et al. (2011). "Cardiac involvement in hypereosinophilic syndrome." Neth J Med 69(5): 240-244. Baumann, S., et al. (2015). "Correlation of cardiac magnetic resonance imaging and histopathology in eosinophilic endomyocarditis." Circ Cardiovasc Imaging 8(1). Kim, N. K., et al. (2015). "A Hypereosinophilic Syndrome with Cardiac Involvement from Thrombotic Stage to Fibrotic Stage." J Cardiovasc Ultrasound 23(2): 100-102. Vandenberghe, P., et al. (2004). "Clinical and molecular features of FIP1L1-PDFGRA (+) chronic eosinophilic leukemias." Leukemia 18(4): 734-742. Lambert, F., et al. (2007). "A case of FIP1L1-PDGFRA-positive chronic eosinophilic leukemia with a rare FIP1L1 breakpoint." J Mol Diagn 9(3): 414-419. Hidron, A., et al. (2010). "Cardiac involvement with parasitic infections." Clin Microbiol Rev 23(2): 324-349. Debl, K., et al. (2008). "Time course of eosinophilic myocarditis visualized by CMR." J Cardiovasc Magn Reson 10: 21. Baumann, S., et al. (2015). "Correlation of cardiac magnetic resonance imaging and histopathology in eosinophilic endomyocarditis." Circ Cardiovasc Imaging 8(1). Seguela, P. E., et al. (2015). "Eosinophilic cardiac disease: Molecular, clinical and imaging aspects." Arch Cardiovasc Dis 108(4): 258-268. Simonnet, B., et al. (2015). "Cardiac involvement in hypereosinophilic syndrome: role of multimodality imaging." Eur Heart J Cardiovasc Imaging 16(2): 228.

Prevalence and pattern of cardiac injury identified by late gadolinium-enhancement of cardiac magnetic resonance image in acute moderate to severe CO poisoning

W. Kwon, J. Lee; Wonju/KR

Purpose Myocardial injury is a frequent consequence of moderate to severe carbon monoxide (CO) poisoning. In addition, long-term mortality is significantly higher in patients who experienced myocardial injury than patients without myocardial injury. No studies have investigated myocardial injury due to carbon monoxide poisoning through cardiac magnetic resonance image (CMR). We want to know whether there are actually cardiac muscle changes identified by late gadolinium-enhancement (LGE) in CMR in acute phase after acute CO poisoning.
Methods & Materials This prospective observational study collected data from consecutive patients who were diagnosed with acute CO poisoning and myocardial injury, defined as elevated high-sensitivity TnI (hs-TnI) level above the upper limit, at the ED between August 2017 and February 2019. CMR was performed to evaluate cardiac muscle changes identified by LGE. Patients with coronary artery disease were excluded. We classified the location of myocardial injury into 4 categories (subepicardium, mesocardium, subendocardium, and transmural) and examined the distribution of injured myocardium.
Results Seventy-five patients were included. Fifteen patients (20.0%) had cardiac injury identified by LGE in CMR. The territory of left anterior descending artery (LAD) (7 patients, 46.7%) was the most common distribution in patients with positive LGE. Patients with LAD territory pattern all showed damage to the subendocardial area. In addition, mesocardium (6 patients, 40.0%) was second common site in patients with positive LGE and there was no transmural damage. Two patients with damage to the subepicardial area also showed in the RCA territory pattern. One patient had global damage distribution, defined as including distribution of all three coronary artery (LAD, left circumflex artery, and right coronary artery). Male sex was significantly more in the positive LGE group than in the negative LGE group ($p = 0.011$). Decreased initial mental status was significantly more in the positive LGE group than in the negative LGE group ($p = 0.006$).
Conclusion Cardiac injury identified by LGE of cardiac MRI was found in 15 patients (20.0%) in acute moderate to severe CO poisoning with elevated hs-TnI.
References Acute myocardial injury from carbon monoxide poisoning by cardiac magnetic resonance imaging. Bennet George B, Ruiz-Rodriguez E, Campbell CL, Leung SW, Sorrell VL. European Heart Journal - Cardiovascular Imaging 2014;15:466 Myocardial fibrosis from severe carbon monoxide poisoning detected by cardiac magnetic resonance imaging. Henry TD, Lesser JR, Satran D. Circulation. 2008;118(7):792.

Incremental Value of Three-Dimensional Printing in Preoperative Planning of Complex Congenital Heart Disease: Single Center Experience

D. H. Yang[1], J. A. Kim[2], S.-H. Park[1], N. Kim[1], T.-J. Yun[1]; [1]Seoul/KR, [2]Goyang/KP

Purpose/Objectives To evaluate an incremental value of three-dimensional (3D) printing in preoperative planning of complex congenital heart disease (CHD) over conventional imaging-based approach.
Methods & Materials Forty patients (median age 8.6 months [range 3 days–59 years]; median body weight 7.5 kg) with complex CHD who underwent both conventional imaging approach and the patient-specific 3D printing were analyzed retrospectively. The 3D printing was performed when the surgical planning (e.g., biventricular repair vs. single ventricular palliation) was unclear even after reviewing conventional imaging modalities in the heart team conference. The surgical strategy was categorized into corrective, equivocally corrective, equivocally palliative, and palliative. Using cardiac computed tomography image, two types of 3D printings were generated: cast models of the blood pool and endocardial wall model. The endocardial wall model with flexible materials allows the detailed evaluation of intracardiac structures (e.g., ventricular septal defect [VSD], papillary muscle, and great vessels). The surgical strategy before and after the use of 3D printing was evaluated.
Results Double outlet right ventricle (DORV) with VSD was the most common indication of 3D printing (30/40, 75%) in our institution, followed by transposition of the great artery with VSD (4/40, 10%) and interrupted aortic arch with VSD (2/40, 5%). Among DORV, remote VSD was the most common type(18/30, 60%). Corrective surgery (e.g., total correction or one and half correction) was performed in 31 (78%), and 9 (22%) patients underwent palliative surgery (e.g., Fontan operation). Before 3D printing, the surgical strategy of 26 (65%) patients was equivocally corrective. Among14 (35%) patients categorized into equivocally palliative before 3D printing, the surgical strategy of 5 (36%) patients were changed to corrective or equivocally corrective. All of these patients underwent corrective surgery based on the information from 3D printing. Mean cost for 3D printing was 1297 USD.
Conclusion In patients with complex CHD, 3D printing may change surgical strategy from palliative to corrective surgery. In patients with an unclear conclusion of surgical strategy using conventional imaging approach, the 3D printing would be a useful complementary tool.

Coronary-to-pulmonary artery fistula in adults: Natural clinical history and management strategies

J. I. Jung[1], S. J. Hong[2], H. Kim[1]; [1]Seoul/KR, [2]Guri-si/KR

Purpose/Objectives To evaluate the natural history of coronary-to-pulmonary artery fistula (CPAF) detected on coronary CT angiography (CCTA) and propose potential treatment strategies.
Methods & Materials We conducted a retrospective multicenter study in 168 CPAF patients collected by review of CCTA reports. Thirty-seven patients were excluded because they had less than 2 years of the follow-up period. Finally, 131 patients were included. Data regarding demographics and clinical history were obtained by reviewing electronic medical records. The treatment administered after the diagnosis of CPAF and the occurrence of major adverse cardiac events (MACE) during the follow-up period were investigated. We analyzed the morphological features of CPAF and evaluated the association between fistula size and surgical ligation. Patients who underwent follow-up CCTA after the CPAF diagnosis were assessed for the morphological change and time interval between diagnosis and last follow-up imaging.

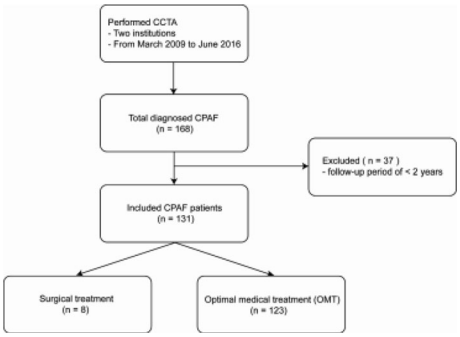

Flow chart of patient inclusion and exclusion.

Results The median age of the study population was 63 years (57–72), and the median follow-up period was 5.72 years (4.08–6.96). There were 65 men and 66 women. Eight patients underwent surgery and 123 (93.9%) patients were observed with optimal medical treatment (OMT). The most common origin of the CPAF was both coronary arteries, with 76 (58.0%) cases. Aneurysm was present in 41 (31.3%) cases. Fifty-four (41.2%) fistulas were less than 2 mm in size. The fistula size (OR 1.120) significantly associated with surgical treatment ($p = 0.028$). Only one patient in the observed with OMT group reported MACE during the follow-up period due to pre-existing coronary artery disease. Twenty-eight patients (21.3%) underwent follow-up CCTA after CPAF diagnosis with 3.81 years of the median time interval. There was no morphological change of CPAF.

Conclusion Most CPAFs detected by CCTA are usually benign prognosis and OMT is sufficient. Continued symptoms and fistula size are possible determinants for surgical treatment.

Comparison of cardiac strain parameters between echocardiography and cardiac magnetic resonance in high-level endurance athletes

Y. Menger[1], E. Janssen[1], M. Heideman[1], M. Saddiqa[1], B. Vande Berg[2], J. Bogaert[3], H. Heidbuchel[4], M. D. M. Claeys[3], M. P. D. R. Willems[3], M. D. K. Lefebvre[1], M. P. D. A. La Gerche[5], M. D. L. Herbots[1], M. D. G. Claessen[3], O. Ghekiere[1]; [1]Hasselt/BE, [2]Leuven, BE/BE, [3]Leuven/BE, [4]Antwerp/BE, [5]Melbourne/AU

Purpose The heart of high-level endurance athletes undergoes substantial structural changes in response to volume overload and increased wall stress. These structural changes are accompanied by changes in both left (LV) and right (RV) ventricular strain. The current standard to evaluate cardiac strains is speckle tracking echocardiography (STE), but cardiac magnetic resonance (CMR) could provide a feasible alternative. The aim of this study is to compare strain measurements between CMR and STE in high-level endurance athletes.

Methods & Materials 43 professional cyclists underwent echocardiography and CMR imaging at rest, as part of the Pro@Heart study. CMR images were acquired in short axis, 2-,3- and 4-chamber views from steady-state free precession (SSFP) sequences on a 1.5T system. Five volunteers were excluded based on gender and software issues. A non-rigid elastic CMR algorithm was used to calculate LV global longitudinal strain (GLS), global circumferential strain (GCS) and global radial strain (GRS), and RV free wall longitudinal strain (RV LS) in 38 male elite cyclists. The strain values on CMR were compared to with STE, using EchoPACS software.

Statistical analysis was performed using linear regression and Bland–Altman analysis.

Results Mean values for STE were more negative than CMR in LV GLS (-18.13 ± 1.89 for STE vs. -12.85 ± 1.79 for CMR), GCS (-20.25 ± 2.52 vs. -15.96 ± 2.31) and RV GLS (-20.49 ± 6.74 vs. -13.78 ± 2.71) and was more positive in GRS (45.25 ± 11.73 vs. 32.90 ± 6.28). Linear regression did not reveal any significant correlation between STE and CMR analysis for neither LV GLS, GCS, GRS or RV GLS. Bland–Altman plots showed a systematic bias between STE and CMR for LV GLS (mean bias 5.28%, limits of agreement $+1$ to $+9$%), for GCS (mean bias 4.30%, limits of agreement -1 to $+10$%), for GRS (mean bias -12.36%, limits of agreement $+10$ to -35%) and for RV GLS (mean bias 6.71%, limits of agreement $+20$ to -7%), respectively.

Conclusion No significant correlation was found between CMR and STE for LV and RV strain parameters in high-level endurance athletes. Therefore, both imaging modalities cannot be used interchangeably for strain analyses in this study population.

References none.

Clinical value of dark-blood late gadolinium enhancement without additional magnetization preparation

R. J. Holtackers[1], C. M. van de Heyning[2], M. S. Nazir[3], I. Rashid[3], I. Ntalas[3], H. Rahman[3], R. Botnar[3], A. Chiribiri[3]; [1]Maastricht/NL, [2]Antwerp/BE, [3]London/UK

Purpose/Objectives For two decades, bright-blood LGE MRI has been considered the reference standard for the non-invasive assessment of myocardial viability. While bright-blood LGE can clearly distinguish between areas of myocardial infarction and viable myocardium, it often suffers from poor scar-to-blood contrast, making subendocardial scar patterns difficult to detect. Recently, we proposed a novel dark-blood LGE approach that increases scar-to-blood contrast and thereby improves subendocardial scar conspicuity (Figure 1). In the present study we sought to assess the clinical value of this novel approach in a large patient cohort with various non-congenital ischemic and non-ischemic cardiomyopathies on both 1.5T and 3T scanners of different vendors.

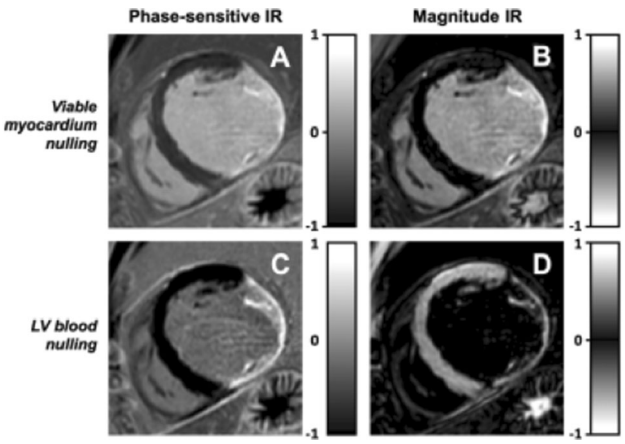

Phase-sensitive inversion-recovery (PSIR) and magnitude IR LGE images with routine myocardium nulling and proposed blood nulling. Image c illustrates the increased scar-to-blood contrast when combining PSIR with a blood nulling inversion time

Methods & Materials 300 consecutive patients referred for clinical CMR were included and randomly assigned to a 1.5T or 3T scanner.

An entire short-axis stack and multiple long-axis views were acquired using conventional phase-sensitive inversion-recovery (PSIR) LGE with TI set to null myocardium (bright-blood) and proposed PSIR LGE with TI set to null blood (dark-blood), in a randomized order. The bright-blood LGE and dark-blood LGE images were separated, anonymized, and interpreted in a random order at different time points by one of five independent observers. Each case was analyzed for the type of scar, per-segment transmurality, papillary muscle enhancement, overall image quality, observer confidence, and presence of right-ventricular scar and intraventricular thrombus.

Results Dark-blood LGE detected significantly more cases with ischemic scar compared to conventional bright-blood LGE (97 vs. 89, $p = 0.008$, Figures 2 and 3), on both 1.5T and 3T, and led to a significantly increased total scar burden (3.3 ± 2.4 vs. 3.0 ± 2.3 standard AHA segments, $p = 0.015$). Overall image quality significantly improved using dark-blood LGE compared to bright-blood LGE (81.3% vs. 74.0% of all segments were of highest diagnostic quality, $p = 0.006$). Furthermore, dark-blood LGE led to significantly higher observer confidence (confident in 84.2% vs. 78.4%, $p = 0.033$).

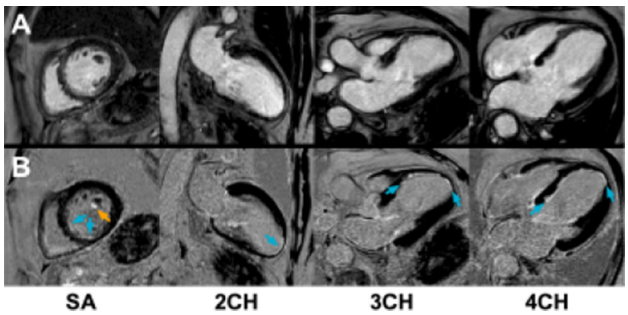

Bright-blood (A) and dark-blood (B) LGE images of a subject with subendocardial infarction, in which only dark-blood LGE was able to define accurate degrees of scar transmurality (blue arrows) and to reveal papillary muscle enhancement (orange arrow).

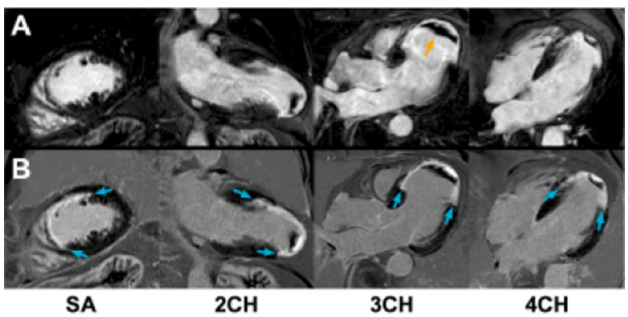

Although myocardial infarction (blue) and thrombus (orange) was clearly seen by both LGE methods in this case, the transmural extent was challenging to assess on the bright-blood LGE images (A) due to poor definition of the border between scar and blood.

Conclusion This study shows that dark-blood LGE is more sensitive than conventional bright-blood LGE in the detection of ischemic scar, regardless of the field strength or scanner vendor, with higher average scar burden, increased overall image quality, and improved observer confidence. These findings make the proposed dark-blood LGE method a viable alternative to conventional LGE. The applicability in routine clinical practice is further strengthened as the proposed dark-blood LGE approach, in contrast to other recently proposed dark- and black-blood techniques, is readily available and does not require any scanner adjustments and/or extensive parameter optimisations.

Compressed sensing 4D flow MRI for the assessment of the left ventricular stroke volume

B. Longere[1], G. Braye[1], J. Pagniez[1], V. Silvestri[1], A. Simeone[1], K. Kasprzak[1], A. Monnet[2], F. Pontana[1]; [1]Lille/FR, [2]Erlangen/DE

Purpose To evaluate the reliability of a compressed sensing prototype free-breathing 4D flow MRI sequence (CS4DF, Siemens Healthineers) for the measurement of the aortic forward volume.

Methods & Materials 15 adult patients (10 males, 5 females; mean age = 50 ± 19.4 y/o) referred for cardiac magnetic resonance (CMR) examination were enrolled. Patients suffering from mitral regurgitation or intracardiac shunt were excluded. The CMR protocol included at least (a) segmented steady-state free precession cine sequences for the assessment of the left ventricular stroke volume (SV), (b) a 2D phase-contrast magnetic resonance imaging (PC-MRI) for direct measurement of the aortic forward volume (AFV_{2D}) and (c) the prototype free-breathing CS4DF sequence. Semi-automated segmentation of cine and PC-MRI images was performed on a clinical workstation. A dedicated software was used for CS4DF post-processing and aortic forward volume measurement (AFV_{CS}). Volumes provided by the three methods were compared using an analysis of variance (ANOVA) and linear regression.

Results The CS4DF sequence mean scan time was $4'10'' \pm 50.4$ s. A mean SV of 96.3 ± 28.4 ml was provided by cine segmentation, mean AFV_{2D} was 95.3 ± 27.3 ml with PC-MRI and mean AFV_{CS} was 93.0 ± 27.2 ml using CS4DF. The one-way ANOVA showed non-significant differences between the three methods ($p = 0.944$). Linear regressions demonstrated strong correlations of AFV_{CS} with AFV_{2D} ($R^2 = 0.89$) and with SV ($R^2 = 0.87$).

Conclusion C4D flow MRI acceleration by compressed sensing does not compromise the reliability of aortic forward volume measurement and may facilitate further works in the field of aorta hemodynamics.

Retro-gated compressed sensing cine imaging for assessment of ventricular functions, volumes and mass

B. Longere, L. Grenier, J. Pagniez, V. Silvestri, A. Simeone, K. Kasprzak, F. Pontana; Lille/FR

Purpose To evaluate the accuracy of a 2D retro-gated compressed sensing (CS) prototype cine sequence for quantification of left (LV) and right ventricular (RV) functions, volumes and mass in clinical routine.

Methods & Materials 20 adult patients (14 males, 6 females; mean age = 47 ± 21.8 y/o) referred for cardiac magnetic resonance (CMR) examination were prospectively enrolled. Grown-up congenital heart disease patients were excluded. Each patient underwent CMR protocol including at least a short-axis stack, one vertical and one horizontal 2-chamber slices using (a) a conventional multi-breath-hold steady-state free precession acquisition (bSSFP) as reference (b) a CS real-time (CSrt) single-breath-hold sequence and (c) the retro-gated CS (CSrg) cine sequence, the latter two providing the same number, position and thickness of slices than the reference technique. Two radiologists independently assessed LV ejection fraction (LVEF), mass (LVM), end-diastolic (LVEDV) and stroke volumes (LVSV) as well as RV ejection fraction (RVEF), end-

diastolic (RVEDV) and stroke volumes (RVSV) for each sequence. Image qualities were compared by edge sharpness measurements.
Results CSrg sequence mean scan time was 58 ± 13.3 s while 24 ± 6.0 s were necessary for CSrt and 523 ± 175.8 s with bSSFP ($p < 0.001$). Analysis of variance did not demonstrate significant difference regarding mean LVEF (bSSFP = 45.7 ± 15.5%, CSrt = 45.3 ± 15.4%, CSrg = 44.9 ± 15.1%; p = 0.991), mean LVEDV (bSSFP = 180.1 ± 57.7 ml, CSrt = 178.6 ± 51.9 ml, CSrg = 175.0 ± 50.7 ml; p = 0.954), mean LVSV (bSFFP = 82.4 ± 29.6 ml, CSrt = 81.4 ± 27.0 ml, CSrg = 78.6 ± 27.8 ml; p = 0.928), mean LVM (bSSFp = 136.1 ± 44.2 g, CSrt = 131.5 ± 46.4 g, CSrg = 126.3 ± 50.4 g; p = 0.825), mean RVEF (bSSFP = 53.2 ± 10.9%, CSrt = 53.0 ± 11.7%, CSrg = 53.0 ± 10.9%; p = 0.998), mean RVEDV (bSSFP = 160.2 ± 51.2 ml, CSrt = 156.3 ± 38.4 ml, CSrg = 154.3 ± 39.2 ml; p = 0.922) and mean RVSV (bSFFP = 83.4 ± 28.1 ml, CSrt = 82.8 ± 26.8 ml, CSrg = 81.8 ± 28.0 ml; p = 0.987). CSrg edge sharpness (0.0782 mm^{-1}) was not significantly different from bSSFP's (0.0718 mm^{-1}; p = 0.131) but higher than CSrt edge sharpness (0.0638 mm^{-1}; p = 0.0006).
Conclusion Retro-gated compressed sensing cine provides in 1 min an accurate assessment of functions and volumes for both left and right ventricles without compromising the sharpness of myocardial boarders, unlike compressed sensing real-time sequence.

Influence of spatial resolution and signal intensity on myocardial strain quantification using feature tracking MRI

F. von Knobelsdorff, T. Schunke, S. Reiter, R. Scheck, B. Höfling, G. Pilz; Agatharied/DE

Purpose Feature tracking is a modern postprocessing algorithm for calculating myocardial strain from cardiac magnetic resonance (CMR) cine images (1). Quantification of myocardial deformation promises to detect myocardial abnormalities early in the course of disease. However, no uniform standards for image acquisition and processing are available. Purpose of the study was analyzing the influence of spatial resolution and signal intensity on myocardial strain results.
Methods & Materials Fifty patients prospectively underwent a standardized CMR exam using a 1.5 Tesla scanner. For feature tracking analysis, steady-state free-precession (SSFP) cine images in long and short axes were acquired in 3 variants: 1. Native standard cine (spatial resolution 1.4 × 1.4 × 8 mm^3). 2. Native cine with lower spatial resolution (2.0 × 2.0 × 8 mm^3). 3. Standard cine equal to variant 1 acquired 5 min after i.v.-administration of 0.2 mmol/kg gadoteracid. All participants were in sinus rhythm, had normal left ventricular ejection fraction, no regional wall motion abnormality and no evidence of fibrosis on Late Gadolinium Enhancement. Using dedicated feature tracking software, circumferential, longitudinal and radial strain were calculated as mean of the six midventricular myocardial segments.
Results Results are summarized in Table 1 and Figure 1. Circumferential and radial strain decreased significantly with higher myocardial signal intensity following Gadolinium administration. Longitudinal strain increased significantly with lower spatial resolution.

Variant of cine acquisition	Longitudinal strain		Circumferential strain		Radial strain	
	Mean ± SD	p-value	Mean ± SD	p-value	Mean ± SD	p-value
1 = Standard	-19.8 ± 3.0	---	-22.3 ± 3.3	---	46.9 ± 12.8	---
2 = Lower spatial resolution	-21.7 ± 3.1	<0.001 *	-22.8 ± 3.4	0.063	48.7 ± 14.2	0.178
3 = After contrast agent administration	-20.0 ± 3.1	0.345	-21.4 ± 3.3	0.001 *	44.4 ± 13.7	0.016 *

Table 1 Summary of the strain results (mean ± standard deviation) for the various acquisition modes (1 = standard, 2 = lower spatial resolution, 3 = after contrast agent administration). The p values stem from paired t tests. SD = standard deviation of the mean. Significant results are highlighted by *

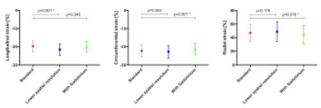

Figure 1 Summary of the strain results (mean ± standard deviation) for the various acquisition modes (standard, lower spatial resolution, after contrast agent administration). p values stem from paired t tests. * = significant results

Conclusion Quantitative myocardial strain results obtained by CMR feature tracking are significantly influenced by variations in spatial resolution and signal intensity. Standardized image acquisition—preferably native cine with sufficient spatial resolution—seems fundamental for reliable and comparable CMR strain analysis.
References (1) Schuster A, Hor KN, Kowallick JT, Beerbaum P, Kutty S. Cardiovascular Magnetic Resonance Myocardial Feature Tracking: Concepts and Clinical Applications. Circ Cardiovasc Imaging. 2016;9(4):e004077.

Effect of nitrates administration before PCI in STEMI patients on CMR feature tracking left ventricular strain at mid term follow up

F. Cilia, C. Calvieri, S. Coco, G. Spano, I. Carbone, N. Galea, M. Francone, C. Catalano; Rome/IT

Purpose CMR-derived myocardial strain has been reported as an useful tool to detect subclinical impairment before LV systolic function deterioration. Furthermore, CMR derived strain has been increasingly used in STEMI patients to assess the efficacy of cardioprotection therapies on clinical end-points. Our aim was to retrospectively evaluate LV remodeling by CMR and the efficacy of nitrates administration before PCI on left ventricular remodelling at three different time points in STEMI patients.
Methods & Materials Forty-two acute STEMI patients, treated by primary percutaneous coronary intervention (PCI) within 12 h after symptoms onset, undergoing CMR in the early post-infarction phase (within 8 days from symptoms onset) between January 2006 and April 2008, were enrolled. STEMI population was divided in two groups on the basis of nitrated administration before PCI.
Results No significant differences were observed in demographic, clinical and angiographic findings between group treated with nitrates and gorup not treated with nitrates. Regarding CMR parameters, as shown in Table 1, a significant reduction of LGE extent as well as an improvement of GRS, GCS and GLS between baseline CMR and CMR at 4–6 months was noted in patients who received nitrates

before PCI. In STEMI patients who received nitrates before PCI, a receiver-operator-characteristics curve analysis identified an area under the curve of 0.864 for GCS difference between acute and intermediate CMR (95% CI 0.684–1.00; p = 0.016) (Fig. 2), determining LV GCS $\geq -9.94\%$ to predict a delta LVESV > 12% with a sensitivity (100%) and specificity (91%).

CMR Parameters (mean, SD)	Total (n=41)	Nitrates Treatment Before PCI (n=25)	Not-Nitrates Treatment Before PCI (n=16)	p Value
LVEDV baseline (ml)	131±36	138±30	134±31	0.713
LVESV baseline (ml)	71±25	70±27	73±23	0.748
LVEF baseline (%)	48±10	50±10	46±9	0.201
LV MASS baseline (g)	120±25	119±25	120±25	0.913
Δ LVEDV Baseline-Intermediate (ml)	6±32	4±26	15±35	0.277
Δ LVESV Baseline-Intermediate (ml)	2±19	1,5±18	2,5±21	0.872
Δ LVEF Baseline-Intermediate (%)	2±6	0,7±6	4±6	0.089
Edema Extent (%)	32±12	33±12	31±14	0.680
Early MVO Extent (%)	4,6±3	4,8±1,8	4,5±4	0.890
Late MVO Extent (%)	3,9±4	2,5±2	5,5±5	0.144
LGE Extent Baseline (%)	21±13	21±12	21±15	0.940
LGE Extent 6 months (%)	14±12	12±13	14±12	0.695
Δ LGE Extent Baseline-Intermediate (%)	-5±11	-11,2±13	-1,7±8	0.014
Δ GRS Baseline-Intermediate (%)	2±7	3,8±8	-0,4±4	0.056
Δ GCS Baseline-Intermediate (%)	-2±3	-2,7±3	-0,7±2	0.044
Δ GLS Baseline-Intermediate (%)	-1±3	-1,1±4	-1±3	0.008

Table 1 .

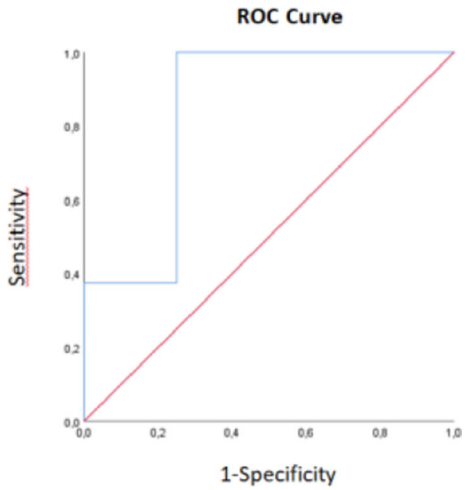

Fig. 2 .

Conclusion In STEMI patients, administration of intravenous nitrates before primary PCI was associated with a greater improvement in LGE extent and in global left ventricular strain at 4 months after PCI. In particular, difference of global circumferential strain between baseline and 4 months CMR seemed to predict LVESV remodelling. Feature-tracking CMR represents a complementary tool to evaluate the benefits of cardioprotective therapies.

Effect of non-significant plaques on first pass myocardial iodine concentration at different injection protocols

S. Boccalini[1], S. A. Si-Mohamed[2], M. Matzuzzi[1], M. Tillier[2], D. C. Rotzinger[3], L. Hanquier[1], L. Boussel[2], D. Revel[1], P. C. Douek[1]; [1]Lyons/FR, [2]Bron/FR, [3]Lausanne/CH

Purpose To compare myocardial iodine distribution at first-pass perfusion imaging between segments subtended by coronary arteries without and with non-significant stenosis at two different contrast injection rates using dual-layer CT (DLCT).

Methods & Materials Between January and July 2018, patients with clinically indicated coronary CT were randomized to undergo spectral coronary DLCT-angiography with different injection protocols. The two protocols were: 35 ml in patients < 80 kg and 0.5 ml/kg in patients > 80 kg (maximum 45 ml) at 2.5 ml/sec (A) or double contrast dose at 5.0 ml/sec (B). Patients with anatomical coronary stenosis > 50% were excluded. Based on the presence of plaques and on the degree of stenosis, coronary arteries (and their subtended segments) of included patients were classified as "without plaques", "stenosis 0–25%", "stenosis 25–50%". For each coronary artery only the plaque determining the highest degree of stenosis was considered. Regions-of-interest were manually drawn on the 16 AHA standard myocardial segments. Iodine concentration was measured on 2-material decomposition (iodine-water) maps in mg/ml. Myocardial iodine values were normalized based on iodine concentration of the left ventricle.

Results 30 patients were included in each of the two groups. In group A, 16 patients had coronary pathology for a total of 22 diseased vessels (19 with a 0–25% stenosis and 3 with a 25–50% stenosis). In group B, 12 patients had 17 diseased vessels with 14 stenosis in the range 0–25% and 3 stenosis in the range 25–50%.

Both group A and B showed significant iodine concentration differences between patients without and with plaques (p < 0.01 and p = 0.04, respectively). In group A, segments subtended by healthy coronary arteries showed significantly higher iodine concentration values than those subtended by vessels with plaques for both normalized and not normalized iodine concentration values (both p < 0.01) (Figure 1). Furthermore, for the same injection protocol, post hoc analysis highlighted a difference between segments subtended by healthy coronaries and both 0–25% and 25–50% stenosis for normalized valued (p < 0.01) (Figure 2). In group B, no difference could be demonstrated for segments vascularized by coronary arteries presenting or not non-significant plaques regardless of normalization (p = 0.6 and p = 0.3) (Figure 3).

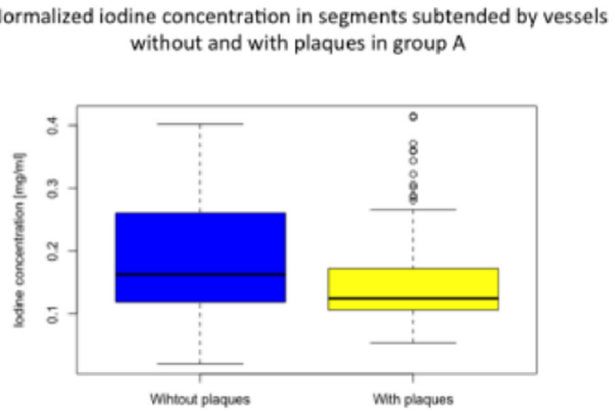

Figure 1 .

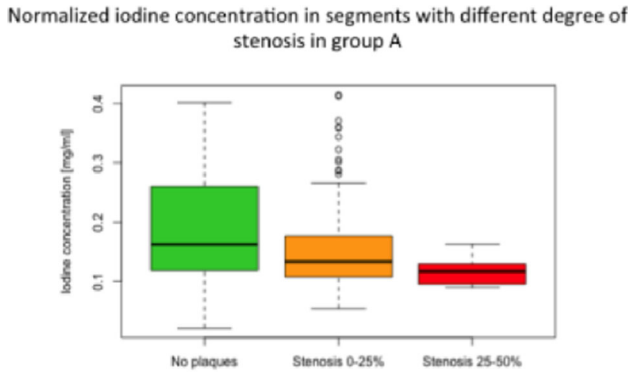

Figure 2 .

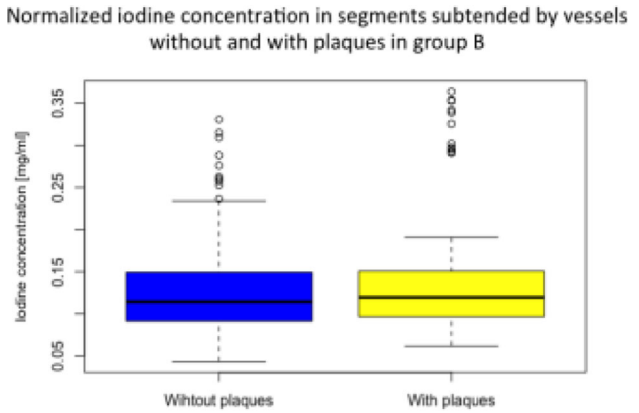

Figure 3 .

Conclusion At lower injection rates and contrast dose, first pass iodine concentration values calculated with spectral CT are significantly different in segments subtended by vessels without any coronary disease and vessels with plaques determining anatomically non-significant stenosis.

Coronary atherosclerosis in apparently healthy master-athletes discovered during pre-participation screening. Role of Coronary CT-Angiography (CCTA)

F. Paciolla[1], G. Rovere[2], G. Savino[2], L. Natale[2], R. Marano[2], R. Manfredi[2]; [1]Rome, RM/IT, [2]Rome/IT

Purpose/Objectives To assess the role of Coronary CT-Angiography (CCTA) and non-invasive detection of coronary atherosclerosis (cATS) in the assessment and clinical management of master athletes (MA) during the pre-participation screening (PPS).
Methods & Materials We retrospectively examined 167 MA who underwent CCTA in our hospital since 2006, analyzing symptoms, stress-test ECG, cardiovascular risk profiles (SCORE) and CCTA findings.
Results Among the whole enrolled population, 153 (91.6%) MA underwent CCTA for equivocal/positive stress-test ECG with/without symptoms, 13 (7.8%) just for clinical symptoms, 1 (0.6%) for the family history. The CCTA showed the presence of cATS in 69 MA (41.3%), congenital coronary anomalies (anomalous origin or deep myocardial bridge) in 8 (4.8%), both in 7 (4.2%). A negative CCTA was observed in 83 MA (49.7%). The risk-SCORE (age, hypertension, hypercholesterolemia, smoking) was a good indicator for the presence of moderate/severe cATS on CCTA. However, mild/moderate cATS was present in 17.8% of MA clinically stratified at a low risk-SCORE.
Conclusion CCTA may be helpful in the PPS of MA with an abnormal stress test ECG and/or clinical symptoms engaged in competitive sports with a high cardiovascular involvement, while the invasive coronary angiography is more indicated in athletes with positive stress-test ECG and high clinical risk. Age, gender, presence of symptoms and clinical risk-SCORE assessment may help sports-physicians/cardiologists to decide whether to request a CCTA or not.

A Missed and Misdiagnosed Case of Pericardial Agenesis

E. Gezmis, C. Altın, E. Ozpelit, E. Ozpelit; Izmir/TR

Purpose To highlight indirect findings of pericardial agenesis, in order to prevent missed and/or misdiagnosis.
Methods & Materials *Introduction:*
Pericardial agenesis is a rare condition which can be complete or partial(1). Patients may either be asymptomatic or present with chest pains, palpitations, dyspnea(2). Herein we present a case of partial pericardial agenesis, which is misdiagnosed with cardiomyopathy, and missed diagnosed.
Case Report:
A 49 years old male referred to our clinic for follow-up of a previous diagnosis of cardiomyopathy. He had been diagnosed based on echocardiography findings at a health check-up 5 years ago. Since than he had been attending follow-ups, during one of which he had underwent cardiac magnetic resonance (CMR). He had no symptoms. Chest X-ray revealed laevorotation of heart (Fig 1). Echocardiography showed laterally displaced left ventricular(LV) apex, and enlarged right ventricle (RV). Coronary computed tomography (CT) angiography revealed leftward displacement of heart with mild RV dilatation. The pericardium was only visible around right atrium (Fig 2). CMR demonstrated mild RV dilatation with reasonable systolic function, and moderate pulmonary valve regurgitation (PR). The absence of pericardium at both left and right sides, except around right atrium, was confirmed, whereas there was no additional finding suggesting cardiomyopathy (Fig 3). The patient was diagnosed with partial pericardial agenesis. The RV enlargement was thought to be due to pericardial agenesis, and associated moderate PR.

Fig. 1 Chest X-ray demonstrating leftward position of the heart

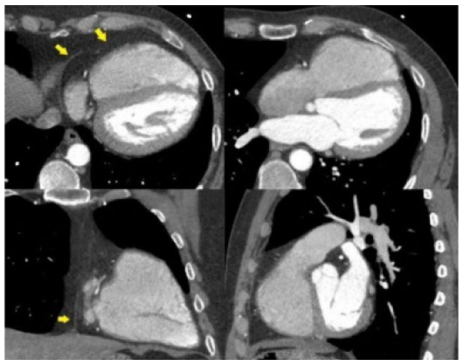

Fig. 2 CCTA revealing pericardial defect at both left and right sides, except around right atrium (arrows)

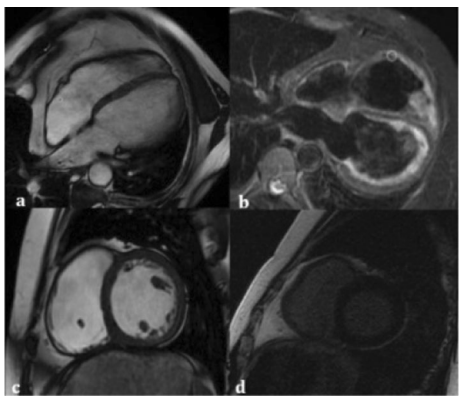

Fig. 3 CMR showing pericard,al agenesis and RV dilatation: (a)4Ch FIESTA, (b)4Ch Triple IR, (c)SA FIESTA, (d)contrast enhanced SA 2D MDE

Results The cross-sectional imaging is largely reliant on detecting the indirect signs for diagnosis of pericardial agenesis. These include laevorotation of heart, interposition of lung tissue, cardiac indentation at the location of defect, excessive motion of left ventricular apex, paradoxic septal motion, hypermobility of the posterior wall (2, 3, 4). Approximately half the cases are associated with RV dilatation(5).
Conclusion Radiologists should be aware of the indirect signs of pericardial agenesis on various imaging modalities.
References 1. Psychidis-Papakyritsis P, De Roos A, Kroft LJ. Functional MRI of congenital absence of the pericardium. AJR Am J Roentgenol. 2007;189(6):W312-4.
2. Gatzoulis MA, Munk M, Merchant N, Van Arsdell GS, McCrindle BW, Webb GD. Isolated congenital absence of the pericardium: clinical presentation, diagnosis and management. Ann Thorac Surg 2000;69:1209–15.
3. Shah AB, Kronzon I. Congenital defects of the pericardium: a review. Eur Heart J Cardiovasc Imaging 2015;16(8):821-7.
4. Scheuermann-Freestone M, Orchard E, Francis J, Petersen M, Friedrich M, Rashid A, et al. Partial congenital absence of the pericardium. Circulation 2007;116:e126–9.
5. Gehlmann HR, Van Ingen GJ. Symptomatic congenital complete absence of the left pericardium: case report and review of the literature. Eur Heart J. 1989;10:670-675.

Plexiform and meandering venous connections in patients with impaired pulmonary venous drainage: Best described by ECG-gated cardiac CT angiography (CTA)

M. S. Juárez-García, G. Burcet Rodríguez, A. Roque Perez, L. Dos, B. Miranda, M. Escobar, H. Cuéllar; Barcelona/ES

Purpose A wide spectrum of anomalies and anatomical variations of the pulmonary veins (PV) has been described in patients with congenital heart disease (CHD). Surgical repair techniques in these patients may also cause PV stenosis or occlusion.
The purpose of this study was to identify unexpected anomalies of the PV in patients who underwent CTA for CHD and to describe alternative drainage routes to the left atrium.
Methods & Materials We reviewed the reports of 509 patients who underwent a CTA for CHD at our institution since 2007 and searched for absence, stenosis or occlusion of a PV. Eight cases were retrieved after excluding patients with partial anomalous pulmonary venous return. A detailed analysis of the left atria and the pulmonary vessels with multiplanar reconstruction and volume rendered images was performed in dedicated workstations.
Results Eight patients (2%) showed anomalies of a single PV (2 agenesia, 1 stenosis, 5 occlusion). In all cases the impaired pulmonary lobe drained into the left atria through venovenous connections of two types: A meandering PV (n = 4), defined as an anomalous PV that drains normally into the left atrium, which has been previously reported as a postsurgical complication in only one occasion. Multiple plexiform connections (n = 4) from the peripheral venous branches of the impaired lobe to those of the adjacent lobe.
Previous surgery for congenital heart disease had been performed in all patients.
PV occlusion was diagnosed in 4 cases where the surgical technique directly involved the atria, but was described as an associated congenital anomaly in the remaining 4 patients.
The venous anomalies were first correctly diagnosed by CTA although all patients had been previously studied by other cardiac imaging techniques, including magnetic resonance.
One case of atrial switch surgery with an occluded PV and a meandering vein presented with hemoptysis, which was attributed to a misdiagnosed pulmonary arteriovenous fistula. 3 patients are asymptomatic and 4 patients show symptoms attributable to their main CHD.

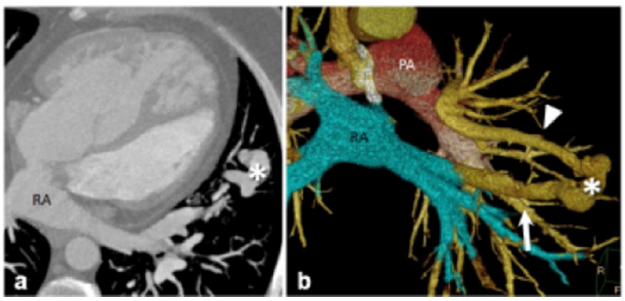

37 y/o man dexto-TGA with atrial switch. (a, b) showing a dilated direct connection between the left upper and lower pulmonary veins (arrowheads), secondary to the surgical occlusion, arrows (b) mark the occluded segment.

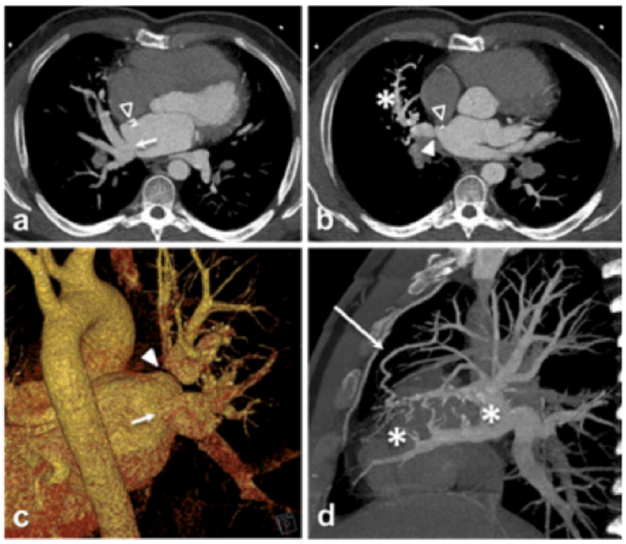

36 y/o man, ASD and PAPVR surgery at 3 mo. (a, b, c) Right superior pulmonary vein ostium interruption (arrowhead) and pulmonary vein flux redirected to LA (arrow) (d) plexiform vessels (*) and meandering vein draining pulmonary vein circuit.

Conclusion We present the largest series of congenital heart disease patients with impaired pulmonary venous drainage and pulmonary venovenous connections, as well as the first CT description of plexiform pulmonary venous connections to our knowledge.

CTA allowed the correct diagnosis of this rare anomaly, which was either not detected or wrongly diagnosed by other imaging techniques.

An exceptional complex coronary anomaly. Is this the new variant in Dual LAD classification system?

N. Lama, V. P. Patris, M. Argiriou; Athens/GR

Purpose We are presenting a remarkable case of a patient with a complex coronary anomaly, with two left anterior descending arteries (LAD), and concomitant anomalous origin of the long left anterior descending coronary artery (ALADAPA) from the pulmonary artery. Each of these entities, Dual LAD and ALADAPA sdr. is a rare anomaly but the combination of them, represent an extremely rare incidence, and Computed Tomography imaging plays a key role, revealing it.

Methods & Materials A previous healthy 58 years-old patient was presented in the ER department with dyspnea on exertion and chest pain. The imaging findings after invasive coronary angiography were inconclusive and required further assessment with CT coronary angiography.

Results Left main coronary artery (LM), had normal origin from the left Valsalva sinus. It was then bifurcated into a short left anterior descending artery (LAD) and the circumflex artery (CMX). A second, longer LAD with anomalous origin from the main pulmonary artery, was found coursing in the anterior interventricular groove up to the cardiac apex causing blood steal by a left-to-right shunt through the coronary system.

During the review of the literature, no reference was found in the previous classification systems of seven types Dual LAD described, for one of two arteries to be originated from Pulmonary Artery. So we are describing what we thought it represents a new variation type.

Regarding the therapeutical approach, two different surgical treatment technics have been purposed (reimplantation of the anomalous vessel or ligation of it combined with grafting of the coronary artery), that may lead to substantial improvement of patient's clinical symptoms.

Conclusion Although both invasive coronary angiography and non-invasive CT coronary angiography are the main diagnostic methods, CT imaging is most of the times the gold standard technique, for patient assessment, providing accurate diagnosis of coronary artery anomalies, regarding their origin and course, with detailed anatomical features.

References Dual Left Anterior Descending Coronary Artery: CT Findings. Prachi P. Agarwal1 Ella A. Kazerooni American Journal of Roentgenology. 2008;191: 1698-1701. https://doi.org/10.2214/ajr.08.1193.

Anomalous Left Anterior Descending Coronary Artery Arising from Pulmonary Artery in a 63 Year-old Male Patient: Case Report and Literature Review. Montasser Y. Ismail, Mohammed I. Nassar, and Mohammed A. Hamad Heart Views. 2015 Jul-Sep; 16(3): 98–103.

Surgical strategies for anomalous origin of coronary artery from pulmonary artery in adults. Rajbanshi BG, Burkhart HM, Schaff HV, Daly RC, Phillips SD, Dearani JA. J Thorac Cardiovasc Surg. 2013:S0022.

Does high heart rate still correlate with high dose and low image quality in coronary CT angiography with modern scanners? Experience with a new generation 256-row CT scanner

D. Tore, A. Depaoli, L. Gianusso, O. Rampado, R. Ropolo, P. Fonio; Turin/IT

Purpose To evaluate the impact of BMI and heart rate on radiation dose and image quality in coronary computed tomography angiography (CCTA) with a 16-cm detector whole-heart coverage single heartbeat CT scanner.

Methods & Materials We retrospectively evaluated 122 CCTAs exams performed at our institution. All exams were performed using prospective ECG-gated single heartbeat axial acquisition (0.28 s gantry rotation time, kV and mA set depending on patient BMI, ECG window 40-80% of R–R cycle) with a whole-heart coverage CT scanner (Revolution CT, GE, USA). Patients were divided in two groups based on heart rate (HR) during imaging. Group 1: 60 patients with low HR ($\leq$ 70 bpm), group 2: 62 patients with high HR ($>$ 70 bpm). CTDI was recorded from the dose report files. BMI data were obtained from clinical documentation. A simulation was also performed using a phantom and the scanner embedded ECG simulator to evaluate CTDI at increasing HR. Statistical analysis was performed using a general linear model and t test.

Results CCTAs had adequate image quality for coronary evaluation in all patients. Mean HR was 76.4 $\pm$ 4.5 for the whole population, 60.5 $\pm$ 1.6 in group 1 and 91.9 $\pm$ 7 in group 2. Mean CTDI was 11.6 $\pm$ 0.9 mGy for the whole population, 12.4 $\pm$ 1.3 mGy in group 1 and 10.9 $\pm$ 1.3 mGy in group 2, without statistically significant difference between the two groups at t test ($p = 0.125$). The general linear model identified a positive correlation between BMI and CTDI (coefficient 0.74 mGy/kg m^2, $p < 0.001$) and a negative correlation between HR and CTDI (coefficient $-$ 0.03 mGy/bpm, $p = 0.011$). Higher heart rates were related with shorter exposure times ($p = 0.02$). Tests performed on the phantom revealed a decrease in CTDI at increasing HR with the same scanning parameters, HR increase from

60 to 120 bpm resulted in a 42% decrease in CTDI without significant difference in image noise.

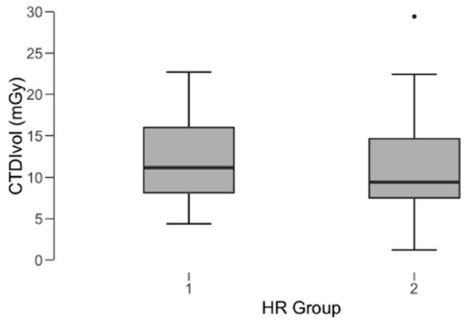

Box plot representing CTDIvol in the patient groups.

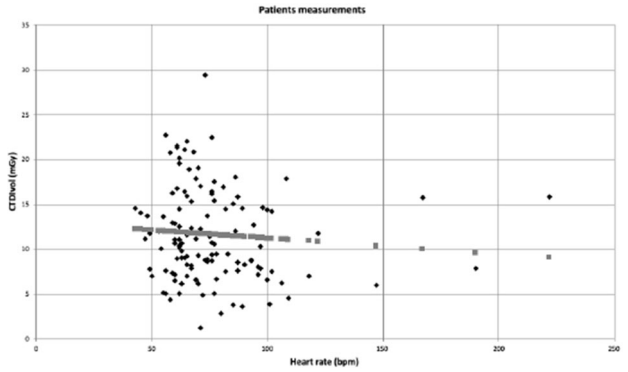

Scatter plot representing CTDIvol and heart rate in the population examined.

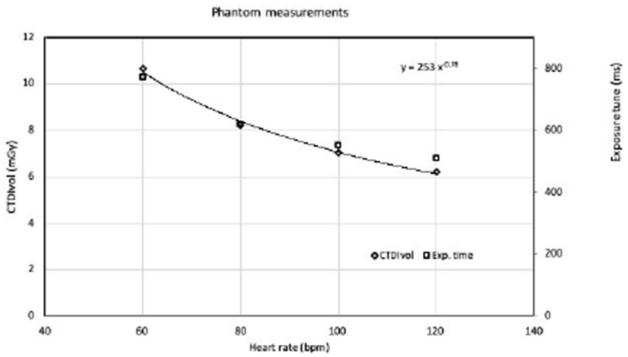

CTDIvol and exposure times obtained from the phantom tests at different heart rates.

Conclusion The mean CTDI was positively correlated with increasing BMI. Interestingly higher HR were related with lower exposure with single heartbeat CCTA acquisition. This phenomenon is probably due to the shortening of diastolic duration at higher HR leading to shorter exposure time. Whole-heart coverage single heartbeat CT scanner, contrary to what happened with older generation scanners, allows coronary diagnostic imaging even at high HR with similar or even with lower exposure compared with lower HR with adequate diagnostic image quality.

Early detection of cardiac involvement in Fabry disease (FD) by using Cardiac Magnetic Resonance

N. Galea, S. Coco, A. Bracci, G. Mancuso, F. Cilia, I. Carbone, C. Catalano, M. Francone; Rome/IT

Purpose Cardiac involvement in Fabry Disease (FD) may have a dramatic impact on morbidity and mortality; medical therapy may prevent progression to cardiomyopathy, however the high cost and undesirable effects require it to be limited to those who actually need. Early identification of cardiac involvement in FD patients may be arduous at pre-hypertrophic stage; our aim was to evaluate the role of Cardiac Magnetic Resonance (CMR) in this clinical setting.
Methods & Materials 16 biopsy proven FD patients with normal maximal wall thickness at echocardiography (< 11 mm) underwent to CMR (1.5 T, Avanto, Siemens, Erlangen, Germany) with following sequence protocol: STIR T2w, cineMR, late enhancement and T1 mapping with MOLLI technique before and 15 min after injection of 0.15 mmol/Kg gadolinium (Gd-DOTA, Guerbet, Paris, France). Indexed LV volumes and mass, native T1 (nT1), extracellular volume fraction (ECV) and tissue tracking (myocardial strain) parameters were analyzed. Results were compared with 16 healthy age and gender matched volunteers.
Results No significative differences were found in myocardial mass (Mass/BSA:45.61 vs. 51.24 g/m^2, p: 0.27), ventricular volumes (EF:58.9 vs. 60.62%, p: 0.62) and left ventricular myocardial strain (Global radial strain: 46.11 vs. 42.75, p: 0.65; global circumferential strain: − 20.4 vs. − 18.8, p: 0.26; global longitudinal strain: − 20.9 vs. − 18.7, p: 0.09) between FD and healthy subjects. No subjects had shown edema or LGE; nT1 was significantly lower (p = 0.01) in FD patients (988 ± 58 ms) than healthy volunteer cohort (1024 ± 63 ms); no significative differences was noted between the two groups in ECV values (23% vs. 24.2%, p: 0.23).
Conclusion Native T1 value appears the only marker of early myocardial involvement in pre-hypertrophic FD patients. No differences in ventricular volumes, myocardial strain and ECV are detectable at early stage of FD compared to healthy subjects.

Comparison of two Methods for Cardiac MR Edema Mapping: Fast Spin-Echo and Steady State Free Precession

P. Krumm[1], P. Martirosian[1], D. Rath[1], M. Gawaz[1], K. Nikolaou[1], B. D. Klumpp[2], A. Hornung[1], U. Kramer[2], F. Schick[1], T. Geisler[1], T. Zitzelsberger[1]; [1]Tübingen/DE, [2]Winnenden/DE

Purpose/Objectives To compare true positive results of myocardial edema mapping in two methods. Myocardial edema may be difficult to detect in cardiac MR due to low contrast between edematous and remote myocardium.
Methods & Materials 76 patients (age 59 ± 11 years, 15 female) with acute myocardial infarction (MI) and 10 healthy volunteers were prospectively included in this single-center study. 1.5T cardiac MR in patients was performed 2.5 days after revascularization (median) for edema mapping: Steady State Free Precession (SSFP) mapping sequence with T_2–preparation pulses (T_2prep); and dual-contrast Fast Spin-Echo (dcFSE) signal decay edema mapping. Late gadolinium enhancement (LGE) was used as reference for expected edema in acute MI.

Results Mean signal increase in edema segments was 74% in dcFSE (245 segments) and 30% in T_2prep SSFP edema mapping (226 segments) compared to healthy volunteers. Mean signal decay time in acutely infarcted segments was 87 ms for dcFSE (pathologic threshold $\geq$ 65 ms) vs. 73 ms for T_2prep SSFP edema mapping (pathologic threshold $\geq$ 68 ms). Acutely infarcted segments were all assigned true positive with a sensitivity of 79% in dcFSE vs. 33% in T_2prep SSFP for each patient, respectively. All other patients had false negative edema in one or more segments. McNemar's test revealed a significant marginal inhomogeneity between methods for false negatives ($p < 0.0001$, power $(1 - \beta) = 0.99$).

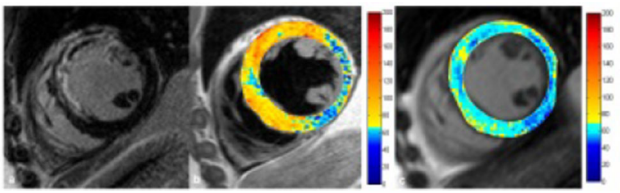

a) LGE in acute STEMI indicating myocardial infarction in septum and anterior segments. b) dcFSE edema mapping overlay with pathologic values in septal segments (yellow and red colors). c) T2prep SSFP map overlay indicates underestimation of edema extent.

Conclusion Signal increase in myocardial edema is relevantly higher in dcFSE than in T2prep SSFP edema mapping. DcFSE edema mapping signal is dependent on T1 and T2 relaxation time, this yields higher signal exploitation in dcFSE edema mapping. Higher signal increase in dcFSE edema mapping may provide higher sensitivity for myocardial edema.

A new method for aortic valve calcium scoring on cardiac computed tomography

B. J. Leenknegt, M. Coeman, D. Devos; Ghent/BE

Purpose/Objectives Aortic valve stenosis (AVS), caused by fibrocalcific changes in the valve leaflets, is the most common valvular heart disease in developed countries. Noninvasive imaging such as computed tomography (CT) has an important role in the workup prior to treatment for AVS. The aortic root however is a complex anatomic structure. Correct quantification of the aortic valve calcification may prove to be challenging. We introduce a new method to quantify the aortic valve calcification based on contrast-enhanced CT scan.

Methods & Materials We retrospectively analysed ECG-gated contrast-enhanced CT scans performed in 91 patients prior to a transcatheter aortic valve implacement (TAVI). All scans were performed on a Somatom Definition Flash CT scan (Siemens). Images were analysed using Syngo.via imaging software (Siemens). After identifying the aortic annular plane, the aortic valve was isolated on a three-dimensional virtual rendering technique (3D VRT) image. Implementing a threshold above 400 Hounsfield units (HU) on the VRT image, calcifications of the aortic valve leaflets were demonstrated. Volumetric analysis, expressed in cm^3, of the aortic valve and the leaflets could then be performed.

Results Combined analysis of CT images in the annular plane and the VRT image allows exclusion of all calcium not related to the valve (Figure 1). After isolating the valve, a calcium volume of the complete valve (Figure 1 above) and of the separate valve leaflets, for example the non-coronary cusp leaflet (Figure 1 below) can be calculated. Moreover, the combined analysis of annular plane CT images and a 3D VRT image allows precise localisation of calcium on the aortic valve leaflets, the commissures, the annulus, within the cusp or towards the mitral valve in complex aortic calcification (Figure 2).

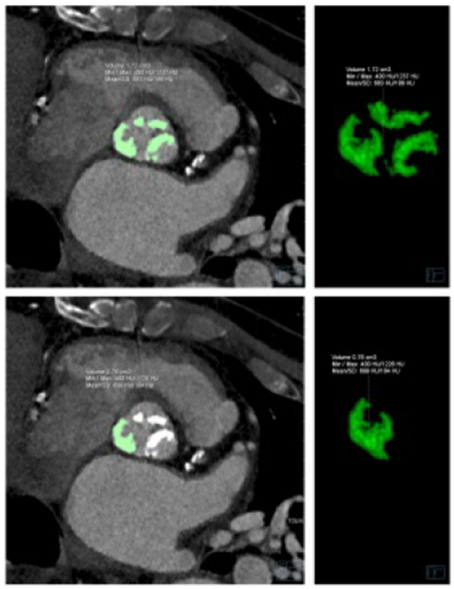

Figure 1 .

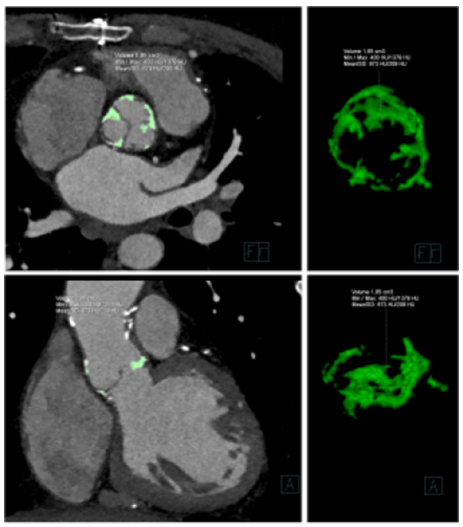

Figure 2 .

Conclusion The aortic root has a complex anatomy and measurement of calcium in this complex structure can be challenging. Volumetric analysis of the aortic valve calcium allows the radiologist to offer the clinician information on the amount and the severity of aortic valve calcification. Performing this analysis on 3D VRT CT images, the radiologist can demonstrate the specific location and distribution of the aortic valve calcium. In the continuously evolving treatment of patients with AVS, with a shift towards treatments which leave the native aortic valve in place, a precise quantification and localisation of aortic valve calcium can prove to be a parameter of use for the clinician.

Extracellular Volume Analysis with Cardiac Magnetic Resonance In Patients With Scleroderma

G. Lastella, C. B. Monti, F. D'angelo, A. Ruffino, P. M. Cannao, F. Sardanelli, F. Secchi; Milan/IT

Purpose To evaluate myocardial extracellular volume (ECV) in patients with scleroderma and the correlations with patient variables.
Methods & Materials Consecutive patients with scleroderma underwent cardiac magnetic resonance, including sequences for the evaluation of T1 values and T1 mapping both before and after contrast injection (0.1 mmol/kg of Gadobutrol). Overall myocardial ECV was then obtained by placing regions of interest both in pre- and post-contrast T1 maps at the septum, anterior wall, lateral wall and posterior wall of the myocardium of left ventricle (LV) in short- and long-axis projections. T1 values obtained from the regions of interest were then averaged to calculate global ECV.
Results 20 scleroderma patients with a median age of 63 years (IQR 51–67 years), of whom 3 were males (15%) were enrolled. Scleroderma patients had a higher global ECV (33.9%, IQR 35.9–39.2%), when compared to healthy subject reference values (25.6%, normality interval of 19.6–31.6%).
Patients had a median LV end-diastolic indexed volume of 67 ml/m^2 (IQR 56–78 ml/m^2), LV end-diastolic indexed volume of 21 ml/m^2 (IQR 17–26 ml/m^2), LV stroke volume of 72 ml (IQR 56 − 85 ml), LV ejection fraction of 69% (IQR 64–72%), and LV mass index of 63 g/m2 (IQR 56 − 72 g/m2). There was a significant negative correlation between ECV and diastolic blood pressure ($\rho = -0.731$, $p = 0.007$), and a borderline positive correlation between ECV and the presence of dyspnoea ($\rho = 0.508$, $p = 0.053$). There were no differences in ECV with regards to different types of scleroderma, or positivity to SCL-70 antibodies.
Conclusion ECV is increased in scleroderma patients despite the normal LV function and it correlates with the presence of dyspnoea. ECV in scleroderma patients may reflect a diffuse myocardial fibrosis and should be helpful in the detection of early myocardial involvement n these patients.

Aortic fluid dynamics in bicuspid valve patients: correlations with valvular morphology using 4D-flow magnetic resonance imaging

G. Pambianchi[1], N. Galea[2], G. Cundari[2], F. Catapano[3], L. Marchitelli[2], I. Carbone[2], M. Francone[2], C. Catalano[2]; [1]Fermo, FM/IT, [2]Rome/IT, [3]Rome, RM/IT

Purpose/Objectives Evaluate the correlation between bicuspid aortic valve (BAV) morphology and the transvalvular flow pattern, aortic flow turbulence and wall shear stress (WSS), using CMR and 4D-Flow imaging.
Methods & Materials 19 healthy BAV participants (aortic diameter $\leq$ 45 mm, lack of severe valvular disease) were studied by CMR on a 3.0T scanner, including cine-MR sequences acquired orthogonal and parallel to the aortic root, contrast-enhanced MR angiography and 4D-flow imaging. Each participant was evaluated measuring, Aortic transversal diameters, valvular morphology (phenotype [RL, RN, RL/RN], leaflet-length, leaflet-asymmetry index), flow general characteristics (peak flow velocity, flow jet angle [FA], flow displacement [FD]), turbulent flow within the ascending aorta (turbulent kinetic energy-TKE, systolic flow reversal ratio-SFRR) and WSS (total, axial and circumferential) at four different levels of the ascending aorta. The statistical analysis consisted of Spearman bivariate correlation and linear regression analyses.
Results In the group the males were 68.4% ± 49 SD, the mean age was 21.8 years ± 9.5 SD. RL-BAV participants (n: 12), RN-BAV (n: 5) and RN/RL-BAV (n: 2) demonstrated peculiar phenotype-related flow patterns. Direct correlations between leaflets asymmetry index, FA (r: 0.64, p: 0.0085) and FD (r: 0.72, p: 0.001) were observed. FD was highly related to Axial and Circumferential WSS in AsAo (r: 0.74, p: 0.004), parameters that showed relation also with SFRR at the same level (r: 0.76, p: 0.001). RN-phenotype partecipants had the greatest AsAo transversal diameters (p: 0.008), higher degree of FD (p: 0.022) and SFRR (p: 0.009).
Conclusion Valve morphology and leaflets asymmetry, in BAV, are directly involved in aortic root flow eccentricity, in particular, FD and FA. These parameters are also correlated to the downstream flow pattern, WSS, SFRR and AsAo diameter. A detailed assesment of valve morpho-dynamics and aortic flow characteristics could ameliorate risk stratification strategy in BAV participants.

Differentiation of Hypertensive and Hypertrophic Cardiomyopathy with CMR

S. Gassenmaier, S. Greulich, K. Klingel, K. Nikolaou, J. M. Brendel, K. A. L. Müller, C. Ruff, P. Krumm; Tübingen/DE

Purpose To systematically compare morphological and functional cardiac MR (CMR) imaging patterns in patients with histopathologically diagnosed hypertensive and hypertrophic cardiomyopathy (CMP).
Methods & Materials 34 patients (8 female; age 50 ± 17 years) with histopathologically diagnosed hypertensive (n = 20) and hypertrophic (n = 14) cardiomyopathy were retrospectively evaluated after consultation of the IRB. 1.5T MR images were analyzed for cardiac morphology, function and late gadolinium enhancement (LGE). All biopsies were performed for hitherto unclear CMP.
Results: Left-ventricular ejection fraction (LV-EF) was significantly lower in hypertensive CMP (mean LV-EF 36%); compared to hypertrophic CMP (mean LV-EF 48%), p = 0.042.
Left-ventricular end-diastolic volume index (LV-EDVI) was pathologically elevated in hypertensive CMP (mean 105 ml/m^2; 55% of patients pathologic); and hypertrophic CMP (mean 95 ml/m^2; 21% of patients pathologic), p = 0.0456.
Left-ventricular myocardial mass index (LV-MMI) was not significantly different between both groups: hypertensive CMP 98 g/m^2; hypertrophic CMP 103 g/m^2, p = 0.65.
Left-ventricular myocardial thickness was not significantly different between both groups: hypertensive CMP septal 12 ± 2 mm, lateral 10 ± 2 mm; hypertrophic CMP septal 13 ± 3 mm, lateral 9 ± 3 mm.
Late-Gadolinium-Enhancement (LGE) was positive in hypertensive CMP in 94% and in hypertrophic CMP in 76% of the patients.

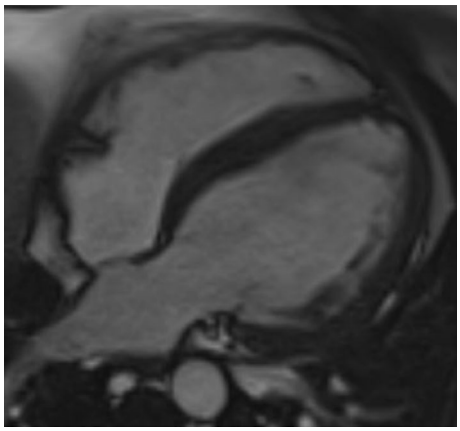

Four-chamber view of a 34 year old patient with hypertensive CMP and a dilated left ventricle.

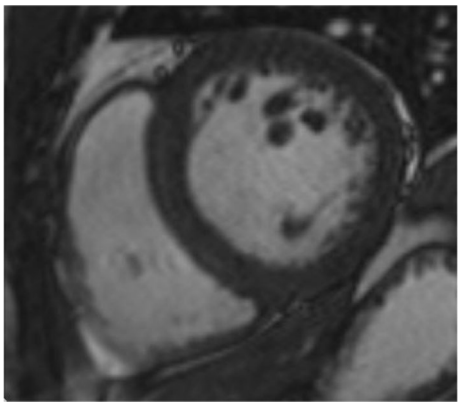

Short-axis view of a 34 year old patient with hypertensive CMP and a dilated left ventricle.

Conclusion Hypertensive and hypertrophic CMP may look similar in CMR and be difficult to differentiate. Morphological and functional parameters can be helpful but without clear cut-off values. Detailed clinical history and presentation should always be taken in consideration.

Variability in manual and automatic aortic measurements on spectral DECT images at different virtual monoenergetic levels

V. de Stasio[1], P. C. Douek[2], S. A. Si-Mohamed[3], L. Hanquier[2], L. Boussel[3], R. P. J. Budde[4], S. Boccalini[5]; [1]Rome/IT, [2]Lyons/FR, [3]Bron/FR, [4]Rotterdam/NL, [5]Genoa/IT

Purpose According to the literature, CT aortic measurements suffer from high variability and scarse reproducibility being influenced by many factors. With the recent introduction of dual energy CT systems and their spectral reconstructions, this problem may be emphasized.
The purpose of our study is to test the variability of aorta diameter measurements on DECT spectral images at different virtual monoenergetic levels for manual and automatic software measurements.
Methods & Materials We retrospectively analysed 30 angio-DECT performed between January and December 2018, using a dual-layer detector CT with retrospective ECG gating. For each exam different series were reconstructed: conventional CT equivalent, monoenergy at 70, 60, 50 and 40 keV. Reconstructions had a slice thickness of < 1 mm.
Two expert radiologists measured the maximum inner-edge to inner-edge diameter of the descendig aorta for conventional, 70 keV and 40 keV reconstructions, at the last slice where the inferior left poulmonary vein was visible on a plane perpendicular to the aorta's longitudinal axis.
Window level was adjusted to the observers preference while other parameters were fixed.
A second set of measurements was obtained by using a commercially available automatic measurement software for all reconstructions.
Results We found significantly higher values of aortic diameter measurements between conventional and spectral 40 keV images for both observers (mean difference: 0.6 ± 0.6 and 0.7 ± 0.6 mm; max difference: 2.4 and 1.8 mm; $p < 0.01$). Differences between conventional and 70 keV images were lower (mean difference: 0.36 ± 0.6 and 0.24 ± 0.42 mm; max difference 1.8 and 1.1 mm; $p < 0.01$). Significant differences between the two expert observers for each reconstruction were found ($p < 0.01$).
The automatic software was affected by a significant measurement variability between conventional and 60 keV images (maximum difference of 1.5 ± 0.4 mm; $p = 0.006$). This was the lowest spectral keV value on which the software was able to identify acceptable vessel contours for at least some of the datasets (20 patients (73%)). Otherwise, the automatic analysis software constantly produced evident errors in the identification of contours for 40 keV and 50 keV monoenergetic reconstructions. No significant difference was demonstrated between automatic measurements on conventional and 70 keV images ($p = 0.16$).

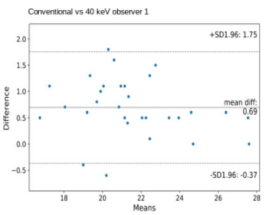

Conventional vs 40 keV observer 1.

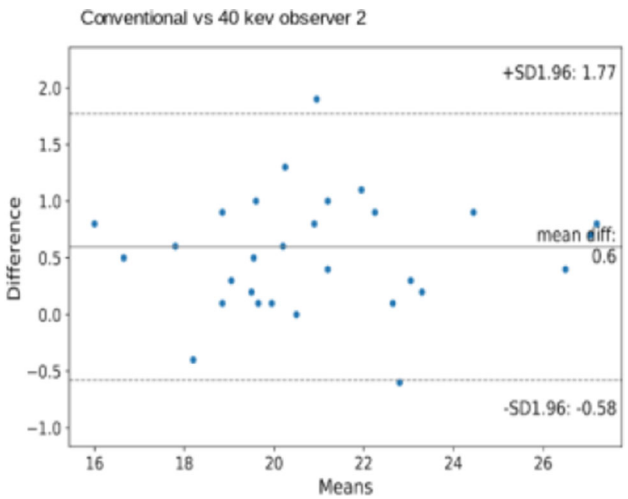

Conventional vs 40 keV observer 2.

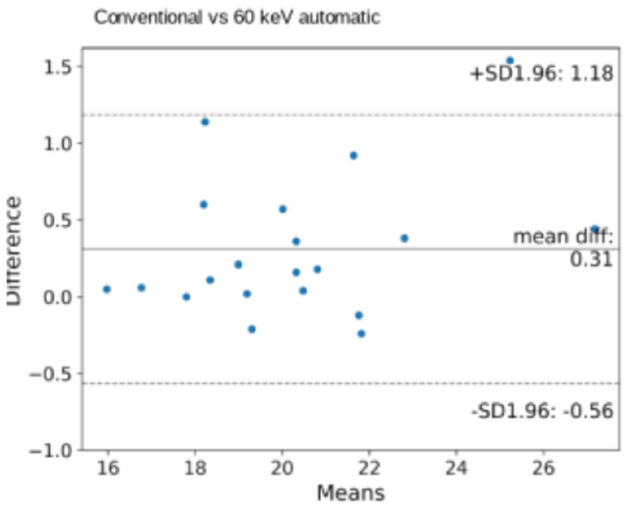

Conventional vs 60 keV automatic.

Conclusion Manual measurements of the two observers were significantly higher for conventional images as compared to 40 keV images. Differences seemed progressively higher for lower virtual monoenergetic levels as compared to conventional images.

Concerning the automatic software analysis, our study found a software running defect for lower nonenergetic reconstructions as well as a significant measurement difference between conventional and 60 keV images.

Dual-energy coronary CT angiography using advanced calcium subtraction algorithm: Feasibility and Initial performance evaluation

Y. Cho, J. Y. Seo, Y. J. Kim, M. J. Yoon; Daejeon/KR

Purpose To investigate the diagnostic impact of prototype dual-energy computed tomography (CT) calcium subtraction algorithm in patients with calcified coronary arteries.

Methods & Materials Twenty-three patients (70% male; mean age, 62 ± 9 years) who had undergone dual-energy coronary CT angiography between May 2018 and April 2019 were included in this IRB-approved, HIPAA-compliant retrospective study. Linearly blended (M_0.5) and calcium-subtracted (CS) images were reconstructed and vascular contrast-to-noise ratios (CNR) were calculated. We assessed subjective image quality using a 5-point scale in a segment based analysis. We also measured the average lumen diameter and area at the point of calcified plaques on both data sets.

Results A total 207 coronary artery segments were evaluated. The subjective image quality analysis showed no significant differences between CS and M_0.5 data sets (mean scores, CS, 4.0 and M_0.5, 4.1, respectively, p = 0.482). CNR also showed no significant differences between CS and M_0.5 data sets (mean scores, CS, 18.3 ± 5.2 and M_0.5, 19.1 ± 3.9, respectively, p = 0.235). The average lumen diameter and area at the point of calcified plaques were significantly higher in CS data sets as compared with M_0.5 data sets (lumen diameter: CS, 2.4 ± 0.6 and M_0.5, 2.1 ± 0.4, respectively, p = 0.032; lumen area: CS, 4.8 ± 2.0 and M_0.5, 3.7 ± 1.5, respectively, p = 0.015). The mean radiation dose was 2.9 ± 0.4 mSv.

Conclusion Prototype dual-energy CT calcium subtraction algorithm might overcome the problem of overestimation of calcified stenosis due to blooming artifacts without differences in conventional subjective and objective measures of image quality.

References 1, De Santis D, De Cecco CN, Schoepf UJ, et al. Modified calcium subtraction in dual-energy CT angiography of the lower extremity runoff: impact on diagnostic accuracy for stenosis detection, Eur Radiol. 2019 Feb 25. https://doi.org/10.1007/s00330-019-06032-y.

2, Jin KN, Chung JW, Park EA, et al. Dual-energy computed tomography angiography: virtual calcified plaque subtraction in a vascular phantom. Acta Radiol Open. 2017 Jul 12;6(7).

3, De Santis D, Jin KN, Schoepf UJ, et al. Heavily Calcified Coronary Arteries: Advanced Calcium Subtraction Improves Luminal Visualization and Diagnostic Confidence in Dual-Energy Coronary Computed Tomography Angiography. Invest Radiol. 2018 Feb;53(2):103-109.

4, Mannil M, Ramachandran J, Vittoria de Martini, et al. Modified Dual-Energy Algorithm for Calcified Plaque Removal: Evaluation in Carotid Computed Tomography Angiography and Comparison With Digital Subtraction Angiography. Invest Radiol. 2017 Nov;52(11): 680-685.

CT in the planning of Transcatheter Mitral Valve Interventions: what is the best cardiac phase?

V. Nicoletti, A. Palmisano, D. Vignale, C. Colantoni, L. Pannone, F. de Cobelli, A. Esposito; Milan/IT

Purpose/Objectives Mitral regurgitation (MR) is one of the most common valvular heart disease lesions, but up to 50% of patients with severe symptomatic MR are not eligible for surgery because of co-existing morbidities. Transcatheter mitral valve intervention (TMVI) is emerging as an alternative treatment option. Cardiac CT plays a crucial role in multimodality imaging for TMVI planning, based on its high spatial resolution and its ability to provide a comprehensive anatomic 3D dataset of valve geometry and cardiac chambers along cardiac cycle. The entity of the modifications of mitral valve geometry throughout the cardiac cycle in patients with severe MR and its potential impact on TMVI planning is still unclear.

Methods & Materials Forty-two patients with severe MR (4 type I, 16 type II and 22 type III according to the Carpentier classification) candidate to TMVI underwent full multiphase ECG-gated cardiac CT. Using a dedicated software, mitral valve anatomy was manually extracted every 10% steps of the R–R interval (0–90%), according to the recommended D-shape mitral valve annulus segmentation model.

Results All patients had enlarged left ventricle (LV EDV = 177.4 ± 94 ml) and left atrium volume (LAV = 124.8 ± 56 ml), with reduced ejection fraction (EF = 47.4 ± 16.1%).

Mean maximum intercommissural diameter was reported in systolic phase (phase 30%: 47.2 ± 7 mm). Mean maximum valvular area and maximum septal-lateral diameter were reported in end-systolic phase (phase 40%: 15.0 ± 4.3 cmq and 38.5 ± 6.6 mm respectively). Mean trigone–trigone diameter showed maximum value in proto-diastole (phase 50%, 24.1 ± 4.5 mm).

In the overall population, comparing the dynamic changes in size and geometry of mitral valve in each phase of cardiac cycle, not significant differences were observed [mitral annulus area (p = 0.861), trigone to trigone (p = 0,359), intercommissural (p = 0.733) and septal-lateral diameters (p = 0.708)]. However, comparing in each patient the maximum and the minimum valvular area, a significant difference was observed (15.9 ± 4.2 cmq and 13,3 ± 3,8 cmq respectively; p = 0.004).

Conclusion Regardless interphase dynamic modification in size and geometry of MV is minimal, larger valvular area was found in systolic phase (40%) suggesting the need to performe MV sizing on systolic phase. The disagreement between phase-to-phase analysis and per patient analysis could be addressed by a certain degree of variability of cardiac phase with larger and smaller valvular area, suggesting the need of a multiphase acquisition for correctly chose the right phase.

Computed Tomography Angiography of two cases of Left Pulmonary Artery Sling with Associated Congenital Anomalies

L. N. Veljanovska Kiridjievska, Z. Atanasov, E. Nakova, I. Milev, R. Rosalia, Z. Mitrev; Skopje/MK

Purpose We present two cases of the aberrant left pulmonary artery, also known as pulmonary sling, diagnosed using thoracic computed tomography angiography.
CT angiography enables detailed evaluation of the suspected anomaly and enables the visualisation of the anatomic relations with surrounding structures. Thus, CT angiography can facilitate the detection of other, commonly associated, congenital anomalies.
Methods & Materials We performed thoracic CT with iodine non-ionic contrast at a dose of 1.5 ml/kg by power injection on two pediatric patients. The 1st patient, a 2-year-old boy, was examined in 2011 using a 64-slice scanner (Lightspeed VCT, GE). In the more recent case (2018) we used a 256-slice scanner (ICT Philips scanner) to examine a 10-months-old girl.
Both cases were characterised by a history of wheezing, repeated respiratory infections and feeding difficulties. Previous ultrasound examinations led to the suspicion of a pulmonary vascular anomaly, furthermore in the first case, clinicians also detected a Patent Ductus Arteriosus (PDA).
Results We diagnosed both cases with left pulmonary artery sling (Figure 1); the anomaly is characterised by an abnormal origin of the left pulmonary artery, arising from the posterior aspect of the right pulmonary artery that crosses the mediastinum, protrudes between the trachea and esophagus causing compression of the trachea and esophagus (Fig. 1a).
Furthermore, in both cases, we detected associated congenital vascular anomalies. In the first case, we confirmed the presence of a persistent ductus arteriosus PDA (Figure 1b), and in the 2nd case, the associated vascular anomaly was persistent left superior vena cava (PLSVC), Figure 1c.

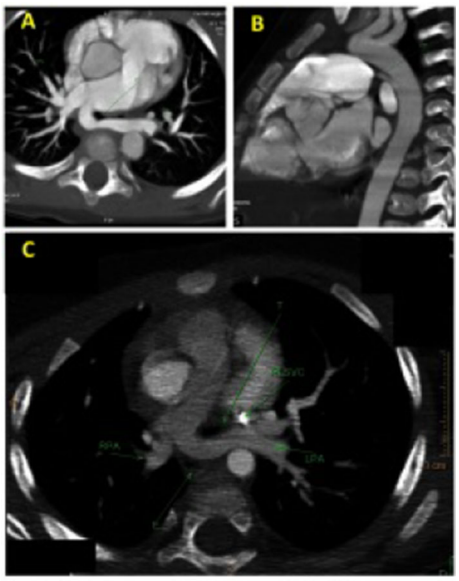

Figure 1 - The Axial MIP images of the left pulmonary artery (LPA) sling in a 2-year-old boy (A), the Sagittal MIP of the associated PDA (B), and (C) the LPA in a 10-months-old girl with the associated persistent left superior vena cava (PLSVC).

The trachea (T), the right pulmonary artery (RPA), the Oesophagus (E) are indicated.

Figure 1 CT Angiography of Left Pulmonary Artery Sling and Associated Anomalies

Conclusion CT angiography is a non-invasive imaging modality to detect left artery pulmonary sling. Moreover, this approach enables the diagnosis of associated cardiovascular anomalies and it allows the assessment of the full anatomical relationships of the tracheo-bronchial tree. Collectively, CT angiography facilitates clinical-decision making.

Lipid panel and DLCN score in the prediction of CAD in patients with familial hypercholesterolemia stratified by genotype: A coronary computed tomography study

G. de Rubeis, A. Ascione, F. Cilia, N. Galea, I. Carbone, C. Catalano, M. Francone; Rome/IT

Purpose/Objectives Assessment of differences and predictive ability of lipid panel and Dutch Lipid Clinic Network (DLCN) score in the search of coronary artery disease in patients with monogenic and polygenic familial hypercholesterolemia (FH).
Methods & Materials Between April 2013 and March 2018, 115 patients affected by FH were studied with coronary CT [51.8 ± 12.3 years, 76 males (66%), 85 (74%) monogenic]. All patients had lipid panel and DLCN score computed.
All 17 coronary segments were analyzed for degree of stenosis, and CAD-RADs score was determined; total calcium burden was computed as well. The predictive model was implemented using linear and logistic regression for CAD-RADs, Agatston score, number of lesions (NL) and number of clinically relevant [> 20% degree of stenosis] lesions (NRL). Analysis of covariance (ANCOVA) was used to investigate differences among groups.
Results Mean DLCN score was 7, mean values (mg/dL) of the lipid panels were: HDL 58 ± 17, TG 126 ± 69, LDL 247 ± 91. The median duration of FH was 25 years [CI 95% 22.3–28.0]. The average NL detected at pre-contrast CT was 4.4 ± 7.4, Agatston score 153.2 ± 352.4. The average NRL detected at angio-CT was 1.8 ± 2.7. Prevalence CAD-RADs ≥ 4 was 8.8% (13 of 115).
Using multiple regression, only TG independently predict CAD-RADs ($r = 0.27$, $p < 0.05$). Performing multiple regression among polygenic and monogenic patients, LDL and TG were shown to independently predict CAD-RADs and NRL in monogenic patients ($r = -0.2579$ and 0.4137; $r = -0.2699$ and 0.2330; $p = 0.05$, respectively), while no single parameter predicts outcomes in the polygenic ones. DLCN is correlated with CAD-RADS only in polygenic patients ($r = 0.5760$, $p < 0.05$). ANCOVA test showed statistically significant differences between polygenic and monogenic patients only for NL (2.5 [CI 95% 0.5–4.4] vs 5.2 ± 7.9 [CI 95% 3.6–6.8]; $p < 0.05$).
Conclusion Lipid panel predicts severity of coronary involvement in monogenic FH. DLCN correlates with CAD-RADs in polygenic FH.

A radiologist as a member of TAVI Heart Team! Fact or fiction in Greek reality?

N. Lama, V. P. Patris, E. Karavasilis, M. Mademli, G. Velonakis, M. Argiriou, N. L. Kelekis; Athens/GR

Purpose Our goal is to investigate and highlight the role and degree of involvement of radiologists in TAVI Heart Teams in Greek reality, by the perspective of the others members, as well as by the viewpoint of the radiologists.

Methods & Materials We designed and distributed in hospitals (University, Public, Private) two different surveys, one about the role of radiologists in TAVI Heart Team to be filled by team members with different medical specialties, and one addressed to radiologists involved in the procedure regarding the way they see themselves as part of this team.
The surveys were anonymous and consent obtained for each participant.
The questions (total of 30, in each one) were focused on key factors affecting everyday practice and role in clinical decisions making.
Additionally, we surveyed key demographics and workplace settings.
Results Selected participants included in the surveys, up to this moment (as the research is still on going and the surveys is planned to be distributed and finalized collected by the end of May in order to begin statistical analysis), are 10 radiologists already involved in pre-TAVI planning and 20 other Heart Team members (Cardiologists, Cardiothoracic Surgeons etc.) from the two biggest cities of Greece.
Conclusion Although we are expecting with great interest the final results, preliminary remarks are not in favor of a well-established role for radiologists in Transcatheter Aortic Valve Implantation programs.
References: SCCT expert consensus document on computed tomography imaging before transcatheter aortic valve implantation (TAVI)/transcatheter aortic valve replacement (TAVR).Stephan Achenbach, MD, FSCCT,*, Victoria Delgado, MD, Jo€rg Hausleiter, MD, Paul Schoenhagen, MD, James K. Min, FSCCT, Jonathon A. Leipsic, MD, FSCCT. Journal of Cardiovascular Computed Tomography (2012) 6, 366–380.
2017 ACC Expert Consensus Decision Pathway for Transcatheter Aortic Valve Replacement in the Management of Adults with Aortic Stenosis. A Report of the American College of Cardiology Task Force on Clinical Expert Consensus Documents. Journal of The American College of Cardiology, A 2017, VOL. 69, NO. 10, 2017 http://dx.doi.org/10.1016/j.jacc.2016.12.006.
Computed tomography imaging in the context of transcatheter aortic valve implantation (TAVI)/transcatheter aortic valve replacement (TAVR): An expert consensus document of the Society of Cardiovascular Computed Tomography, Philipp Blanke, Jonathan R. Weir-McCall, Stephan Achenbach, Victoria Delgado, Jörg Hausleiter, Hasan Jilaihawi, Mohamed Marwan, Bjarne L. Norgaard, Niccolo Piazza, Paul Schoenhagen, Jonathon A. Leipsic. Journal of Cardiovascular Computed Tomography January–February 2019 Volume 13, Issue 1, Pages 1–20, DOI: https://doi.org/10.1016/j.jcct.2018.11.008.

Assessment of myocardial fibrosis by CMR in aortic stenosis. A systematic review of literature

N. Lama, V. P. Patris, G. Velonakis, M. Mademli, E. Karavasilis, M. Argiriou, N. L. Kelekis; Athens/GR

Purpose The aim of our systematic review is to provide a more global perspective of myocardial fibrosis in patient with stenosis of aortic valve and to attempt to distinguish normal and pathological ranges through diverse expressions of the disease in different stages, in combination with the use of distinctive CMR techniques (late gadolinium enhancement, T1native, ECV).
Methods & Materials We performed a systematic search using MEDLINE and Google Scholar. Keywords included in our research were CMR, Aortic Stenosis and Myocardial Fibrosis. The chosen articles were included in our study, if they supported a solid approach in left ventricular changes in patients with aortic valve stenosis.
Subgroup analysis was performed dividing patients and healthy control groups, focal and diffuse myocardial fibrosis, as well as different degrees of it. Also we evaluated potential impact of technical (1.5T or 3T MRI scanners—use of T1 mapping and/or Late Gadolinium enhancement) and multiple biological factors (ex. age, sex, family history, body mass index, left ventricle characteristics etc.). We also assessed risk of bias in included studies.
Results We retrieved and analyzed 36 different studies. Aortic valve stenosis is a disease with a complex phenotype, and its assessment is challenging as various stages provoke different expressions often discordant with ultrasonographic results. All parameters were evaluated through subgroup analysis, looking for potential relation between them.
Conclusion As new insights in an old disease, provided by the use of cardiac MRI (which is the reference standard for the assessment of myocardial fibrosis) highlighted potential re-staging of affected patients, we believe that a more proper therapeutic approach is on the way.
References Imaging and Impact of Myocardial Fibrosis in Aortic Stenosis. Rong Bing, João L. Cavalcante, Russell J. Everett, Marie-Annick Clavel, David E. Newby and Marc R. Dweck JACC: Cardiovascular Imaging, Volume 12, Issue 2, February 2019.
Myocardial T1 and T2 mapping in severe aortic stenosis: Potential novel insights into the pathophysiology of myocardial remodeling. Ana Fehrmanna, Melanie Treutleina, Tanja Rudolphb, Volker Rudolphb, Kilian Weissc, Daniel Giesea, Alexander C. Buncka, David Maintza, Bettina Baeßlera, European Journal of Radiology, October 2018, Volume 107, Pages 76–83.
Late gadolinium enhancement as a potential marker of increased perioperative risk in aortic valve replacement. Quarto C1, Dweck MR, Murigu T, Joshi S, Melina G, Angeloni E, Prasad SK, Pepper JR. Interact Cardiovasc Thorac Surg. 2012 Jul;15(1):45-50.

Coronary computed tomography in the analysis of CAD in familial hypercholesterolemia patients: Validation of lipid panel and DLCN score as predictive tools

A. Ascione, G. de Rubeis, L. Marchitelli, N. Galea, I. Carbone, C. Catalano, M. Francone; Rome/IT

Purpose/Objectives To assess the ability of lipid panel and Dutch Lipid Clinic Network (DLCN) score to predict presence and severity of coronary artery disease as observed with cardiac CT.
Methods & Materials Between January 2014 and March 2018, 104 patients (51.8 ± 12.3 years, 76 males [66%]) affected by Familial Hypercholesterolemia (FH) were analyzed with coronary CT. Determination of lipid panel and DLCN score was performed for each patient.
CAD-RADs score was assessed after analysis of the degree of stenosis for all 17 coronary segments; total calcium burden was computed as well.
Linear and logistic regression was used to implement the predictive model.
Results Mean values (mg/dL) of the lipid panels were: Total cholesterol 338.9 ± 84.0, HDL 58.6 ± 17.2, TG 126.7 ± 69.4, LDL 246.8 ± 91.4; mean DLCN score was 7 before genotyping and 13 after genotyping.
Prevalence of significant Coronary Artery Disease (CAD – RADs $\geq$ 4) was 12,5% (13 out of 104).
The average number of lesions detected at pre-contrast CT was 4.4 ± 7.3, Agatston score 153.2 ± 352.4.
TG, LDL cholesterol and HDL cholesterol levels were not able to predict the Agatston score ($r = -0.02$; $r = -0.01$; $r = -0.9$; $p > 0.05$). Only the TG value was able to predict the level of CAD—RADs ($r = 0.3$ [$p < 0.05$]); neither DLCN score nor any lipid panel value can predict significant coronary artery disease (CAD—RADs > 4).

Conclusion Neither lipid panel nor DLCN score can predict presence of significant Coronary Artery Disease at cardiac CT in FH patients.

Cardiac-MRI in patients with hypertrophic cardiomyopathy associated with arrhythmias

O. Y. Dariy, S. Aleksandrova, V. Makarenko, L. Bockeria; Moscow/RU

Purpose The purpose of our study was to determine the relationship between the MR-parameters of the heart and the most frequent cardiac arrhythmias in patients with hypertrophic cardiomaopathy HCM.
Methods & Materials We performed 56 cardiac magnetic resonance studies on 3T Philips Achieva ans 1.5T Siemens of the patients with HCM in the age 45 ± 12.36 before the surgical intervention. Male (57%; n = 32). 66% (n = 37) patients were with cardiac arrhythmias by ECG-data. Observation period was during 9 years. 71.4% (n = 40) patients underwent surgical correction of HCM after MRI, 17.5%, n = 7 of them interventional one. We estimated the functional parametrs of the ventricles (LV/RV), the size of left atrium (LA), mitral/tricuspid annular plane systolic excursion (MAPSE/TAPSE), LVOT obstruction datas and LV fibrosis.
Results we've divided patients into 4 groups—the 1st one were patients with HCM without arrhythmias (33%, n = 19); the IId—patients with HCM and atrial fibrillation (AF), (21.4%, n = 12); the IIId–HCM and ventricular tachycardia (VT) (35.7%, n = 20); the IVth HCM and AV-block (8.9%, n = 5). We've got minimal LVEDV value in the II group (115.3 ± 20.8 ml), the maximal—in the I'st one (131.3 ± 24.1 ml), LVEF the maximal value in II group (87 ± 13.5%), the minimal in IVth (70.4 ± 4.2%). The maximal value of myocardial mass (228.5 ± 59.5 g) and the highest percentage of myocardial fibrosis(11 ± 4.9%) we had in III group, 50% (n = 10) of them had quantity of myocardial damage > 15%. We obtained a weak correlation of myocardial relative thickness index and myocardial fibrosis (p = 0.034l). We had the extreme hypertrohy (> 30 mm) of LV in 11% (n = 5) patients. Between III and I groups we found statistically significant differences in LVOT obstruction frequency (r = 0.58; p > 0.05). In the II group we obtained the maximal LA volume size (122 ± 22 ml) and decrease of MAPSE/TAPSE (4.9 ± 1.7 mm, p < 0.0001). We've got a good correlation between I and II groups in epicardial fat increase (r = 0.63; p < 0.05).
Conclusion Analysis of MRI markers indicates an important role in association with various arrhythmias in patients with HCM. Changes in the functional parameters of the LV and RV, and the volumetric parameters of the LA depend on the presence of arrhythmias.

Image quality and reliability of a novel dark blood late gadolinium enhancement sequence in ischemic cardiomyopathy

G. Muscogiuri[1], M. Gatti[2], S. Dell'aversana[3], A. I. Guaricci[4], M. Guglielmo[1], A. Baggiano[1], L. Fusini[1], G. Pontone[1]; [1]Milan/IT, [2]Turin/IT, [3]Naples/IT, [4]Bari/IT

Purpose/Objectives To assess the reliability of a novel dark-blood LGE (DBLGE) technique compared to standard bright-blood LGE (SBBLGE) sequence in patients with ischemic cardiomyopathy.
Methods & Materials This prospective study included 78 patients (63.1 ± 12.6 years, 62 males) with clinical history of ischemic cardiomyopathy who underwent CMR at 1.5T (Discovery MR450, GE Healthcare, Waukesha, WI) with postcontrast SBBLGE and DBLGE acquisition. Two observers performed the imaging analysis in a double blinded fashion. The endpoints were: a) qualitative and quantitative analysis of signal intensity ratio (SIR) b) n° segments involved. c) transmurality index (i.e. 025% .25 50%, 5075% and 75,100%) d) papillary muscle enhancement e) microvascular occlusion (MVO). Statistical analysis was performed with nonparametric test.
Results There were no interobserver variability (all p > 0.05). Subjective image quality in DBLGE compared to SBBLGE was higher for the discrimination between LGE and blood signal (p < 0.001), inferior (p < 0.001) between LGE and myocardium and similar between blood and myocardium (p = 0.56). DBLGE provided higher SIR between LGE and blood signal (1.18 ± 1.15 vs. 0.18 ± 0.42. p < 0.001), lower SIR between LGE and myocardium (0.91 ± 4.95 vs. 1.96 ± 1.64. p < 0.001) and between blood and myocardium (0.26 ± 0.71 vs. 1.57 ± 1.26. p < 0.001). The n° segments involved was similar (p = 0.08). The transmurality index was inferior for DBLGE (3.09 ± 1.02 vs. 3.30 ± 1.11. p = 0.007). DBLGE was superior in identifying papillary muscle hyperenhancement (25 vs. 17 cases.p < 0.001) and inferior in MVO detection (7 vs. 12 cases.p < 0.001).
Conclusion The DBLGE sequences when compared to SBBLGE provided better contrast between LGE and bloodpool, seemed to be superior in identifying papillary muscle hyperenhancement, whereas underestimated the trasmurality extension of LGE and the presence of MVO.

Feasibility and diagnostic accuracy of a deep learning algorithm for the evaluation of CADRADS classification with coronary computed tomography angiography

G. Muscogiuri[1], M. Chiesa[1], M. Trotta[1], M. Guglielmo[1], A. Baggiano[1], A. I. Guaricci[2], M. Gatti[3], S. Dell'aversana[4], V. Palmisano[5], G. Rizzon[6], A. Cavaliere[6], A. Del Torto[1], P. Vivona[1], G. Cicala[7], A. Loffreno[1], F. Ricci[8], F. Baessato[1], L. Fusini[1], G. Pontone[1]; [1]Milan/IT, [2]Bari/IT, [3]Turin/IT, [4]Naples/IT, [5]Cagliari/IT, [6]Padua/IT, [7]Parma/IT, [8]Rome/IT

Purpose To develop a deep convolutional neural network (CNN) to classify coronary computed tomography angiography (CCTA) in the correct Coronary Artery Disease Reporting and Data System (CADRADS) category.
Methods & Materials Two hundred eighty-eight patients who underwent clinically indicated CCTA were included in this single-center retrospective study. The CCTAs were stratified by CAD RADS scores by expert readers and considered as reference standard. Fifty patients for each class of CADRADS from 0 to 4 and 38 patients for CADRADS 5 were included in the analysis. A deep CNN was designed and tested on the CCTA dataset and compared to onsite reading. The deep CNN analyzed the diagnostic accuracy of the following three Models based on CADRADS classification: Model A (CADRADS 0 vs. CADRADS 12 vs. CADRADS 3,4,5), Model 1 (CADRADS 0 vs. CADRADS > 0), Model 2 (CADRADS 02 vs. CADRADS 35). Time of analysis for both physicians and CNN were recorded.
Results Model A showed a sensitivity, specificity, negative predictive value, positive predictive value and accuracy of 47%, 74%, 77%, 46% and 60%, respectively. Model 1 showed a sensitivity, specificity, negative predictive value, positive predictive value and accuracy of 66%, 91%, 92%, 63%, 86%, 89%, respectively. Conversely Model 2 demonstrated the following sensitivity, specificity, negative predictive value, positive predictive value and accuracy: 82%, 58%, 74%, 69%, 71%, 78%, respectively. Time of analysis was significantly lower using CNN as compared to onsite reading (530.5 ± 179.1 vs. 104.3 ± 1.4 s, p:0.01).

Conclusion Deep CNN yielded accurate automated classification of patients with CADRADS.

The role of multislice computed tomography (MSCT) angiography in the diagnosis of calcific aortic stenosis: Could MSCT be more informative then Echocardiography in diagnosis?

R. R. Mironchuk, A. Skripnik, V. Fokin, G. Trufanov, O. Moiseeva, O. Irtuga, E. Malev, P. Murtazalieva; Saint-Petersburg/RU

Purpose The study aims to figure out the correlation between a modified protocol of Computed tomography (CT) and echocardiography in assessing pathological changes in patients with calcific aortic stenosis.

Methods & Materials The study involved 30 women and 36 men, aged 41 to 72 y.o., with suspected aortic stenosis, who were performed CT and Echocardiography in a short time.

CT study was performed in 2 phases: native CT series of the study made it possible to evaluate such parameters as the mass, volume, density, and score of calcifications on the valve leaflets.

Computed tomography angiography (CTA) performed with retrospective electrocardiographic gating after the intravenous contrast injection (iodine flux 1.85 g/s) allowed to assess the condition of the valve leaflets in systole and diastole by using special software, the average effective dose was 16.5 ± 6.8 milli-Sieverts.

Results On CTA series of the study, the aortic valve phenotype was identified: bicuspid—38 patients, tricuspid − 28 patients. Comparison of native CT and CTA scans allowed to estimate the location and the degree of expression of calcifications on each aortic valve leaflets. A planimetric evaluation of the aortic valve aperture (AVA) in a state of maximum disclosure of the valve leaflets was performed.

Patients were divided into 3 groups according to their degree of aortic stenosis: mild (AVA = 1.5–2.0 cm^2)—22 patients, moderate (AVA = 1.0–1.5 cm^2)—29 patients, and severe (AVA < 1.0 cm^2)—8 patients. In 7 patients, the AVA area was within normal limits. The performed paired Spearman Rank Order Correlations analysis revealed a positive strong relationship between AVA calculated by CTA and Echo AVA calculated using the velocity time integral (VTI) ($r = -0.6$, $p = 0.05$) and moderate negative correlation between Aortic valve calcifications score (AVC score) and AVA calculated by CTA ($r = -0.39$, $p = 0.001$), and AVC score and Echo AVA VTI ($r = -0.35$, $p = 0.004$).

Average values of AVC score (according to the patient's degree of aortic stenosis): mild—1278.63 ± 257.22 AU, moderate—1754.07 ± 312.71 AU, severe—2509.42 ± 278.32 AU.

Conclusion CT of the aortic valve is a minimally invasive method that allows to determine the valve phenotype, asses quantity and quality of the calcium deposits on the leaflets, evaluate pathological changes of the valve function in one study and has a good correlation with Echocardiography AVA VTI.

CarDiac MagnEtic Resonance for Primary Prevention Implantable CardioVerter DefibrillAtor ThErapy International Study in non-ischemic dilated cardiomyopathy patients

A. I. Guaricci[1], P. Masci[2], G. Muscogiuri[3], M. Guglielmo[3], A. Baggiano[3], L. Fusini[3], V. Lorenzoni[4], J. Schwitter[5], G. Pontone[3]; [1]Bari/IT, [2]London/IT, [3]Milan/IT, [4]Pisa/IT, [5]Lausanne/CH

Purpose/Objectives The aim of this study was to evaluate the additional prognostic value of a cardiac magnetic resonance (CMR) based score over standard of care (SOC) in a large cohort of non-ischemic cardiomyopathy (NICM) patients evaluated for primary implanted cardioverter-defibrillator (ICD) therapy.

Methods & Materials In this Study 1000 (derivation cohort) and 508 (validation cohort) NICM patients with chronic heart failure (HF) and left ventricular ejection fraction (LVEF) < 50% were included. All-cause mortality and major adverse arrhythmic cardiac events (MAACE) were the primary and secondary endpoints, respectively.

Results During a median follow-up of 959 days, all-cause mortality and MAACE occurred in 72 (7%) and 93 (9%) patients, respectively. Age and > 3 midwall segments with late gadolinium enhancement (LGE) were the only independent predictors of mortality (HR 1.037, 95% CI: 1.018–1.057, $p < 0.001$ and HR: 1.78, 95% CI 1.062–3.005, $p = 0.029$, respectively). Gender, left ventricle end-diastolic volume index as detected by CMR (CMR-LVEDVi), and > 2 midwall segments with LGE were independent predictors of MAACE (HR 2.13, 95% CI 1.231–3.690, $p = 0.007$; HR 3.16, 95% CI 1.750–5.709, $p < 0.001$ and HR 1.69, 95% CI 1.084–2.644, $p < 0.02$ respectively). A weighted CMR score, including these three variables, was calculated and when added to the model based on SOC provided a net reclassification improvement (NRI) of 63.7% ($p < 0.001$). When the CMR-score was applied to the validation cohort, NRI of 31.3% (p:0.022) was demonstrated with good prognostic stratification (p:0.001).

Conclusion CMR provides incremental prognostic stratification as compared to SOC, which may have direct impact on the indication of ICD implantation.

Stanford A aortic dissection: pre- and post- surgery Computed Tomography Angiography (CTA) features

E. Muscogiuri[1], T. Polidori[1], M. Pignatelli[1], G. Fraietta[1], M. Zerunian[1], D. Caruso[2], D. de Santis[3], M. Di Girolamo[1], A. Laghi[1]; [1]Rome/IT, [2]Rome, LT/IT, [3]Rome, ITALIA/IT

Purpose To describe and evaluate the main features of acute aortic dissection (AAD) on computed tomography angiography (CTA). To describe the role of CTA in post-surgical follow-up. To emphasize the added value of ECG-gated CTA in the evaluation of Stanford A aortic dissection.

Methods & Materials We retrospectively evaluated 20 patients who underwent CTA of the aorta in Radiology Emergency Department and were diagnosed with Stanford A acute aortic dissection (AAD). The main features of aortic dissection were evaluated for each patient at baseline (involvement of coronary arteries, epi-aortic vessels, abdominal vessels, iliac arteries, extension of dissection, etc.). Post-surgery CT scans of the same patients were evaluated to assess the procedure' success or the progression of disease. A few patients underwent more than one post- surgery CTA and/or ECG-gated CTA.

Results The majority of the patients evaluated (12 pts, 60%) were diagnosed with a Stanford A AAD with an extensive involvement of both thoracic and abdominal aorta at baseline (iliac bifurcation involvement). We evaluated post-surgery CTA scans focusing on the detection of pivotal CT signs concerning the procedure's outcome (absence of new intimal tears, false lumen patency, etc.). Only 4 (20%) of the patients evaluated had a non-patent false lumen after surgery, while the remaining patients had a patent false lumen with absent or minimal involvement of ascending aorta and aortic arch. In some cases patients underwent ECG-gated CTA as a follow-up, with a great improvement of the image quality.

Conclusion CTA is a powerful diagnostic technique and plays a key role in management of Stanford A AAD. Image findings in CTA post-surgery scans allow to assess the procedure' success or progression of disease. ECG-gated CTA is a useful technique to improve image quality and possibly improve the diagnostic performance concerning Stanford A AAD.

References Ueda T, Fleischmann D, Rubin GD et al., Imaging of the thoracic aorta before and after stent-graft repair of aneurysms and dissections, Semin Thorac Cardiovasc Surg. 2008 Winter;20(4):348-357. Meyersohn NM, Ghemigian K, Shapiro MD et al., Role of Computed Tomography in Assessment of the Thoracic Aorta, Curr Treat Options Cardiovasc Med. 2015 Aug;17(8):395.

Extended region growing algorithm for whole heart segmentation from cardiac MRI images

R. Marginean, L. Popa, M. Coman, S. Manole, V. Coman, A. Andreica, L. Diosan, Z. Bálint; Cluj/RO

Purpose We aimed to assess the reliability of an automatic solution for whole-heart segmentation of MRI images of patients with atrial fibrillation (AF). We propose a semi-interactive image segmentation algorithm based on region growing, GrowCut[1], using novel neighborhood structures based on Cellular Automata. We complemented the algorithm with a global view of the signal using remote neighbors outside standard neighborhoods (Moore and Von Neumann). We validated the proposed semi-interactive algorithm on a clinical dataset from our AtFib study.

Methods & Materials Our data consisted of stacks of 2D MRI images from 10 AF patients and 10 healthy controls, captured with a Discovery MR 750 w General Electric 3.0T. The manual segmentations of each slice of each acquisition, prepared independently by two radiologists, were treated as ground truth. The raw images were segmented using our GrowCut extension. To simulate a minimal interaction, we used the ground truth to generate a seed in the shape of a pixel-width vertical bar traversing the foreground and background. These served as starting points for region expansions. We heuristically identified a region of interest (ROI) and filtered the raw segmentation using a ROI mask. To find the ROI, we used two iterations of erosion, a cluster analysis with a filtering step, and a dilation. The automatic results were compared against the ground truth images, to validate our method. We measured all VISCERAL reported metrics[2]. We performed the evaluation in two regimes: image-based (the slice with the greatest structure) and patient-based (stacks of images).

Results For the image-based evaluation, we obtained a median Dice coefficient of 0.80 with an Interquartile Range (IQR) of 0.13 for the 20 datasets. There was a significant improvement versus the classical GrowCut algorithm (median Dice: 0.29, IQR 0.09). The median precision was 0.69 (IQR 0.12), significantly higher than the classical method (median precision: 0.17, IQR 0.07).

For patient-based cases, we segmented each individual slice and reported the average performance across all slices in a volume. The median Dice coefficient was 0.40 (IQR 0.27), with a 29% increase over the classical algorithm (median Dice: 0.31, IQR: 0.25). The median precision was 0.57 (IQR 0.42), with 285% higher than the classical algorithm (median precision: 0.20, IQR 0.22).

Conclusion Our automatic algorithm for whole-heart segmentation, based on neighborhood extension of the classical GrowCut algorithm, outperforms the classical method. This solution can serve as a building block of an automatic computer-aided diagnostic system.

Fabry's disease—strain imaging can show primal differences without conventional changes in cardiac MRI

S. Benz, M. C. Halfmann, A. Lollert, C. Düber, K.-F. Kreitner, T. Emrich; Mainz/DE

Purpose/Objectives Myocardial involvement in Fabry disease is a common manifestation and leads in higher stages to begin of an enzyme replacement therapy (ERT). The extent of hypertrophy and fibrosis of the heart is commonly acquired in cardiac magnetic resonance (CMR) with late gadolinium enhancement (LGE) and T1 mapping. In early disease stages, CMR can be normal regarding left ventricular hypertrophy, T1 Mapping and presence of fibrosis. The aim of this retrospective study was to evaluate the diagnostic value of strain imaging in Fabry's disease without obvious cardiac involvement in CMR.

Methods & Materials In our study, 57 healthy volunteers with no history of cardiac events and 61 patients with a diagnosis of Fabry's disease underwent CMR imaging at 3T. We identified 20 patients without phenotypic cardiac involvement in CMR. Using a semi-automatic tissue tracking software (CVI Circle®), we measured global strains for both ventricles from multiple axes. The strain parameters acquired from this group were compared with healthy volunteers.

Results All common parameters in CMR as ejection fraction, end-diastolic volume, myocardial mass, LGE or T1 relaxation time showed no significant difference between healthy volunteers and Fabry patients in the early accumulation phase. In contrary, all feature tracking strain parameters differed significantly between both groups. The most powerful parameter was left ventricular longitudinal strain with a mean of 20.6% (± 2.6) for healthy volunteers and 16.3% (± 4.1) for Fabry's disease in early accumulation phase ($p < 0.0001$).

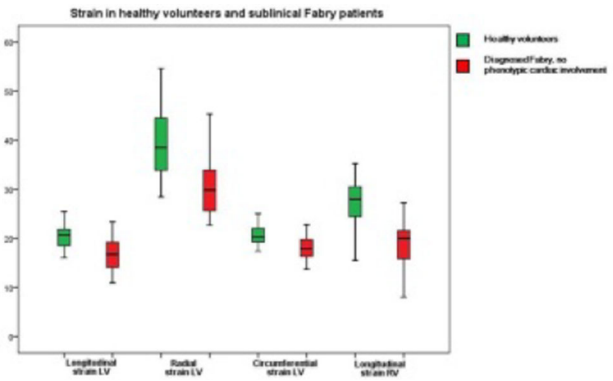

Strain in healthy volunteers and subclinical Fabry patients

Conclusion Feature tracking strain parameters perceive subclinical changes in Fabry's disease. Accumulation of sphingolipids in Fabry's disease is a lifelong process and cardiac involvement seems to begin earlier than anticipated. We recommend adding strain imaging as a parameter to evaluate cardiac involvement in early disease stages. Implications on initiation of ERT have to be determined.

Inverse Association Of Density And Size Of Calcified Plaques With Features Of Plaque Instability, Independent Of Total Coronary Artery Calcium Score

M. Chiocchi, L. Pugliese, L. Spiritigliozzi, F. D. T. Di Tosto, C. Di Donna, A. U. Cavallo, M. Forcina, M. Presicce, V. de Stasio, F. Ricci, R. Floris; Rome/IT

Purpose/Objectives Coronary artery calcium score (CACS) has been found to improve cardiovascular (CV) risk stratification in asymptomatic patients with low-to-intermediate risk. However, several studies have shown that patients with stable disease are more heavily calcified than those with an unstable disease, thus suggesting that CACS is a marker of CV disease burden rather than a predictor of the likelihood of a CV event from an individual plaque. To address this issue we have evaluated the relationship of calcium density and size of coronary artery plaque with features of plaque instability in patients undergoing coronary computed tomographic angiography (CCTA).

Methods & Materials One-hundred and fifty consecutive patients undergoing CCTA at the Department of Diagnostic Imaging and Interventional Radiology, University of Tor Vergata, Rome, Italy. CAC was measured according to the standard Agatston method. Then, plaques were classified as calcified, fibrous or lipid according to their density, as measured in Hounsfield units(HU); calcified plaques were further classified as large or spotty, based on whether their maximal diameter was $>$ or $<$ 3 mm. Other features of plaque instability, such as positive remodeling and napkin-ring sign, were recorded, together with a stent or by-pass presence and patency, and a plaque instability score was obtained. Each patient was then assigned to a Coronary Artery Disease Reporting and Data System (CAD-RADS) category, based on the degree of maximal coronary stenosis. Finally, the epicardial fat thickness was assessed on the left and right ventricle lateral free wall at the base of the ventricles in the short-axis view.

Results Patients had a mean age of 65.7 $\pm$ 11.1 years, 31% were female, 22% had diabetes, 67% had dyslipidemia and 83% had hypertension. Plaque instability score was higher in patients with spotty vs. large calcification (3.37 $\pm$ 1.06 vs. 1.88 $\pm$ 0.73, $p < 0.0001$) and was independently and inversely associated with plaque density ($p = 0.003$), but not with CACS ($p = 0.264$). Also, the epicardial fat thickness was inversely associated with plaque density ($p < 0.012$).

Conclusion Density and size of calcified plaques correlate with features of plaque instability more than CACS and should be considered, in addition to total CACS, in risk stratification of patients undergoing CCTA.

A multiparametric native CMR approach to acute and chronic cardiac diseases with increased myocardial mass using mapping and feature tracking strain

M. C. Halfmann, S. Benz, C. Düber, K.-F. Kreitner, T. Emrich; Mainz/DE

Purpose The diagnoses of acute myocarditis (AM) and hypertensive heart disease (HHD) remain difficult and are commonly based on a combination of clinical expertise and a multi-parameter diagnostic workup including contrast enhanced cardiac magnetic resonance imaging (CMR). It was our purpose to evaluate a multiparametric set of native imaging parameters for their diagnostic accuracy.

Methods & Materials A total of 33 AM and 21 HHD patients who were referred to our department between 09/2014 and 09/2017 as well as 50 carefully selected healthy volunteers underwent CMR at 3T. Subsequent feature-tracking strain analysis as well as native T1 and T2 mapping was performed using dedicated cardiovascular imaging software (cvi42 circle) and results were processed in form of binary logistic regressions using statistics software (SPSS 21, IBM). Cut-off values and corresponding sensitivities and specificities were derived from receiver operator characteristic curves and their respective areas under the curve (AUC) by means of smallest distance to the top left corner.

Results For HV versus AM the combination of global circumferential strain, myocardial mass per body surface area (MYM) and native T1 values performed best, reaching an AUC of .92 with a cut-off $\geq$ .247 yielding 94% sensitivity and 76% specificity. In HV versus HHD, the triad of global longitudinal strain (GLS), MYM and native T1 values discriminated best between groups reaching an AUC of .99. with a cut-off $\geq$ .052 delivering 100% sensitivity and 84% specificity and in AM versus HHD, with a cut-off $\geq$ .244, an AUC of .92 was reached by the combination of GLS, MYM and native T2 values, thereby achieving 90% sensitivity and 76% specificity.

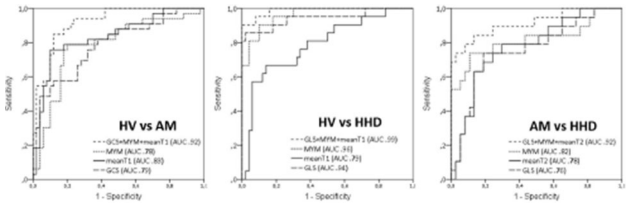

Sensitivity and specifity in acute myocarditis and hypertensive heart disease compared to healthy volunteers

Conclusion Our proposed multiparametric approach was able to precisely discriminate between healthy individuals and patients as well as different patient populations without the need for contrast agents. The proposed multiparametric approach holds great potential to increase the diagnostic accuracy while simultaneously being entirely non-invasive.

Additional role of FFRct and stress CT perfusion in the management of patients with stable chest pain compared to cCTA

A. Baggiano[1], M. Guglielmo[1], G. Muscogiuri[1], L. Fusini[1], M. Soldi[1], A. Del Torto[1], D. Andreini[1], S. Mushtaq[1], E. Conte[1], A. D. Annoni[1], A. Formenti[1], E. Mancini[1], A. I. Guaricci[2], A. L. Bartorelli[1], M. Pepi[1], G. Pontone[1]; [1]Milan/IT, [2]Bari/IT

Purpose/Objectives Computed tomography-derived fractional flow reserve (FFRCT) and stress computed tomography perfusion (stress-CTP) are new techniques that combine anatomy and functional evaluation to improve assessment of coronary artery disease (CAD) using coronary computed tomography angiography (cCTA). This study sought to determine the effect of adding FFRCT and stress-CTP to cCTA alone for assessment of lesion severity and patient management of patients referred for chest pain.

Methods & Materials 289 patients with stable chest pain scheduled for clinically indicated invasive coronary angiography (ICA) plus invasive FFR were evaluated with cCTA, FFRCT, and stress-CTP. Of 289 patients, 147 underwent static stress-CTP, while 142 were evaluated with dynamic stress-CTP.

Management plan with optimal medical therapy (OMT) or percutaneous coronary intervention (PCI) for each patient according to results of each non-invasive technique was recorded, and then compared to what effectively applied according to results of reference standard technique (ICA + FFR). The primary endpoints for the study were the correct allocation of patients to OMT or PCI using cCTA, cCTA + FFRCT and cCTA + stress-CTP, and the correct assessment of non-invasive techniques for all three vessels in relation to angiographically and FFR-defined significance.

Results Compared to cCTA alone, the addition of FFRCT and stress-CTP to cCTA alone increased the agreement in allocating patients to OMT from 24% to 38% and 44%, respectively, while the addition of FFRCT and stress-CTP to cCTA alone increased the

agreement in allocating patients to PCI from 29% to 32% and 36%, respectively. Using ICA + FFR as standard reference, cCTA showed agreement for all three vessels in 56% of patients, while combined approaches of cCTA + FFRCT and cCTA + stress-CTP showed agreement in 66% and 82% of patients, respectively.

Conclusion The addition of functional assessment with FFRCT or Stress-CTP to cCTA has a substantial effect on the evaluation of the relevance of coronary artery disease and therefore on the management of patients compared to cCTA alone.

Prospective noninferiority study of low iodine dose dual-layer spectral detector coronary CT angiography

D. C. Rotzinger[1], S. A. Si-Mohamed[2], L. Boussel[2], R. A. Meuli[1], P. C. Douek[3]; [1]Lausanne/CH, [2]Bron/FR, [3]Lyons/FR

Purpose/Objectives To demonstrate the non-inferiority of low iodine dose and low injection rate dual-layer spectral detector coronary CTA (CCTA), compared to standard injection conventional CCTA for the evaluation of coronary artery disease; to compare the contrast-to-noise ratio between monochromatic and conventional CCTA reconstructions.

Methods & Materials 108 patients with clinically indicated CCTA were prospectively randomized to receive either a standard iodine injection protocol A (flow rate, 5 ml/s; iodine delivery rate, 2 g/s), or a reduced flow rate and iodine dose protocol B, (flow rate, 2.5 ml/s; iodine delivery rate, 1 g/s). The contrast agent (400 mg I/ml) and the duration of injection (16 s) was the same across both protocols. All patients were examined on a dual-layer spectral detector CT system. Conventional images only were reconstructed for protocol A. For protocol B, 55 keV monochromatic images were reconstructed. Contrast-to-noise ratio (CNR) between lumen and fat was measured in 5 coronary segments (LM, distal LAD, distal LCx, proximal RCA, distal RCA). Two independent radiologists rated 17 coronary segments per patient regarding image quality on a 4-point Likert scale (1 = worst score, non-diagnostic, 4 = best score, excellent). Segments deemed non-diagnostic were further classified as motion artifact-related or not. An examination was considered diagnostic if no segment was scored 1.

Results Injected contrast agent volume was 72.2 ± 9.8 ml and 42.5 ± 10.5 ml for protocol A and B, respectively ($p < 0.001$). Mean coronary attenuation was 397.5 ± 138.2 HU in protocol A (conventional reconstruction) and 354.9 ± 128.2 HU in protocol B (55 keV monochromatic reconstruction). CNR was 23.3 ± 14.2 and 28.9 ± 18.2 in protocol A and B, respectively ($p = 0.015$). The rate of diagnostic CCTA was 89.3% (n = 50/56) and 96.2% (n = 50/52) in protocols A and B, respectively. Non-inferiority of protocol B compared to A was inferred (95% CI of the difference = − 0.1651 to 0.0277), with a pre-specified non-inferiority margin of 10%. All segments deemed non-diagnostic (n = 30/1492) had motion artifacts.

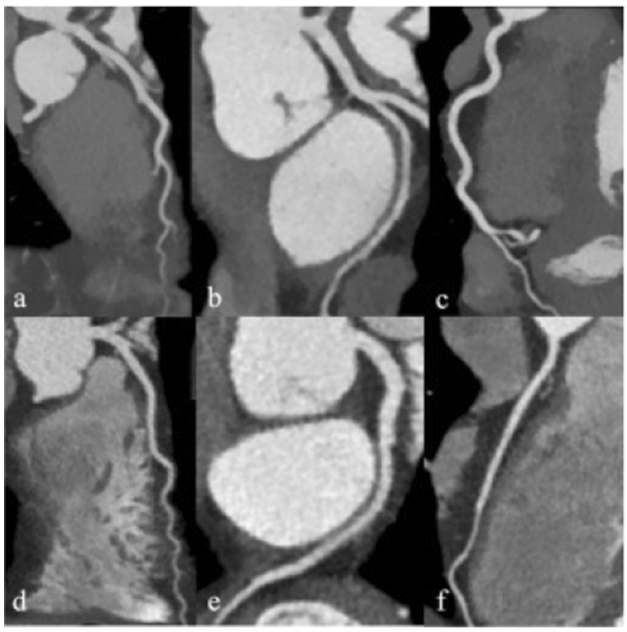

Fig 1: CCTA obtained with 40 mL contrast agent injected at 2.5 mL/s, 55 keV monochromatic reconstructions of the LAD, LCx and RCA (a-c). CCTA obtained with 70 mL contrast agent injected at 5 mL/s, conventional reconstructions of the LAD, LCx, and RCA (d-f).

Conclusion Dual-layer spectral detector CT angiography with 55 keV monochromatic reconstructions allows for a 50% reduction in contrast agent flow rate, and a 40% reduction in iodine dose, compared to conventional CT angiography of the coronary arteries. Additionally, monochromatic reconstructions can improve the CNR between the coronary lumen and surrounding fat.

T1.mapping and CMR Feature Tracking in Mitral Valve Prolapse

M. Guglielmo[1], L. Fusini[1], G. Muscogiuri[1], A. Baggiano[1], A. Loffreno[1], F. Baessato[1], G. Rizzon[2], A. Cavaliere[2], A. I. Guaricci[3], G. Bonalumi[1], M. Zanobini[1], F. Alamanni[1], M. Pepi[1], G. Pontone[1]; [1]Milan/IT, [2]Padua/IT, [3]Bari/IT

Purpose Several studies suggest that mitral valve prolapse (MVP) can be related to sudden cardiac death, owing to sustained ventricular arrhythmias (VAs). In patients with sudden cardiac death and complex VAs, a high percentage of either left ventricle (LV) papillary muscle fibrosis or inferobasal fibrosis has been described using cardiac magnetic resonance (CMR) with late gadolinium enhancement technique (LGE). However, LGE presents several technical limitations and requires contrast agent administration. Thanks to T1 mapping (T1-map) and feature tracking (FT) techniques, CMR may identify myocardial fibrosis and deformation abnormalities respectively. We sought to demonstrate that, in patients with MVP, T1 map can accurately identify the presence of myocardial fibrosis which, being related to myocardial stiffness, is associated to abnormal deformation indexes at CMR FT strain evaluation.

Methods & Materials Consecutive patients with indication to mitral valve surgery for severe mitral regurgitation due to mitral valve prolapse were prospectively enrolled. CMR including Modified Look-Locker (MOLLI) sequences for T1 mapping was performed in each patient. In addition, CMR FT analysis of steady state free precession (SSFP) cine images was performed to obtain 2D global and segmental circumferential and radial strains.

Results 70 consecutive patients (age: 59 ± 12) were successfully evaluated with CMR. T1 native values were significantly higher in the basal and mid LV inferolateral wall compared to the remote myocardium (1074 ± 67 vs. 1046 ± 40 ms, $p < 0.001$). Moreover, the average radial and circumferential strains of the basal and mid LV inferolateral were significantly reduced compared to those of the remote myocardium (21.1 ± 10.4 and − 12.8 ± 5.6 vs. 31.6 ± 9.1 and − 17.3 ± 3.6 respectively, $p < 0.001$).

Conclusion In patients with MVP and severe mitral regurgitation native T1 values of the LV inferolateral are higher as compared to remote myocardium and associated with reduced circumferential and radial strains. T1 mapping and CMR FT strain may be used as tools for the early identification of tissue changes in the LV inferolateral myocardial segment. Further studies are needed to evaluate if these changes are able to predict LGE development and are associated with higher risk for VAs.

FT—CMR derived strain ratios provide incremental value in the diagnosis of acute and chronic heart conditions with increased myocardial mass

M. C. Halfmann, S. Benz, C. Düber, K.-F. Kreitner, T. Emrich; Mainz/DE

Purpose Both acute myocarditis (AM) and hypertensive heart disease (HHD) commonly require a multi-parameter diagnostic workup including cardiac magnetic resonance imaging (CMR). Feature tracking (FT)-CMR strain has the potential to assess complex motions based on the different layers of muscle fiber orientation within the myocardium and a pathological increase of myocardial mass results in altered deformation patterns. Thus, the combination of both parameters might yield incremental diagnostic value and was therefore the focus of our study.

Methods & Materials A population of AM patients (n = 43) and HHD patients(n = 29) referred to our department between 09/2014 and 09/2017 and a carefully selected group of 61 healthy volunteers (HV) underwent CMR at 3T. Subsequent FT-strain analysis was done using dedicated software (cvi42 Circle) and strain values were evaluated for gender and age specific differences and subsequently adjusted using statistics software (SPSS Statistics 21, IBM). Strain ratios using the myocardial mass per BSA were calculated and their diagnostic accuracy was evaluated by receiver operator characteristic curves with their respective areas under the curve (AUC), while the Youden index (YI) was used to determine cut-offs and calculate corresponding sensitivity and specificity.

Results We report statistically significant differences between genders ($p < .05$) but not between age groups. In the comparison between gender-adjusted (gStrain) and ratio strains (rStrain), rGCS performed best in the differentiation between HV and AM reaching an AUC of 0.86, a cut-off < 0.305 and a YI of 0.6, yielding 79% sensitivity and 82% specificity. The rGLS performed best for HV vs. HHD as well as AM vs. HHD reaching AUCs of 0.96/0.79, respectively and a cut-off values < 0.226/< 0.197 with YI of 0.78/0.54, yielding 92%/89% sensitivity as well as 86%/66% specificity, respectively.

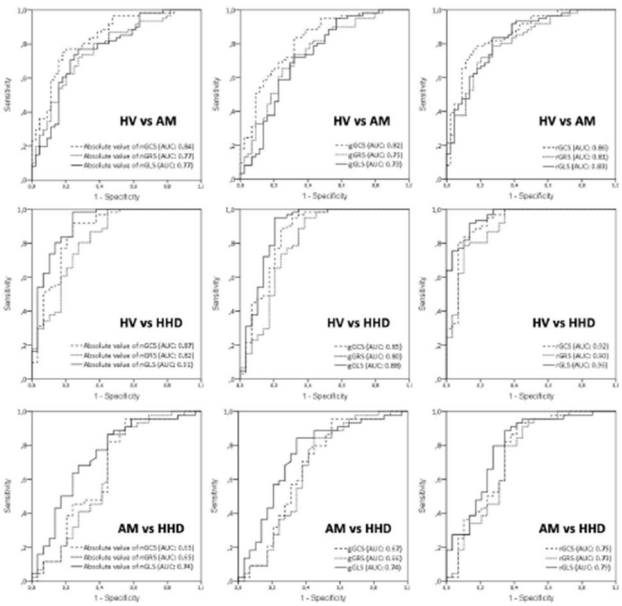

Accuracy of strain ratios for hypertensive heart disease and acute myocarditis

Conclusion The reported increases in the areas under the curve show the incremental value of adding the myocardial mass into the equation when using strain parameters in a diagnostic setting. This observation was made across all three settings and all three strains.

Strain ratios can improve the overall diagnostic accuracy, sensitivity and specificity for all global strain parameters, thereby moving another step forward on the path of noninvasive imaging biomarkers in the heterogeneous field of myocardial diseases with increased myocardial mass.

Comparisons between conventional and compressed sensing 4D flow in healthy volunteers and aortic diseased patients

T. Emrich[1], N. Ring[1], N. Jin[2], D. S. Dohle[1], C. Bussalb[1], M. Thalheimer[1], C. Noll[1], R. S. Strecker[3], C. Düber[1], K.-F. Kreitner[1]; [1]Mainz/DE, [2]Cleveland/US, [3]Frankfurt am Main/DE

Purpose/Objectives Four-dimensional flow measurement (4D Flow) is an emerging quantitative imaging biomarker. Widespread clinical application is currently limited due to its long acquisition time. Compressed Sensing (CS) is a relatively new method to accelerate MRI acquisitions by incoherently undersampling k-space and recovering image quality through iterative reconstruction. The aim of this prospective study was to assess the feasibility of applying CS 4D flow in healthy volunteers and aortic dissection patients after surgical repair and comparing the blood flow measurements to a conventional 4D flow prototype.

Methods & Materials CS and the conventional non-CS 4D flow were acquired in 30 healthy volunteers and 22 patients on a 3-Tesla MRI scanner. All patients had undergone aortic surgery for treatment of aortic dissection with supracoronary aortic replacement and "frozen elephant trunk" antegrad stentgraft implantation. 4D flow was performed in sagittal orientation to cover the whole heart and the thoracic aorta during free-breathing with navigator gating CS 4D flow

was acquired with rate 7.7 acceleration, and non-CS 4D flow was acquired with rate 3 GRAPPA acceleration. Flow measurements were performed with a dedicated 4D flow software tool (cvi42, Circle, Calgary, Canada) at the ascending aorta and a within a region of highest flow (typically in the middle part inside the stent graft) (Figure).

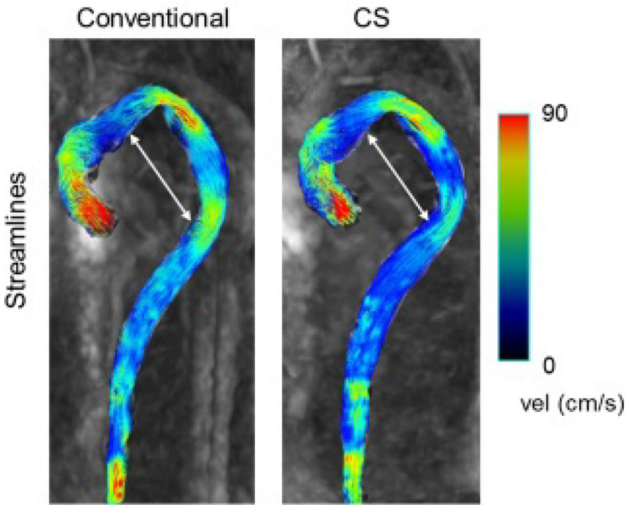

Results Compared to the conventional non-CS acquisition, CS 4D flow significantly shortened the image acquisition time. Overall, there were no statistically significant differences between non-CS and CS measurements regarding net flow, mean pressure gradient, maximum mean velocity, and maximum flow, e.g. p for CS vs. conventional net flow = 0.353. Nevertheless, compared to the conventional 4D flow, CS 4D flow tends to slightly underestimate net flow (− 8.68%) and velocity (− 7.35%).
Conclusion Acceleration of 4D flow measurements will improve the implementation of this emerging imaging technique in daily routine. Before that, the effect of the acceleration on quantitative flow measurements have to be understood in physiologic and pathologic flow patterns. Our work shows that CS 4D flow enables reliable blood flow quantification in health and disease with the advantage of reduced acquisition time.

Comparison of Feature Tracking strain parameters derived from highly accelerated CINE images versus conventional CINE images

R. Oberle[1], T. Klimzak[1], C. Forman[2], M. Schmidt[2], R. S. Strecker[3], C. Düber[1], K.-F. Kreitner[1], T. Emrich[1]; [1]Mainz/DE, [2]Erlangen/DE, [3]Frankfurt am Main/DE

Purpose A future goal of cardiac magnetic resonance (CMR) imaging is to establish reliable imaging biomarker from accelerated sequences. The purpose of this study was to evaluate the accuracy of strain parameters derived by feature tracking (FT) from highly accelerated CINE-sequences in comparison to regular CINE sequences in two commercial available software solutions.
Methods & Materials In this prospective study, CINE sequences from 40 healthy volunteers and 40 patients with various cardiac diseases were analysed. For every patient, CINE-images in typical long- and short-axis were acquired using conventional sequences as well as highly accelerated sequences using compressed sensing (CS). Every examination was performed at 3T. Subsequently, CMR FT strain parameters were calculated using two different commercial available post-processing software. Temporal and spatial resolution was comparable between both CINE techniques. Contour correctness was carefully checked by comparison of basic volumetric parameters (slice by slice) in both the accelerated and regular CINE sequences.
Results First, for both software solutions, no significant changes in quantification of basic volumetric parameters (e.g. enddiastolic volume, myocardial mass, stroke volume) were found between conventional and accelerated sequences. Second, Software A showed a mild underestimation of FT parameters (Fig 1, left), while Software B calculated significant lower FT parameters from highly accelerated CINE images (Fig. 1, right) (e.g. Software A: Mean Peak Circumferential Strain (Conventional vs. CS): − 13.49 ± 5.08 vs. − 13.17 ± 4.74/Software B: Mean Peak Circumferential Strain (Conventional vs. CS): − 14.90 ± 4.96 vs. − 12.58 ± 4.15).
Conclusion Calculation of FT strain parameters from conventional and highly accelerated CINE images differ between different software solutions, potentially caused by different strength and weakness of used algorithms. Standardization of sequences and FT algorithms is needed before FT parameters from accelerated sequences are useable in clinical routine.

Feature Tracking strain parameters in highly accelerated CINE images with varying regularization factors compared to standard CINE sequences in Cardiac MRI

R. Oberle[1], C. Forman[2], M. Schmidt[2], R. S. Strecker[2], C. Düber[1], K.-F. Kreitner[1], T. Emrich[1]; [1]Mainz/DE, [2]Erlangen/DE

Purpose Future cardiac magnetic resonance (CMR) examinations aim to acquire reliable imaging biomarkers from various sequences. Contemporaneous, there is an attempt to accelerate image acquisition. Differences in Feature Tracking (FT) strain parameters between conventional and highly accelerated sequences using compressed sensing (CS) have been reported recently. The purpose of this prospective study was to evaluate the influence of different regularization factors on the accuracy of FT strain parameters from CS Cine images compared to conventional Cine images.
Methods & Materials This study included CINE-images from 8 patients with various cardiac diseases. For every patient, CINE-images in typical short-axis orientation were acquired using a conventional CINE as well as highly accelerated CS Cine sequence at 3T. The data acquired using compressed sensing was reconstructed with different regularization factors (R1: 0.00001, R2: 0.00005, R3: 0.0001, R4: 0.0003 and R5: 0.0005). Subsequently CMR FT strain parameters were calculated using an ML-algorithm of a commercial available post-processing software. Contour correctness was carefully checked by comparison of basic volumetric parameters (slice by slice) in both the reconstructed CS and conventional CINE sequences.
Results FT strain parameters from CS Cine sequences differ from conventional Cine sequences. The mean absolute deviation rised significantly with increasing regularization factors (e.g. global radial strain R1 = 0.79 ± .0.65; R2 = 0.93 ± 0.81; R3 = 1.12 ± 0.96; R4 = 1.22 ± 0.95 and R5 = 1.31 ± 1.00; p (R1 vs. R5) = 0.036) (Figure).
Conclusion The amount of regularization significantly affects FT strain parameters calculated from highly accelerated Cine images. Standardisation of sequences, reconstructions and FT algorithms are needed to allow acquisition of reliable imaging biomarkers. Therefore further evaluation is needed which regularization factor should be used to get comparable strain parameters in clinical routine.

Multiparametric cardiac magnetic resonance imaging in Fabry diseases improves diagnostic accuracy compared to T1 Mapping

T. Emrich, S. Benz, M. C. Halfmann, S. Rueppel, S. Lyschik, C. Kampmann, J. Hennermann, C. Düber, K.-F. Kreitner; Mainz/DE

Purpose/Objectives Fabry's Disease (FD) is a hereditary, x-chromosomal linked storage disease that lead to accumulation of sphingolipids. Recently published work highlight the diagnostic potential of T1 Mapping in the detection of Fabry's disease. The aim of this study was to evaluate a combined diagnostic approach using basic cardiac parameters, T1 and T2 Mapping as well as left and right ventricular strain values.
Methods & Materials In this retrospective study, 61 patients in all phenotypic stages of Fabry's disease and 57 healthy volunteers were included. CMR was performed at 3T and incorporated CINE imaging, T1 and T2 Mapping as well as Late Gadolinium Enhancement imaging. In a post-processing manner, cvi42 (Circle, Calgary, Canada) was used to calculate global and septal T1 and T2 times as well as left and right ventricular function and Feature-tracking based strain parameters.
Results In univariate analysis, longitudinal strain parameters outperform conventional and mapping parameters in detection of Fabry's disease. Nevertheless, the combination of left and right ventricular global longitudinal strain (GLS) with T1 Mapping yielded the highest diagnostic accuracy with a sensitivity and specificity of 83.3 and 82.4% (Figure). The combined approach results in significant improvement of diagnostic accuracy compared to a univariate approach, demonstrated by increasing Youden's indexes (YI): YI (T1 Mapping) 0.468 vs. YI (LV GLS) 0.623 vs. YI (combination) 0.657.

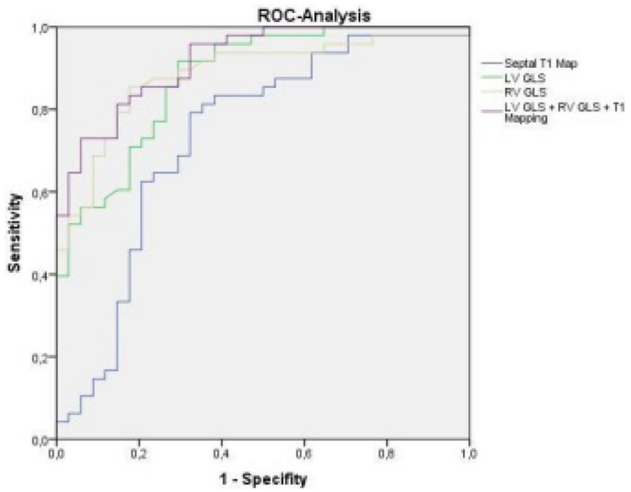

ROC-analysis for uni- and multivariate models
Conclusion A multi-parametric imaging approach incorporating FT strain parameters and T1 Mapping improved the diagnostic accuracy of CMR for detection of Fabry's disease in all stages of disease. Further research is needed to establish Strain imaging as a surrogate for prognosis and therapy.

Remote MRI indicators of blood flow in the aorta in patients with coarctation

M. Shlyappo, L. A. Yurpolskaya, V. Makarenko, M. Makarenko, A. Svobodov; Moscow/RU

Purpose: To assess blood flow using the MR 4D Flow in patients with aortic coarctation in the late postoperative period.
Methods & Materials Cardiac MRI was performed in 10patients, mean age 9.6 + 1.8 years who underwent resection of aortic coarctation with an end-to-end anastomosis between the ages of 2 weeks and 10 months. At the time of the MRI all patients were at the next stage of dynamic observation without drug treatment.
Results A flow change with acceleration and loss of the signal in the region of minimal residual aortic narrowing, local and extended was detected in all patients in systole. In four patients, an additional vortex flow was observed below the aortic narrowing area, a spiral flow in the descending aorta, which persisted throughout diastole. The gradient on the aortic isthmus, obtained by calculating 4DFlow MRI and standard 2D phase-contrast MRI, was not significantly different ($p < 0.05$).
The gradient on the isthmus was directly related to the LV myocardium mass index (r = 0.65; p = 0.04) and blood flow indicators (peak velocity and stroke volume) in the ascending and descending aorta (p = 0.03; p = 0.026). The arc-level gradient depended on the peak velocity in the ascending and descending (r = 0.64; p = 0.048) aorta, the inverse relationship with the age and duration of the history of the disease (r = 0.63; p = 0.049), a direct correlation with the heart index (r = 0.70; p = 0.02).
There is no reliable connection between the blood flow indicators and the arc geometry (H/L). Geometry (H/L) had inverse correlations with indexed diffuse reflectance (r = 0.74; p = 0.015), with indexed SV (r = 0.69; p = 0.027) and LV mass index (r = 0.74; p = 0.015). With delayed MR contrasting, fibrous changes in the myocardium were found in 9patients. 7 examined had an additional lesion of the RV free wall. The expression of fibrosis was inversely correlated with the EF RV (r = 0.65; p = 0.04) and directly depended on the gradient on the aortic isthmus (r = 0.63; p = 0.05).
Conclusion MR 4DFlow allows retrospective investigate the bloodstream, including its geometry, in detail under natural conditions in combination with an MR-assessment of the overall functional parameters of the heart and the presence of fibrotic changes in the myocardium.
References 1. Aortic hemodynamics in patients with and without repair of aortic coarctation: in vivo analysis by 4D flow-sensitive magnetic resonance imaging. Frydrychowicz A, Markl M, Hirtler D, Harloff A, Schlensak C, Geiger J, Stiller B, Arnold R. *Invest Radiol*. 2011 May;46(5):317-25. https://doi.org/10.1097/rli.0b013e3182034fc2.
2. Non-invasive radiologic diagnostics in modern cardiosurgery clinic. V.N. Makarenko, L.A. Yurpol'skaya. *The Bulletin of Bakoulev Center Cardiovascular Diseases. Volume 17. N 3. 2016. P. 124-134.*

Effect of Machine Learning support on quantification of ventricular function and volumes in untrained residents—is Machine Learning Support ready for prime time?

D. Werner[1], R. Oberle[1], K. Stroh[1], F. Stöhr[1], A. Sojoudi[2], C. Bussalb[1], C. Düber[1], K.-F. Kreitner[1], T. Emrich[1]; [1]Mainz/DE, [2]Calgary/CA

Purpose/Objectives Luijnenburg et al. reported inter-observer variability in trained observers from 3.9 to 6.0% for EF, 4.3–5.3% for EDV and 3.7–6.1% for MYM. The aim of this prospective study was to evaluate the inter-observer variability of ventricular volume measurements in untrained residents with and without the support of machine learning algorithms compared to an expert.

Methods & Materials Quantification of ventricular function and volumes was performed by 5 residents with 0-5 years' experience in radiology, and no experience in cardiac magnetic resonance imaging. After introduction into the software for 30 min, every resident performed measurements of ventricular function and volumes using cvi42 (Circle, Calgary, Canada) in 10 patients without support (manual = M), with semi-automatic support (SM), and entirely automated (AM). We investigated the variability of results in required examination time, ejection fraction (EF), end-diastolic volume (EDV) and myocardial mass (MYM).

Using dedicated statistics software the 3 sub-groups were compared to an expert having 9 years of experience in cardiac imaging by means of t tests and bland–altman plots.

Results First, we discovered a significant reduction of time for contouring of the left ventricle (M: 06:15 min, SM: 03:15 min, AM: 01:30 min). The relative deviation of EF compared to the expert for the respective sub-groups was M: 3.35%, SM: 4.12% and AM: 2.98% ($p = 0.012$ between SM and AM). There were no statistically significant differences in EDV (M: 8.00%, SM: 7.11% and AM: 8.99%), but MYM (M: 9.17%, SM: 13.58% and AM: 6.76%; $p < 0.001$ for SM vs. AM). The variance of error between the sub-groups in Bland–Altman plots was smallest in the AM group.

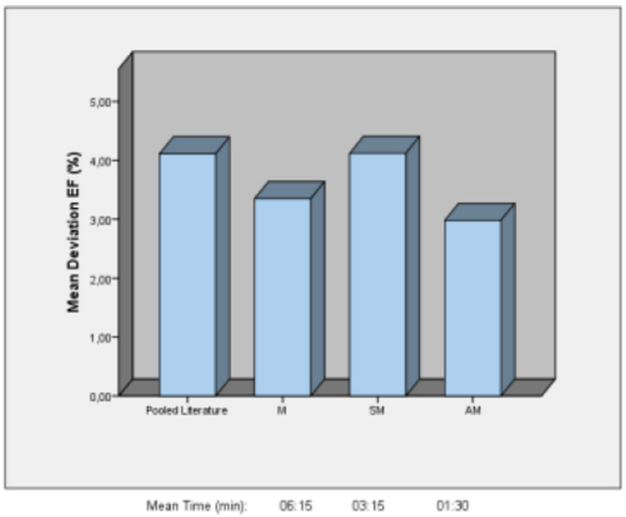

Conclusion In summary, the measurements of untrained residents using automated software were non-inferior to those of an expert. We were able to prove, that using machine learning rather than performing manual measurements can save up to 75% of time. In addition, the inter-observer variability in EF was below the previously published values between trained observers and deviation in MYM and EDV was comparable to previously reported results.

Prognostic Implications of CMR Feature Tracking in Acute Myocardial Injury

T. Leckebusch, T. Emrich; Mainz/DE

Purpose/Objectives The term "myocardial infarction with non-obstructed coronary arteries" (MINOCA) was created for patients presenting with acute chest pain, elevated cardiac enzymes and unobstructed coronary arteries in coronary angiography. Nevertheless, beside coronary causes ("true" MINOCA), non-coronary aetiologies like myocarditis can cause this clinical setting. To separate coronary from non-coronary aetiologies, the term "acute myocardial injury" was recently established (1).The aim of the here presented work is to evaluate the prognostic role of CMR feature tracking in patients with acute myocardial injury.

Methods & Materials This retrospective single centre study included 121 patients presenting with acute chest pain, elevated troponins and non-obstructed coronary arteries in coronary angiography. CMR examinations were realized within a median of 3 days after cardiac catheterization. Patients with "true infarction"/MINOCA were excluded from analysis. We followed these patients by telephone interview and/or analysis of the medical record during a median time of 4.2 years. The primary endpoint was defined as MACE (including death, stroke, congestive heart failure, recurrent hospitalization or interventional/surgical procedure).

Results First, cut-off values for strain parameters were calculated from 62 healthy volunteers (HV) by following equitation: mean value (Strain HV) ± 2*standard deviation. Subsequently, Kaplan–Meier analyses were performed for groups of patients with normal and abnormal FT-CMR parameters. Patients with abnormal strain values showed a significant higher rate of primary endpoints ($p < 0.05$ for all) (Figure). In univariate analysis, abnormal FT-CMR parameters increase the risk of adverse events, e.g. HR for Longitudinal Strain: 2.94; Circumferential Strain: 2.99; Radial Strain: 2.54.

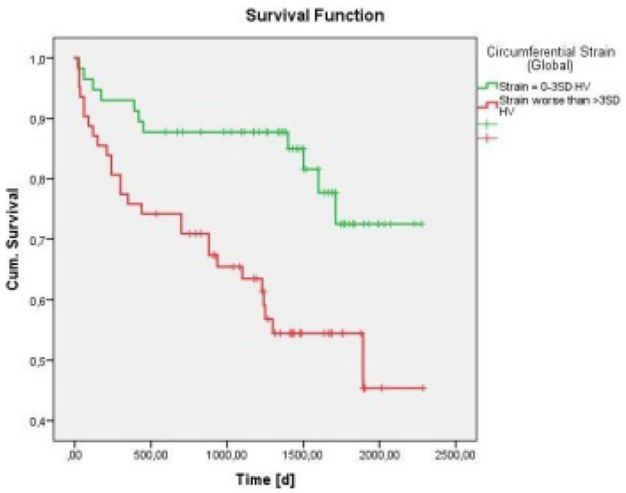

Conclusion Patients with acute myocardial injury and pathologic strain values show a significant higher risk of MACE. Larger (multicenter-) studies are needed to give general recommendations and establish cut-off values for FT-CMR in this population.

Tailorizing pre-TAVI assessment: our experience with CT and MR protocols

F. D. T. Di Tosto, M. Chiocchi, L. Pugliese, F. Ricci, A. U. Cavallo, M. Forcina, V. de Stasio, M. Presicce, L. Spiritigliozzi, C. Di Donna, F. D'errico, M. Pasqualetto, L. Benelli, R. Floris; Rome/IT

Purpose: The aim of our study is to show the importance of precise evaluation of aortic anulus size, coronary ostia height, aortic valve shape and access vessels evaluation in patients undergoing trans-

catheter aortic valve implantation (TAVI). These tools are fundamental in preprocedural evaluation and management of TAVI candidates.
Methods & Materials Between June 2017 and January 2019, 323 patients with severe aortic stenosis, not eligible for surgery, were enrolled for TAVI at the Interventional Cardiology Department of Tor Vergata Polyclinic. All patients underwent pre-procedural diagnostic examination: 218 patients without chronic kidney disease were examined by Computed tomography angiography (CTA) using a retrospectively ECG-triggered high-pitch spiral acquisition mode with low-dose radiation, other 105 patients with chronic kidney disease were divided in 2 groups: 78 patients with 30 ml/min < e GFR < 45 ml/min were studied by a CT acquisition protocol with low-dose contrast injections and 27 patients with e GFR < 30 ml/min underwent MRI assessment without contrast media administration.
Results CT is a gold standard methodic for pre TAVI planning because allows accurate visualization and measures of the aortic annulus coronary ostia, height evaluation of arterial calcifications and peripheral vascular accesses and also extracardiac finding. Furthermore our study shows that acquisition protocol with low-dose contrast injections allows the operator to adequately visualize the intima of the large vessels and the segments of the aortic valve system in order to obtain adequate measures. Non contrast MRI 2D sequences offer a promising approach, because the aortic root can be visualized and measured without the use of contrast media, even if it has some limitations.
Conclusion From our experience in the pre-procedural evaluation of TAVI candidates is fundamental to adapt each patient to the best protocol, in order to minimize possible complications and improve the quality of planning.

Loss of kinetic energy over the aortic arch after surgical repair of acute aortic dissection—a prospective 4D flow study

T. Emrich[1], R. Bülow[2], N. Ring[1], C. Bussalb[1], C. Noll[1], M. Thalheimer[1], M. C. Halfmann[1], C. Düber[1], K.-F. Kreitner[1], D. S. Dohle[1]; [1]Mainz/DE, [2]Greifswald/DE

Purpose Four-dimensional flow measurement (4D Flow) is an emerging imaging technique. Beside traditional flow parameters, 4D flow enables the calculation of advanced parameters as wall shear stress or loss of kinetic energy. The aim of this prospective study was to evaluate differences in loss of kinetic energy over the aortic arch between healthy volunteers and aortic dissection patients after surgical repair with implantation of an antegrad stentgraft ("frozen elephant trunk"; FET).
Methods & Materials In 17 healthy volunteers (HV) and 11 patients, 4D flow imaging was performed using a 4D flow prototype on a 3-Tesla MRI scanner. All patients had undergone aortic surgery for treatment of acute aortic dissection (Type A) with supracoronary aortic replacement and "frozen elephant trunk" antegrad stentgraft implantation. 4D flow was performed in sagittal orientation to cover the whole heart and the thoracic aorta during free-breathing with navigator gating with rate 3 GRAPPA acceleration. Flow measurements and calculation of loss of kinetic energy were performed with a dedicated 4D flow software tool (cvi42, Circle, Calgary, Canada) from the aortic annulus to the descending aorta.
Results Mean maximum and average loss of kinetic energy was 2 to 3 times higher over the aortic arch in FET patients compared to healthy volunteers (mean maximum energy loss FET vs. HV: 9.0 ± 6.1 vs. 3.7 ± 1.3 mW; p = 0.016 and mean average energy loss FET vs. HV: 2.4 ± 1.3 vs. 0.9 ± 0.3 mW; p = 0.003).
Conclusion FET repair of acute aortic dissection leads to a significant increase in loss of kinetic energy measured by 4D flow MR imaging. The prognostic implications of these changes on end-organ perfusion and cardiac remodeling have to be determined in prospective studies.

Type I Kounis Syndrome or Hypersensitivity Myocarditis? Dilemma Solved by Cardiac Magnetic Resonance

E. Gezmis, C. Altın; Izmir/TR

Purpose To highlight role of CMR in differentiation of Kounis Syndrome and Hypersensitivity Myocarditis.
Methods & Materials: Introduction Kounis syndrome(KS) is the concurrent acute coronary syndrome due to coronary vasospasm, in the setting of hypersensitivity reactions. Three variants of KS have been described: type I includes normal coronary arteries, type II includes preexisting atheromatous disease, and type III includes coronary artery stent thrombosis(1). Hypersensitivity myocarditis(HM) is myocarditis provoked by a hypersensitivity reaction(2). These two entities are often inseparable, as their clinical presentation is very similar. Here we report a case of penicillin induced HM, in which definitive diagnosis was made using CMR.
Case Report
37 years old male admitted to emergency department with acute chest pain, starting after intramuscular administration of penicillin, which had been prescribed for acute tonsillitis four days ago. His medical and family histories were unremarkable. Erythematous rashes were observed on his hands, and abdomen. Troponin-I level were high. ECG showed ST eleva-tion. Coronary angiography was performed, which revealed normal coronary arteries. Echocardiography showed global hypokinesia with LVEF of 50%. The findings were suggestive of both Type I KS and HM. CMR demonstrated hypokinesia, myocardial edema, midwall and subepicardial early gadolinium enhancement (EGE) in midventricular inferolateral, apical anterior, apical septal segments(Fig 1). However there were neither subendocardial perfusion defects nor subendocardial contrast enhancement. The patient was diagnosed with HM. CMR at the 3 months follow-up showed resolution of previous findings.

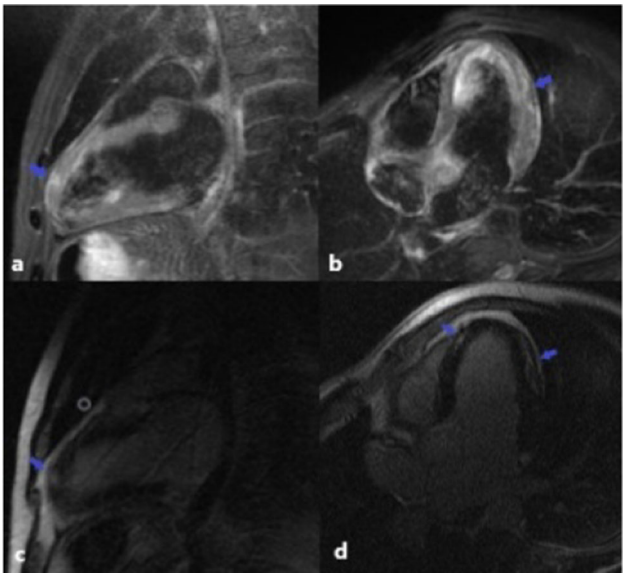

Fig. 1 CMR: 2Ch Triple IR (a) and 4Ch Triple IR (b) showing myocardial oedema, 2Ch 2D MDE (c) and 4Ch 2D MDE (d) showing midwall and subepicardial EGE

Results: Discussion The symptoms, laboratory, ECG and echocardiography findings of HM ans KS are usually indistinguishable. So it is challenging to establish a definitive diagnosis(3). Recent studies about KS showed that perfusion defects, EGE and/or LGE involve subendocardial area conforming a coronary artery distribution (1,4,5). However in HS, the EGE/LGE is subepicardial or mid-wall (5).
Conclusion CMR may be pivotal, in patients presenting with chest pain and hypersensitivity reaction, for making the definitive diagnosis of HS or KS.
References: References:
1. Kounis NG. Coronary Hypersensitivity Disorder:The Kounis Syndrome. Clin Ther. 2013;35(5):563-71.
2. Park Y et al. Hypersensitivity myocarditis confirmed by cardiac magnetic resonance imaging and endomyocardial biopsy. Korean J Intern Med. 2014;29(2):236-40.
3. Almpanis GC et al. The conundrum of hypersensitivity car-diac disease: hypersensitivity myocarditis, acute hypersensitiv-ity coronary syndrome(Kounis syndrome) or both? Int J Cardiol. 2011;148(2):237–40.
4. Okur A et al. The utility of cardiac magnetic resonance imaging in Kounis syndrome. Postepy Kardiol Interwencyjnej. 2015;11(3):218-23.
5. Baillie TJ et al. Kounis syndrome and hypersensitivity myocarditis–One and the same? Insights from cardiac magnetic resonance imaging. J Cardiol Cases. 2015 Oct;12(4): 119-122.

Mapping techniques for detection of myocardial inflammation persistence in acute myocarditis convalescent phase and impact on left ventricle remodeling: MIAMI study

A. Palmisano[1], R. Faletti[2], G. Benedetti[3], M. Gatti[2], P. M. Rancoita[1], M. Francone[4], N. Galea[4], F. de Cobelli[1], A. Esposito[1]; [1]Milan/IT, [2]Turin/IT, [3]London/UK, [4]Rome/IT

Purpose/Objectives Acute myocarditis is a multifaceted disease with non-specific clinical presentations and variable outcome, ranging from complete recovery to end-stage dilated cardiomyopathy. A key element in the unfavorable left ventricle remodeling is the chronicization of the inflammation. Pixel-wise mapping techniques resulted more sensitive than conventional CMR images in the diagnosis of acute myocarditis. However, the role of mapping in the detection inflammation trend in the convalescent phase is still under investigation, as well as its prognostic meaning.
Methods & Materials Thirty-eight patients with clinical suspicions of acute myocarditis underwent cardiac MR (CMR) at 1.5 T scanner for the evaluation of morpho-functionality and hyperaemia with ce-SSFP images, oedema with STIR, T1-mapping and T2 mapping, myocytes necrosis with LGE and ECV. When clinically indicated endomyocardial biopsy (EMB) was performed. A second CMR was performed 2 month after baseline. Forty-five healthy volunteers underwent CMR as control group.
Results Thirty-three patients out of 38 completed CMR follow-up. EMB was performed in 26 patients and confirmed CMR diagnosis. Clinical presentation was with Infarct-like syndrome in 21 patients (55%), heart failure in 10 (27%) and sudden cardiac death/arrhythmia in 7 (18%).
At baseline CMR mean LV-EDV and EF were 135 ml 53%, respectively. Lake-Louise criteria (LLC) were positive (T2-ratio:2.8, Hyperemia:13%, LGE:6%). Mapping parameters were positive (T1: 1124 ms, T2: 56 ms, ECV:32%) without differences among clinical presentation ($p > 0.05$).
Mapping parameters showed excellent diagnostic accuracy for myocarditis in acute phase (AUC: 95%, 98%, 90% for T1 map, T2 map and ECV) and convalescent phase (90%, 85%, 89% for T1 map, T2 map and ECV).
At short-term follow-up, a slight recovery of EF was experimented with a reduction of all LLC and mapping parameters without differences among clinical presentations. The modification of native-T1 values correlated to the recovery of EDV (**$R = 0.8242$, $p = 0.0005$**) and ejection fraction (**$R = -0.4559$, $p = 0.0378$**).
Conclusion T1 value is the most accurate mapping parameter to detect persistence of inflammation in the convalescent phase, which negatively impacts on LV EDV and EF recover.

Myocardial extracellular volume assessment in esophageal cancer patients using routine contrast-enhanced CT

D. Capra[1], C. B. Monti[2], M. Melloni[2], C. Gumina[2], A. Luporini[2], F. Lombardi[2], A. Sironi[2], E. Asti[2], L. Bonavina[2], F. Sardanelli[2], F. Secchi[2]; [1]Segrate/IT, [2]Milan/IT

Purpose To assess the feasibility of estimating the myocardial extracellular volume fraction (ECV) through routine contrast-enhanced computed tomography (CT) in esophageal cancer patients and to investigate the correlation between an increase in ECV and exposure to radiation therapy.
Methods & Materials Patients with esophageal cancer who had undergone routine CT examinations before and after radiation therapy were retrospectively analyzed. Patients with pre-existing cardiovascular conditions, who previously had undergone cardiotoxic chemotherapy, with CT images with artifacts were excluded. ECV was measured using round ROIs in the septum at mid-level and in the left ventricular chamber at the same level. Wilcoxon statistical test was used to compare the measurements.
Results Twenty-seven subjects were analyzed, with a median age of 66 years (interquartile range (IQR) 59–71 years), six of which were women. Pre-treatment median ECV was 28.6% (IQR 26.2–31.8%) and post treatment median ECV was 30.7% (IQR 26–36.2%) with a median interval of 35 days. Post-treatment ECV was significantly higher than pre-treatment ECV ($p = 0.027$).
Conclusion ECV in esophageal cancer patients is found to be significantly higher after treatment, its rise after radiation therapy could play a role in the screening of myocardial condition in esophageal cancer patients undergoing such treatment.

Image quality of late gadolinium enhancement in cardiac magnetic resonance with different doses of contrast material in patients with chronic myocardial infarction

C. B. Monti, L. Saggiante, M. Alì, A. Cozzi, M. Codari, F. Sardanelli, F. Secchi; Milan/IT

Purpose/Objectives Contrast-enhanced cardiac magnetic resonance (MR) is pivotal in assessing patients with chronic myocardial infarction (CMI) over time. However, issues concerning the safety of gadolinium-based contrast agents (GBCA) have led to the pursuit of GBCA dose reduction. Our purpose was to assess image quality of scar tissue in a series of cardiac MR examinations performed with different GBCA doses in CMI patients.

Methods & Materials CMI patients who underwent GBCA-enhanced cardiac MR were divided into three subgroups, with regards to the gadobutrol dose they received (A:0.10 mmol/kg, B:0.15 mmol/kg, C:0.20 mmol/kg) and retrospectively evaluated. Signal-to-noise ratio was calculated for scar tissue (SNR_{scar}), and contrast-to-noise ratios were calculated between scar tissue and both remote myocardium ($CNR_{scar-rem}$), and blood ($CNR_{scar-blood}$). Data were reported as median and interquartile range (IQR), differences were tested with Kruskal–Wallis and post hoc tests.
Results Out of 94 retrieved patients, 37 belonged to group A, 26 to group B, and 31 to group C. SNR_{scar} was lower in group A (50.8, IQR 43.4–63.7) than group B (70.1, IQR 52.2–111.5; $p = 0.014$) and group C (72.1, IQR 59.4–100.0), while $CNR_{scar-rem}$ was lower in group A (71.0, IQR 61.3–84.6) than group B (96.5, IQR 73.1–152.8; $p = 0.003$) and group C (103.9, IQR 83.9–132.0; $p < 0.001$). There were no other significant differences in SNR_{scar}, $CNR_{scar-rem}$ or $CNR_{scar-blood}$ ($p > 0.856$).
Conclusion Using 0.15 mmol/l of gadobutrol does not seem to hinder image quality compared to 0.20 mmol/l, while using 0.10 mmol/l appears to provide lower image quality. Thus, 0.15 mmol/kg of gadobutrol could be suggested instead of 0.20 mmol/kg.

Prevalence and characterization of myocardial bridging detected on cardiac ct

E. Detorakis[1], I. Papadopoulou[1], R. Illing[2]; [1]Heraklion/GR, [2]Budapest/HU

Purpose Myocardial bridging (MB) is a congenital anomaly in which a segment of a coronary artery is covered by myocardium, mostly involving the mid-portion of the left anterior descending (LAD) artery. We retrospectively studied the prevalence of MB in local population and to identify its possible clinical significance.
Methods & Materials Ninety-eight patients (64 men, 34 women) of median age 52 years, with low to intermediate risk of coronary artery disease underwent cardiac CT in our department on a 128-slice CT scanner (GE Optima CT 660). A beta-blocker was administrated orally according to heart rate. Contrast media (Ultravist 370, *Bayer* HealthCare) was i.v administered. A prospectively ECG-triggered protocol was implemented in 68 patients and a prospective protocol in the remaining 30 due to cardiac arrhythmias. Atherosclerotic lesions were evaluated (CAD-RAD system) while the presence and extent of MB was recorded. Statistical analysis was performed using Student t test and Chi square test. A p value of < 0.05 was considered statistically significant.
Results Myocardial bridging was detected in 52 of 98 patients (53%) in all cases of the superficial type involving the mid part of the LAD. The mean length of MB was 2.2 cm (Figure 1). In 48 patients the lumen diameter was found reduced along the MB portion, while in those patients where retrospective ECG-gated protocol was used, a further reduction of 10–30% of lumen diameter was recorded during systole (Figures 2 and 3). 42 patients belonged to CAD-RADS 0 category and 38 of them reported chest pain under exercise or stress conditions the last 3-8 months. A statistically significant correlation was found between the presence of myocardial bridging and chest pain ($r^2 = 0.3218$, $p = 0.00032$).

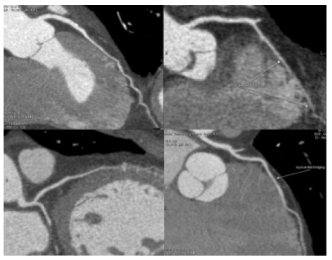

Figure 1 Curved reconstruction images of LAD, showing a superficial type of myocardial bridge of various length (white arrows)

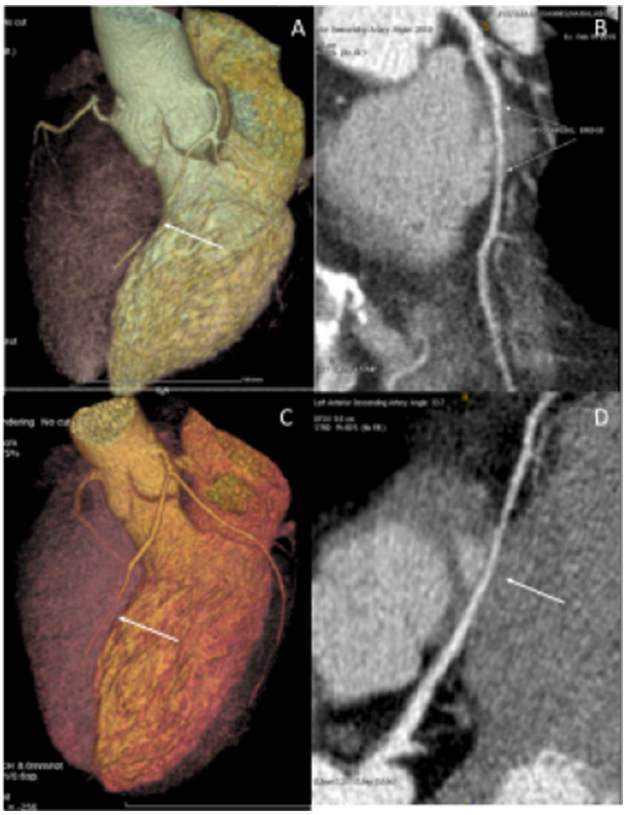

Figure 2 Myocardial bridging (white arrow), as depicted in volume rendering technique (a and c) and in curved reconstruction images (b and d). The reduction of LAD diameter along the MB is obvious

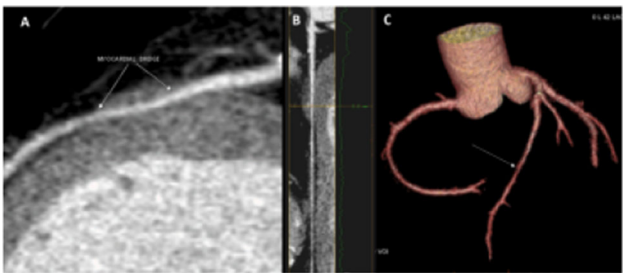

Figure 3 Curved reconstruction (a), linear reconstruction (b) and coronary tree volume rendering technique (c), where myocardial bridge (white arrows) is clearly depicted. MB length as well as the lumen diameter reduction is recorded

Conclusion A high prevalence of superficial type myocardial bridging was detected in our study population, involving the mid part of the LAD, with diameter reduction along the MB segment The presence of MB was strongly correlated with chest pain/discomfort. Additional diagnostic imaging, such as the use of non-invasive fractional flow reserve CT (FFR-CT) technique in the future, may further clarify the clinical significance of MB.

References 1.Nakanishi R et al. Myocardial bridging on coronary CTA: an innocent bystander or a culprit in myocardial infarction? J Cardiovasc Comput Tomogr. 2012 Jan-Feb;6(1):3-13.

2.Forsdahl SH et al. Myocardial Bridges on Coronary Computed Tomography Angiography- Correlation With Intravascular Ultrasound and Fractional Flow Reserve. Circ J. 2017 Nov 24;81(12):1894-1900. https://doi.org/10.1253/circj.cj-17-0284. Epub 2017 Jul 7.

Breast Arterial Calcification Predicts Progression of Coronary Atherosclerosis in Asymptomatic Women

Y. E. Yoon[1], B. L. Yun[1], K. M. Kim[1], W. Lee[1], J. S. Han[1], E. J. Chun[2], S. Ahn[1], H. E. Park[3], J.-B. Park[3], S. I. Choi[2], J.-W. Suh[1]; [1]Seongnam/KR, [2]Seongnam-Si/KR, [3]Seoul/KR

Purpose Evidence that the presence of breast arterial calcification (BAC) is associated with an increased risk of cardiovascular disease morbidity and mortality is currently accumulating. Recently, the BBC study demonstrated that BAC evaluation in asymptomatic women provides an independent and incremental value over conventional risk factors for the prediction of subclinical coronary atherosclerosis. However, to date, it is unknown whether BAC evaluation is also helpful for the prediction of coronary atherosclerosis progression. Therefore, we aimed to assess whether the evaluation of BAC could predict the progression of coronary atherosclerosis on coronary computed tomography angiography (CCTA) in asymptomatic women.

Methods & Materials This retrospective observational cohort study analyzed asymptomatic women from the BBC registry, which included 2100 asymptomatic women. Among these, 126 women (age 54.5 ± 7.0 years) who underwent repeated CCTA examinations were included in the final analysis. Coronary arterial calcification score (CACS) and segment-stenosis score (SSS) were evaluated for the progression of coronary arterial calcification (CAC) and coronary atherosclerotic plaque (CAP). CAC and CAP progression rates were calculated as the annualized difference between the baseline and follow-up $\sqrt{}$CACS and SSS, respectively.

Results CAC and CAP progression were observed in 42 (33.3%) and 26 (20.6%) women, respectively (median interscan time, 4.3 years), and were associated with the presence of BAC and a higher BAC score at baseline. When we stratified by the presence of BAC, women with BAC demonstrated significantly higher CACS and SSS at both baseline and follow-up and significantly higher progression rates of CAC and CAP. (Figure 1). Women with BAC also showed higher chances for CAC and CAP progression during follow-up (log-rank $p < 0.001$ for both). (Figure 2) Both BAC presence and score were significantly associated with CAC and CAP progression rates. In multivariable analyses, the BAC score remained as an independent predictor for both CAC and CAP progression rates even after the adjustment for clinical risk factors ($\beta = 0.087$; $p = 0.029$, and $\beta = 0.020$, $p = 0.010$, respectively) and with additional adjustment for baseline CACS ($\beta = 0.080$; $p = 0.040$, and $\beta = 0.019$, $p = 0.012$, respectively) or SSS ($\beta = 0.079$; $p = 0.034$, and $\beta = 0.019$, $p = 0.011$, respectively).

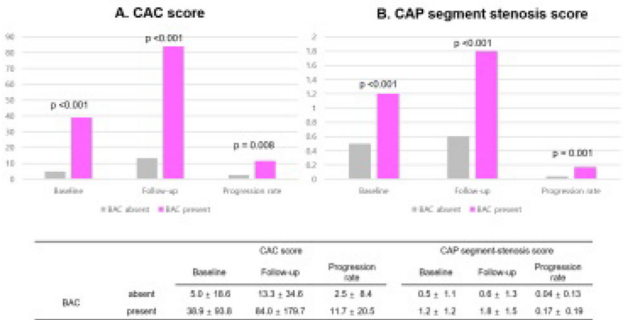

		CAC score			CAP segment-stenosis score		
		Baseline	Follow-up	Progression rate	Baseline	Follow-up	Progression rate
BAC	absent	5.0 ± 16.6	13.3 ± 34.6	2.5 ± 8.4	0.5 ± 1.1	0.6 ± 1.3	0.04 ± 0.13
	present	38.9 ± 93.8	84.0 ± 179.7	11.7 ± 20.5	1.2 ± 1.2	1.8 ± 1.5	0.17 ± 0.19

Figure 1 Progression of CAC (a) and CAP (b) according to the presence and absence of BAC

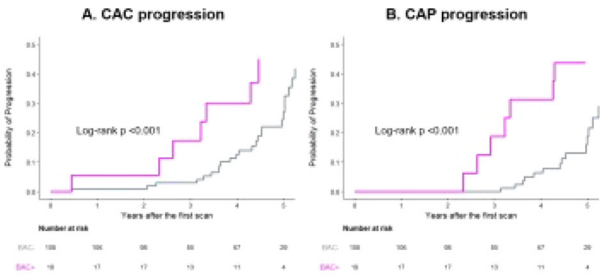

The cumulative proportion of CAC (A) and CAP (B) progression according to the presence and absence of BAC.

Conclusion BAC, which is suggested as a potential women-specific risk marker for coronary artery disease, also predicts the progression of coronary atherosclerosis.

References Yoon YE, Kim KM, Han JS et al. (2018) Prediction of Subclinical Coronary Artery Disease With Breast Arterial Calcification and Low Bone Mass in Asymptomatic Women: Registry for the Women Health Cohort for Breast, Bone, and Coronary Artery Disease Study. JACC Cardiovasc Imaging.

Comparison of image quality between higher- and lower-concentration contrast medium on low-dose coronary computed tomography angiography (CCTA)

T. H. Kim, J. M. Shin, E.-Y. Choi, C. H. Park; Seoul/KR

Purpose/Objectives To compare the image quality between higher- and lower-concentration contrast material (CM) on coronary computed tomography angiography (CCTA) with low tube voltage, volume reduction of CM, and a knowledge-based iterative model reconstruction (IMR) algorithm.

Methods & Materials Eight-two patients who underwent CCTA (a 64-slice CT scanner) for suspected coronary artery disease were randomly categorized into two groups; group A with CCTA using low-osmolar iodine CM (ioversol, 350 mg/ml) and group B, using iso-osmolar iodine CM (iodixanol, 270 mg/ml). An 80-kVp protocol was used for patients with a BMI < 22 kg/m^2, whereas a 100-kVp protocol for patients with a BMI 22 to 28 kg/m^2. Iodine delivery rate/body weight (gI/s/kg) was fixed as 0.018 for 100-kVp and 0.012 for 80-kVp during 15 s in both groups. All CT images were reconstructed using a knowledge-based IMR algorithm. The attenuation value and image noise of CCTA were measured from the ascending aorta. The SNR and CNR were calculated from the RCA and LM artery. Image quality was assessed via a 4-point grading scale from the RCA, LM artery, LAD, and LCx, as follows: grade 1 (poor/non-diagnostic), grade 2 (adequate), grade 3 (good), and grade 4 (excellent; no image degradation). The radiation dose was compared as the DLP (mGy $\times$ cm).

Results Forty-two patients were enrolled in group A and 40 in group B. Age, height, body weight, BMI and mean HRs were not different between the two groups ($p > 0.05$). The radiation dose, mean attenuation, and image noises of CCTA were 194.1 ± 128.1 mGy $\times$ cm, 422.6 ± 64.4 HU, 29.3 ± 2.7 in group A and 191.9 ± 130.2, 419.3 ± 58.6, and 28.7 ± 5.9 in group B, respectively ($p > 0.05$). The SNRs did not differ between the groups in the RCA (14.3 ± 2.9 vs. 15.7 ± 3.4) and LM artery (15.0 ± 2.3 vs. 15.2 ± 3.7) ($p > 0.05$). The CNRs of CCTA did not differ between the groups in the RCA (17.6 ± 3.1 vs. 19.1 ± 3.8) and LM artery (18.3 ± 2.6 vs. 18.9 ± 4.6) ($p > 0.05$). The mean image quality of the RCA, LM artery, LAD, and LCx was 3.47 in group A and 3.53 in group B ($p = 0.420$).

Conclusion Iso-osmolar contrast agent with a lower iodine concentration might be feasible for CCTA with low tube voltage, volume reduction of contrast media, and a knowledge-based IMR algorithm.

Cardiac remodeling in elite cyclists: a 2-years follow-up magnetic resonance imaging study

B. Vande Berg[1], J. Bogaert[2], M. D. L. Herbots[1], M. D. K. Lefebvre[1], M. D. G. Claessen[2], M. D. M. Claeys[2], M. P. D. R. Willems[2], H. Heidbuchel[3], M. P. D. A. La Gerche[4], D. Hansen[1], O. Ghekiere[1]; [1]Hasselt/BE, [2]Leuven/BE, [3]Antwerp/BE, [4]Melbourne/AU

Purpose/Objectives To assess right (RV) and left ventricular (LV) volumetric, myocardial strain and tissue characteristics over time obtained by cardiac magnetic resonance (CMR) in elite professional endurance cyclists.

Methods & Materials Eighteen male cyclists of U23 Worldtour team (mean age 19 ± 1 year) underwent CMR at baseline and at 2-years follow-up on a 1.5T system as part of the Pro@Heart study. Gobal volumetric and functional parameters included (indexed) LV/RV end-systolic and end-diastolic volumes and ejection fraction (LVEF/RVEF). A non-rigid elastic algorithm was used to calculate global LV and RV myocardial strain. Native and post-contrast T1 mapping with extracellular volume (ECV) calculation was performed in septal and lateral wall LV on a 4-chamber view. Nonparametric Wilcoxon signed ranks test was used to compare differences between baseline and follow-up CMR.

Results Lateral LV wall thickness (mean value baseline/follow-up: $7.6 \pm 1.1/8.5 \pm 0.9$ mm, $p < 0.05$) and LV global longitudinal strain (mean value baseline/follow-up: $-11.8 \pm 1.9/-13.2 \pm 2.0\%$, $p < 0.05$) significantly increased at 2-years follow-up. Similarly, there was an increase of global RV longitudinal strain at 2-years follow-up (mean value baseline/follow-up: $-12.9 \pm 3.4/-15.4 \pm 2.5\%$, $p < 0.05$). No statistically significant difference over time was observed for the other strain measurements (LV global radial and circumferential strain), for the volumetric parameters, the LV myocardial mass, septal wall thickness, native T1 mapping and ECV ($p > 0.05$).

Conclusion Whereas cardiac volumes and myocardial mass did not change, biventricular global longitudinal strain and LV lateral wall thickness significantly increased after 2 years of endurance competition in young elite cyclists.

Reduction of Radiation Exposure in the Cardiac Catheter laboratory

M. R. Rees[1], S. Dalvi[2], C. Bellamy[3]; [1]Gwynedd/UK, [2]Liverpool/UK, [3]Rhyl/UK

Purpose To assess the effct of changing the method of using cine magnification in the cardiac catheter laboratory from camera factors to digital image enhancement.

Methods & Materials Following a study carried out using a chest and cardiac phantom, it was discovered that using a digital mangnification method using a large screen it was not necessary to use the electronic x ray tube magnification to achieve satisfactory imaging. Patient doses were monitored for a period of 4 months prior to the change in methodology and for a period of 3 months after the method change. Radiation dosage, screening time and patient body weight for each operator were analysed 4 months before and 4 months after a large screen was installed enabling the use of digital magnification in a catheter laboratory. :Three variables for each operator, were recorded 1. Number of patients, 2. Screening time and 3.patient body weight.

Results There was 37% reduction in average Dose Area Product (DAP) per patient and 45.5% reduction in average skin dose per patient.

There was a 46.1% reduction in average DAP per minute and 53.4% reduction in average skin dose per minute.

There was 42.8% reduction in average DAP per kg of patient's body $p < 0.0001$ weight and 50.5% reduction in average skin dose per kg of patient 's body weight. $p < 0.0001$.

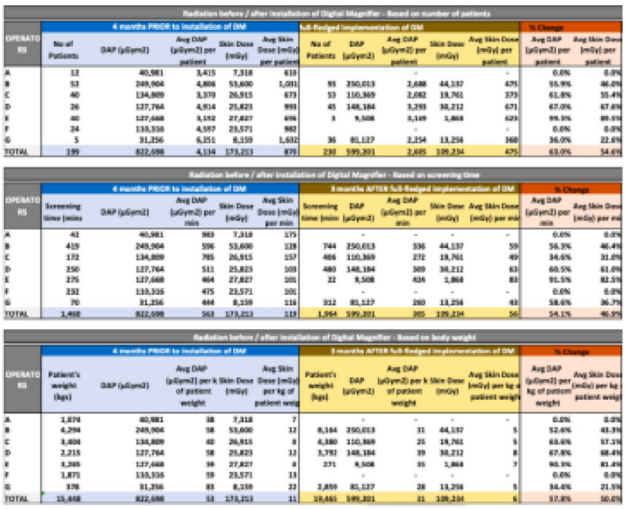

Radiation audit results

Conclusion Radiation dose reduction in the cardiac catheter laboratory can be achieved by using digital magnification technology with a range of dose reduction from 31% to 84% dependent on operator with an average reduction in DAP of 46.1%.

References: 2018 ACC/HRS/NASCI/SCAI/SCCT Expert Consensus Document on Optimal Use of Ionizing Radiation in Cardiovascular Imaging—Best Practices for Safety and Effectiveness, Part 2: Radiological Equipment Operation, Dose-Sparing Methodologies, Patient and Medical Personnel ProtectionHirshfeld JW, Ferrari VA, BengelFM,BergersenL,Chambers CE, EinsteinAJ,Eisenberg MJ, Fogel MA, Gerber TC, Haines DE, Laskey WK, Limacher MC, Nichols KJ, Daniel DA, Raff GL, Rubin GD, Smith D, Stillman, AE, Thomas SA, Tsai, TT,Wagner LK, L. Wann SJournal of the American College of Cardiology Jun 2018, 71 (24) 2829-2855.

The association between carotid arterial calcium score and silent cerebrovascular lesions on the obstructive sleep apnea patient: using the airway CT and brain MRI

E.-J. Kang, K.-N. Lee, M. S. Kim; Busan/KR

Purpose To investigate the relationships of carotid arterial calcium score on airway computed tomography (CT) and silent cerebrovascular.

lesions in patients with obstructive sleep apnea (OSA).

Methods & Materials This study included 60 consecutive OSA patients who underwent both upper airway CT and brain magnetic resonance image (MRI).

The CarACS on each airway CT were quantified using the modified Agatstone scoring method. The severity of OSA was divided into four groups (normal, mild, moderate and severe) using the respiratory disturbance index (RDI) as the results of polysomnography. The silent cerebrovascular lesion was evaluated by T2-weighted and fluid-attenuated inversion recovery images on brain MRI using the grading of periventricular hyperintensity (PVH): PVH grade 0 to 4. Various clinical characteristics including age, gender, body mass index, comorbid disease, blood pressure, and total cholesterol were analyzed in each patient; we also investigated the history of cerebral infarction.

Results The carotid arterial calcification was found in 14 patients (23%), and mean CarACS was 45.74 ± 112.3. The numbers of patient of each PVH grade were as followed: 26 patients (43.3%) for PVH 0; 14 patients (23.3%) for PVH 1; 14 patients (23.3%) for PVH 2; 4 patients (6.7%) for PVH 3; and 2 patients (3.3%) for PVH 4, respectively. In univariate analysis, the presence of CarAC (standardized coefficient [ß] = 0.483, $p < 0.001$), CarACS (ß = 0.482, $p < 0.001$), and the age (ß = 0.36, p = 0.010) showed significant association with PVH grade. The severity of OSA (RDI index) was not showed any association with PVH grade. In multivariate analysis, CarACS was v.

Conclusion CarACS was associated with the severity of silent cerebrovascular lesion and age, whereas the severity of OSA did not contribute.

Therefore, additional analysis of CarACS on OSA patients may provide more information for cerebrovascular status.

Diagnostic accuracy of dual-energy CT in patients with suspect acute pulmonary embolism: a systematic review and meta-analysis

M. Zanardo[1], C. B. Monti[1], S. Schiaffino[2], A. Cozzi[1], P. M. Cannao[2], F. Secchi[1], F. Sardanelli[1]; [1]Milan/IT, [2]San Donato Milanese, PLEASE SELECT AN OPTION BELOW/IT

Purpose/Objectives To review the diagnostic accuracy of dual-energy CT (DECT) in diagnosing acute pulmonary embolism (PE), with regards to radiation dose, and to compare DECT and single-energy CT in the same setting.

Methods & Materials After study protocol registration on PROSPERO, in February 2019 a systematic search was performed in Medline/EMBASE for articles reporting the diagnostic performance of DECT in diagnosing acute PE including numbers of true positive, true negative, false positive and false negative cases. Pooled sensitivity, specificity, positive and negative likelihood ratios (LR) and diagnostic odds ratio (DOR) were calculated according to the approach by Reitsma. A summary receiver operating characteristics (sROC) curve was constructed, reporting both pooled data and data from single studies. Data were reported as estimate and 95% confidence interval (CI). The pooled effective radiation dose for the chest was calculated using the random effect model. Risk of publication bias was assessed using the Egger test.

Results Of 159 initially retrieved articles, 14 studies were identified, including 23 independent study parts (Figure 1), involving 993 patients. Patients' mean or median age ranged from 40 to 68 years, the percentage of male patients ranged from 32 to 79%. Out of 14 studies, 12 used a dual-tube/dual-detector DECT, while 2 used rapid-kV switching DECT. Lower voltages ranged from 80 to 100 kVp, while high voltages ranged from 135 to 140 kVp.

Pooled sensitivity was 84.1% (95% CI 78.3–88.6%), pooled specificity was 88.6% (95% CI 83.9–92.1%), positive LR was 7.52 (95% CI 5.21–10.60), negative LR was 0.18 (95% CI 0.13–0.25), DOR was 42.8 (95% CI 24.2–70.3). The sROC curve had an area under the curve of 0.93 (Figure 2).

Effective radiation dose to the chest showed high heterogeneity ($I^2 = 97\%$), and its pooled estimate was 4.52 mSv (95% CI 3.68–5.36 mSv). Significant risk of publication bias regarding effective radiation dose was found (Egger's test p = 0.006).

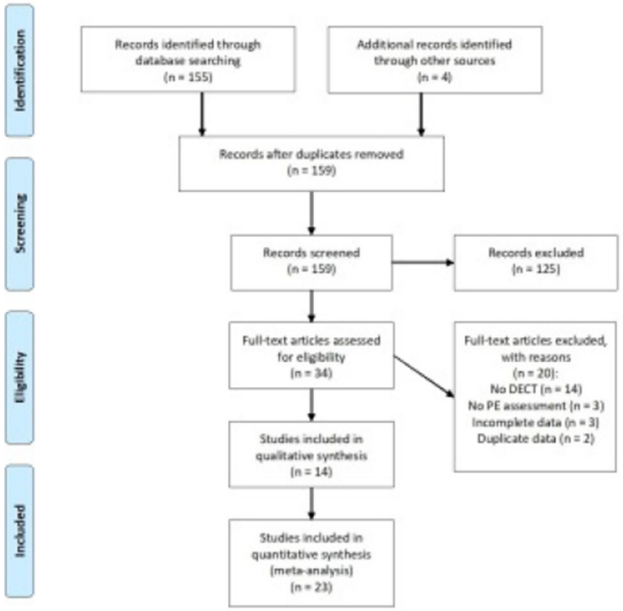

Flow chart of the analysed articles

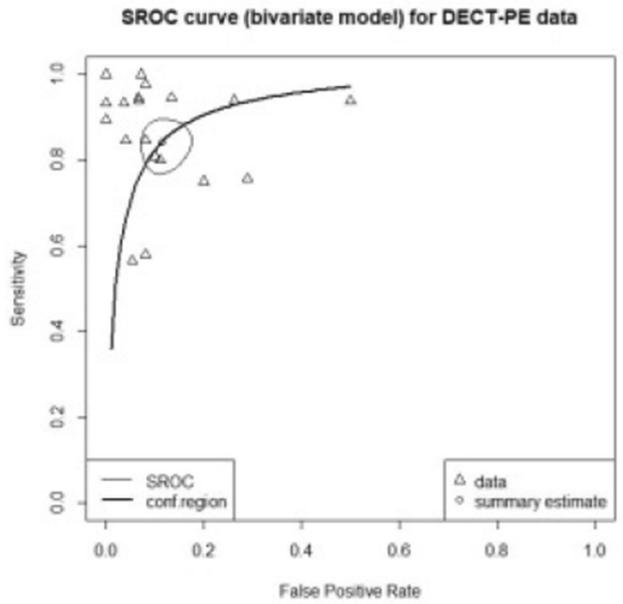

Summary receiver operating characteristics curve (bivariate model) for dual-energy CT for pulmonary embolism data

Conclusion This systematic review showed that the diagnostic accuracy of DECT in acute PE is substantially comparable to that of single-energy CT, in presence of a comparable effective radiation dose to the chest, also providing more accurate evaluation of the lung ventilation and tissue characterization.

Cardiovascular magnetic resonance in acute myocarditis—May LGE distribution reveal the underlying cause?

E. Detorakis[1], G. Antemisaris[1], R. Illing[2]; [1]Heraklion/GR, [2]Budapest/HU

Purpose Myocarditis is an acquired cardiomyopathy related to acute or chronic inflammation of the myocardium either focal or diffuse. In Europe and North America viral infections constitute the most frequent causative agent of acute myocarditis. The present study aims to reveal any possible correlation between LGE distribution and the underlying causative viral agent.

Methods & Materials 48 consecutive patients included in this prospective study (44 men, 4 women, median age 29 years) with suspected acute myocarditis. 45 patients reported a viral infection within the last 15–25 days, 41 of the upper respiratory tract and 7 of gastrointestinal tract. About 5–10 days before CMR examination 44 presented episodes of chest pain and 42 had elevated cardiac troponin blood levels. Serological tests focused on Coxsackie virus B, Ebstein-Barr virus, Cytomegalovirus, Influenza virus, HHV6 and Parvovirus B19. ECG-gated CMR imaging was performed in a 1.5 T system (Signa CV/i, GE Medical Systems, WI,USA). The imaging protocol focused on LGE images acquired 8-15 min following i.v administration of 0.1 mmol/kg of Gadobutrol Gd-CA (Gadovist®, Bayer, Germany) using a PSIR sequence, continuously adapting the TI values for nulling of normal myocardium. All images in LGE were acquired in apical, mid-cavity and basal short axis levels covering all AHA segments. Statistical analysis was performed and Student t test and Chi square test were used. A p value of < 0.05 was considered statistically significant.

Results LGE was depicted in 42/48 patients with subepicardial to mesocardial extent, in 31 involved inferior/inferolateral segmets of the left ventricle wall (AHA segments 4,5,6,11 and 12, Group A) and in the remaining 11 patients the septal/anteroseptal segments, together or not with lateral wall segments (AHA segments 1,2,3,8,9 + -4,5,6,11,12, Group B). Serological tests identified Parvovirus B19 antibodies in 28 patients, HHV6 antibodies in 9 and Coxsackie virus B in 2 patients. A significant correlation was recorded between Group A and the presence of Parvovirus B19 antibodies ($r =+ 0.949$, $p < 0.0001$) as well as another significant correlation between the presence of HHV6 antibodies and Group B ($r =+ 0.8229$, $p < 0.00010$.

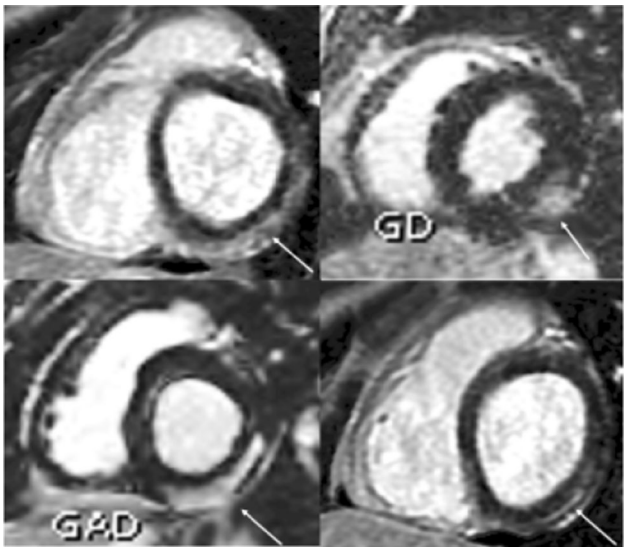

Figure 1 LGE involving inferior/lateral segments (white arrows) in 4 different cases of acute myocarditis where Parvovirus B19 antibodies were detected

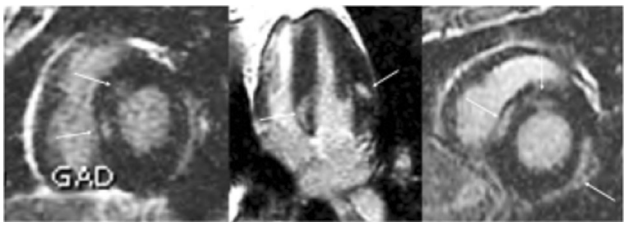

Figure 2 LGE involving septal and anteroseptal segments, together involved with inferolateral segments (white arrows) in 3 different cases of acute myocarditis where HHV6 antibodies were identified

Conclusion In patients with acute myocarditis Parvovirus B19 seems to have a predilection target for inferior/lateral segments and HHV6 for septal/anteroseptal segments where LGE was depicted on CMR. Both correlations proved to be statistically significant.

References Aquaro GD et al. Cardiac MR With Late Gadolinium Enhancement in Acute Myocarditis With Preserved Systolic Function: ITAMY Study. J Am Coll Cardiol. 2017 Oct 17;70(16):1977-1987.

Myocardial damage in patients with muscular dystrophy: Correspondence between muscle degeneration and myocardial dysfunction

H. Liu[1], H.-Y. Xu[1], Z.-G. Yang[1], R. Xu[1], Y.-K. Guo[1], H. Fu[1], H. Fu[2], L. Xie[1], C. Fu[1], X. Li[1], X. Zhou[3]; [1]Chengdu/CN, [2]Chengdu, Sichuan/CN, [3]Shanghai/CN

Purpose/Objectives Progressive cardiomyopathy is common in patients with DMD, affecting one-third of children at 14 years, and is universal by 18 years. The aim of this study was to explore the onset of myocardial injury with the reference of lower limb muscles and further analysis the site of the first involvement lesions.

Methods & Materials A total of 82 DMD patients and 40 age- and gender-matched healthy individuals were enrolled and underwent CMR imaging of heart and hip muscles with a 3T MR scanner (MAGNETOM Skyra, Siemens Healthcare, Erlangen, Germany). Myocardial strain analysis was performed after loading long-axis (4-chamber and 2-chamber) and a series of short-axis slices into the tissue tracking module of a commercial software (cvi42; Circle Cardiovascular Imaging, Inc., Calgary, Canada). The tissue tracking parameters were acquired automatically, including myocardial radial strain, circumferential strain and longitudinal strain of basal, mid and apical of left ventricular. The patients were divided into two groups according to the severity of Gluteus maximus: group A with early stage (fat lesion grade 1–2, less than 10%, 10–40% grade 2) and group B with progressive stage (fat lesion grade 3–4, 40–70% grade 3, and $> 70\%$ grade 4).

Results The average age of DMD patients was 8.9 years. There were 57(70%) patients without LGE and 25 patients (30%) with positive LGE. Among the 82 patients, there were 42 cases of group A and 40 cases of group B. Delayed enhancement was 5 (12%) in group A and 20 (50%) in late stage patients. Compared with the normal volunteers, the basal radical strain of group A was significantly lower than that in the normal volunteers (59.65 ± 15.26 vs. 43.76 ± 8.26, $p = 0.03$). The apical radical strain of group A was significantly higher than group B (54.76 ± 12.67 vs. 44.43 ± 10.78, $p = 0.02$). There was no significant difference in left ventricular function, basal or mid strain in three directions ($p > 0.05$) between group A and group B.

Conclusion The degree of cardiomyopathy was gradually aggravated with lower limb muscle degeneration commonly and occurs early in muscular degeneration of lower limb muscles. Magnetic resonance tissue tracking technology has early diagnostic value for DMD patients with early stage and the basal part of the heart is the first to be involved.

The Impact of Visceral and General Obesity on Cardiovascular Function and Geometry: a Cross-Sectional Magnetic Resonance Imaging Study of the UK Biobank

I. Dekkers, M. van Hout, J. J. M. Westenberg, M. Schalij, A. Scholte, H. J. Lamb; Leiden/NL

Purpose/Objectives To evaluate associations of body fat distribution with cardiovascular function and geometry in the middle-aged general population. Obesity has been associated with decreased cardiovascular function and heart failure, however it remains unclear to what extent this is attributable to metabolic distinctive visceral obesity.

Methods & Materials In this cross sectional analysis of the UK-biobank, 4590 participants (54% female, mean age 61.1 ± 7.2 years) who underwent magnetic resonance imaging for assessment of left ventricular [LV] parameters (end-diastolic volume [EDV], ejection fraction [EF], cardiac output [CO] and index [CI]) and body composition (subcutaneous adipose tissue [SAT] and visceral adipose tissue [VAT]) were included. Body fat percentage [BF%] was assessed by bioelectrical impedance. Linear regressions were performed using visceral (VAT) and general (SAT and BF%) obesity measures as determinants, and cardiac function and geometry as outcome variables.

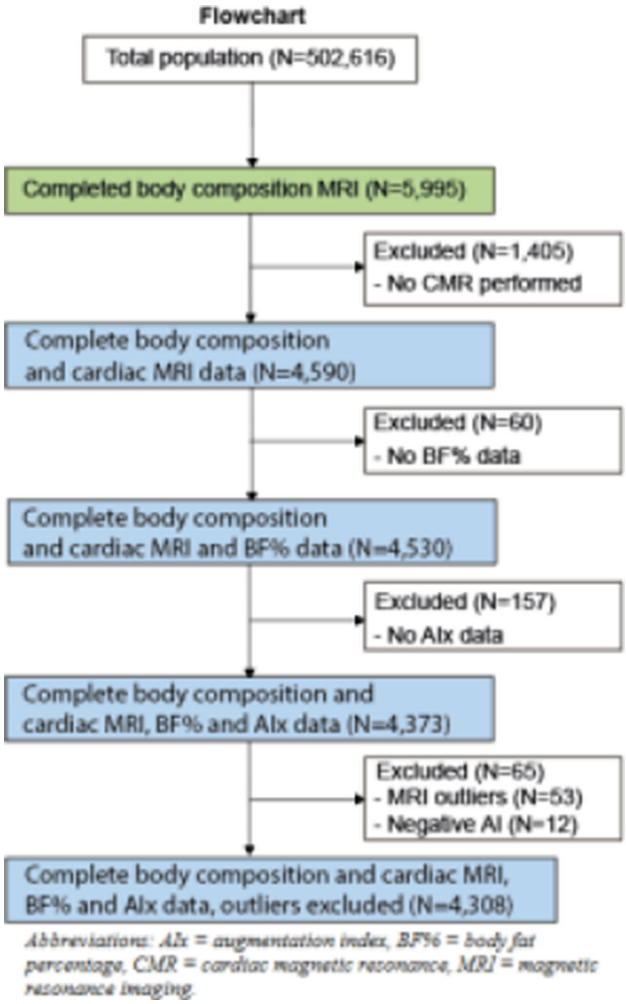

Abbreviations: AIx = augmentation index, BF% = body fat percentage, CMR = cardiac magnetic resonance, MRI = magnetic resonance imaging

Flowchart

Results Visceral obesity was associated with smaller EDV (VAT: β − 1.74 [− 1.15; − 2.33]), where general obesity was associated with larger EDV (SAT: β 1.01 [0.72; 1.30], BF %: β 0.37 [0.23; 0.51]). Furthermore, visceral obesity was associated with lower systolic LV function, with lower EF (VAT: β − 0.24 [− 0.12; − 0.35], SAT: β 0.02 [− 0.04; 0.08], BF%: β 0.02 [− 0.02; 0.06]) and the strongest negative association with CI (VAT: β − 0.05 [− 0.06; − 0.04], SAT β − 0.02 [− 0.03; − 0.01], BF% β − 0.01 [− 0.013; − 0.007]). In contrast, only general obesity was significantly associated with higher CO (SAT: β 0.06 [0.05; 0.07], BF %: β 0.02 [0.01; 0.03]). In gender specific analysis, only men had a significant association between VAT and EF (β − 0.35 [− 0.19; − 0.51]).

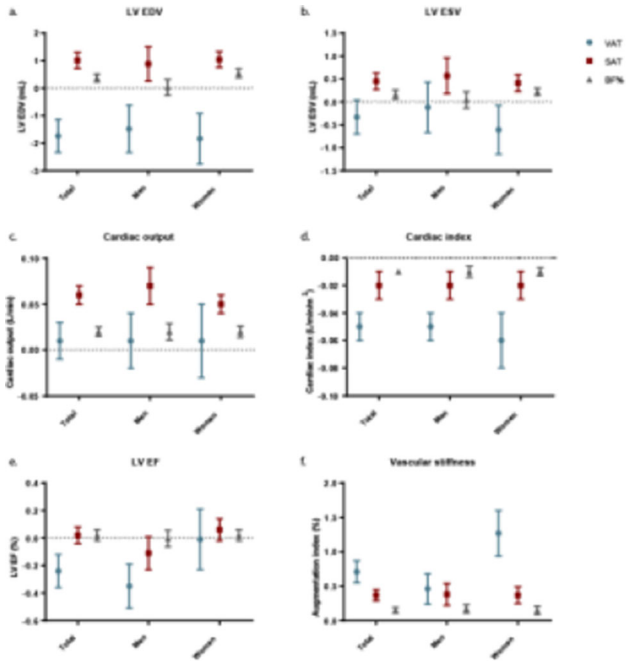

Figure 2a–f. *Associations (β with 95% confidence interval) of measures of obesity with: **a:** LV EDV, **b:** LV ESV, **c:** cardiac output, **d:** cardiac index, **e:** LV EF, **f:** augmentation index.*

Figure 2a–f Associations (β with 95% confidence interval) of measures of obesity with: a LV EDV, b LV ESV, c cardiac output, d cardiac index, e LV EF, f augmentation index

Conclusion Visceral obesity was associated with smaller LV end-diastolic volume and subclinical lower LV systolic function in men, suggesting that visceral obesity plays a more important role compared to general obesity in the development of obesity associated cardiomyopathy.

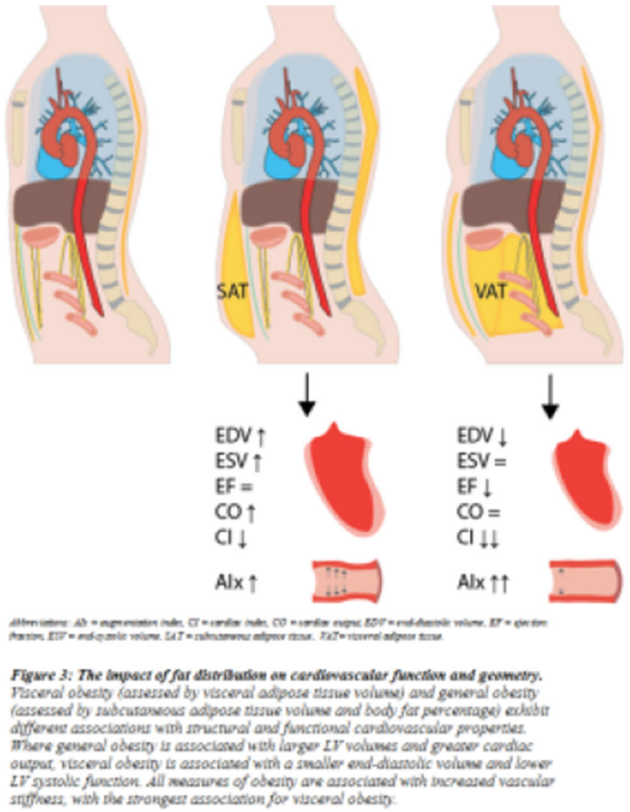

Figure 3 The impact of fat distribution on cardiovascular function and geometry

Quantification of mitral valve regurgitation from 4D flow MRI using semi-automated flow tracking

C. P. S. Blanken[1], J. J. M. Westenberg[2], J.-P. Aben[3], G. P. Bijvoet[3], S. A. J. Chamuleau[4], A. J. Nederveen[1], T. Leiner[4], N. R. Planken[1], P. van Ooij[1]; [1]Amsterdam/NL, [2]Leiden/NL, [3]Maastricht/NL, [4]Utrecht/NL

Purpose/Objectives Cardiac 4D flow MRI offers novel possibilities to quantify mitral valve regurgitation (MVR). Retrospective valve tracking enables forward blood flow quantification over the heart valves, taking into account valvular motion. However, quantification of MVR at valve level can suffer from flow incoherency, causing an underestimation of regurgitant flow. A suggested solution is to measure 1–2 cm proximal to the valve and perpendicular to the regurgitation: flow tracking. This study's purpose was to compare regurgitant flow as quantified by semi-automated flow tracking and valve tracking in clinical MRI data.

Methods & Materials 26 MVR patients (8 mild-moderate, 8 moderate-severe, 10 severe, as diagnosed by echocardiography) underwent 4D flow MRI at 1.5T (30 cardiac phases, free-breathing, retrospective ECG-gating, three-directional VENC of 150–280 cm/s, spatial resolution of $2.89 \times 2.89 \times 3.5$ mm^3 for severe MVR and $1.45 \times 1.45 \times 6$ mm^3 in the other groups). Mitral valve (MV) and aortic valve (AV) flow volumes were quantified from 4D flow MRI by dedicated software (CAAS MR Solutions 5v1, Pie Medical Imaging) with through-plane valve motion correction as assessed on two-, three- and four-chamber cine bSSFP. 1) MV regurgitant flow volume (Rvol) was quantified using flow tracking and valve tracking (Figure 1). 2) To test inter-valve consistency, MV and AV forward flow were quantified using valve tracking at annulus level. 3) Left-ventricular stroke volume (LVSV) was quantified by short-axis bSSFP volumetry for indirect MVR quantification ($Rvol_{INDIRECT}$ = LVSV–AV flow).

Agreements between MV and AV net flow and between 4D flow MRI-derived Rvol and $Rvol_{INDIRECT}$ were evaluated with a Wilcoxon signed-rank test. Orthogonal regression and Bland–Altman analysis were performed with $p < 0.05$ considered significant.

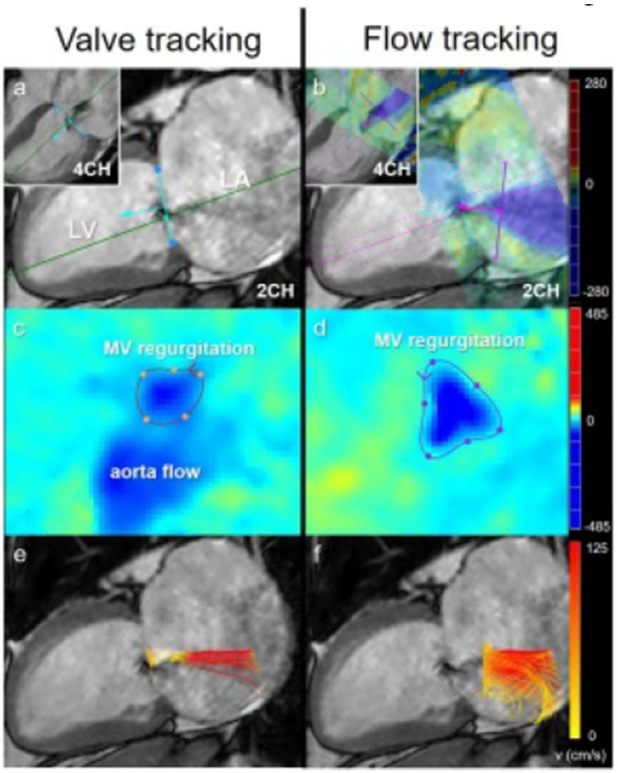

Figure 1 Valve tracking and flow tracking in severe MVR. a, b Measurement plane initialization, with an additional plane for flow tracking during regurgitation. c, d Flow area contouring in 4D flow velocity projection. e, f) Streamlines

Results Flow tracking measured higher Rvol than valve tracking ($p < 0.001$, Figure 2). MV net flow turned out higher than AV net flow for valve tracking ($p < 0.001$) but not when Rvol was quantified with flow tracking ($p = 0.97$, Figure 3) Interestingly, when comparing with $Rvol_{INDIRECT}$, Rvol measured with flow tracking was higher ($p = 0.005$) whereas Rvol measured with valve tracking was not ($p = 0.253$), despite a trend towards underestimation of Rvol for severe MVR using valve tracking.

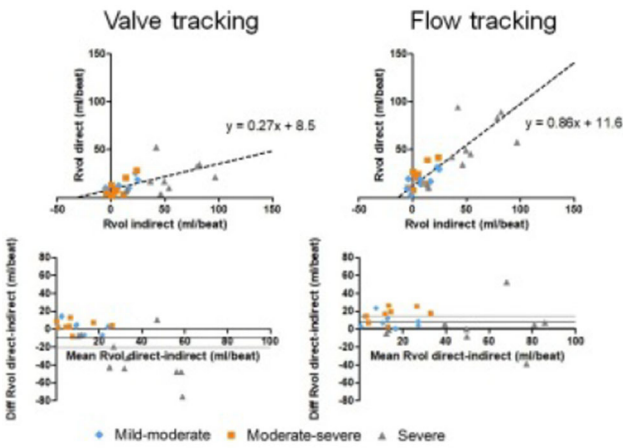

Figure 2 Orthogonal regression (top) and Bland–Altman plots (bottom) of Rvol measured with valve tracking (15 ± 12 ml, left) and flow tracking (33 ± 25 ml, right) versus indirectly quantified Rvol (= LVSV-AV flow)

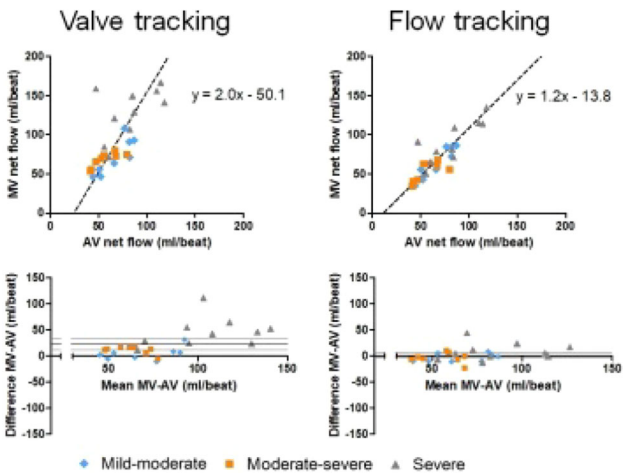

Figure 3 Orthogonal regression (top) and Bland–Altman plots (bottom) of MV and AV net flows (forward—backward flow volume) resulting from valve tracking (left) and flow tracking (right). MV and AV net flows should be equal

Conclusion In this study, the application of semi-automated flow tracking provided better quantification of MVR by 4D flow MRI than valve tracking, particularly in severe MVR. Good agreement between MV and AV net flows indicated good accuracy of flow tracking. We found that flow tracking provided more accurate quantification of MVR than valve tracking due to measurement at a location of less incoherent flow.

Open 1.0-T versus Closed 1.5-T Cardiac MR: Image Quality Assessment

M. Alì, C. B. Monti, B. Gold, G. Lastella, S. Papa, F. Secchi, F. Sardanelli; Milan/IT

Purpose Cardiac magnetic resonance imaging (MRI) in closed magnets is difficult/impossible for claustrophobic/obese patients. Whether open cardiac MRI provides adequate image quality is unclear. Thus, the aim of our study was to compare an open 1-T system (O-1T) with a closed 1.5-T system (C-1.5T) for cardiac imaging.

Methods & Materials In this retrospective inter-individual study, two concurrent cohorts of consecutive patients with suspected or known cardiac disease, each including 100 subjects, were re-evaluated.

One hundred examinations were performed using a vertical O-1T MRI, while the other half were performed using an horizontal C-1.5T magnetic field MRI. For each examination the following sequences were performed: bright-blood cine, T1-weighted (T1), T2-weighed short-tau inversion recovery (T2-STIR), delayed enhancement (DE). Signal-to-noise ratio of blood (SNRb) or myocardium (SNRm), and contrast-to-noise ratio of myocardium (CNRm) were calculated. Subjective image quality (SIQ) of each sequence was graded by a 10-year-experienced radiologist (R1) and a trained medical student (R2) as 0 = poor, 1 = intermediate, or 2 = optimal. Each examination was considered as diagnostic when the report answered the clinical question.

Differences between SNR and CNR distributions of open MR examinations, compared to closed-bore MR, were evaluated using Mann–Whitney *U*. When possible, Pearson's χ^2 was performed on the more expert reader (R1) evaluation in order to assess differences throughout scores given using the 3-point scale, while the inter-reader agreement was estimated using linearly weighted Cohen κ. Concordances in absolute terms and as a percentage were also reported.

Results C-1.5T was better than O-1T on cine for SNRb (median 172 vs. 452), SNRm (71 vs. 160) and CNRm (107 vs. 265) and on T2-STIR for SNRb (10 vs. 29), SNRm (74 vs. 261) and CNRm (− 67 vs. − 233) ($p < 0.001$). On DE, SNRm was higher with O-1T than for C-1.5T (312 vs. 79; $p < 0.001$) while CNR was lower (158 vs. 389; $p < 0.001$). No significant differences were found for SNRb on DE and both SNRm and CNRm on T1 ($p \geq 0.215$).

SIQ of O-1T was not significantly different from that of C-1.5T for both R1 and R2 for cine, T1, and DE ($p \geq 0.157$); for T2-STIR, SIQ of O-1T was significantly lower (p = 0.003). R1-R2 concordance was almost perfect (k = 0.816–0.894), and all examinations were diagnostic.

Conclusion O-1T cardiac examinations were diagnostic. Even though quantitative measurements mostly favored C-1.5T, the SIQ of O-1T was not significantly different for all the sequences, with the only exception of T2-STIR.

Cardiac magnetic resonance in myotonic dystrophy type 1: A contribution to risk assessment

M. Alì, C. B. Monti, L. Melazzini, B. Fossati, R. Cardani, G. Meola, F. Sardanelli, F. Secchi; Milan/IT

Purpose The aim of our study was to evaluate left ventricular extracellular volume (ECV) and strain on cardiac magnetic resonance

(CMR) as potential imaging-biomarkers of subclinical cardiac pathology in myotonic dystrophy type-1 (DM1) patients.
Methods & Materials We retrospectively analyzed CMR examinations of DM1 patients with preserved ejection fraction performed between 2014 and 2016. ECV was calculated from native and post-contrast T1-mapping, referring to normal values reported in literature. Global circumferential strain (CS) was calculated and negative non-contrast CMR scans in age- and sex-matched subjects without history of cardiac disease were used as controls.
Results Nine patients and nine controls without significant difference for age ($p = 0.931$) and sex ($p = 1.000$) were analyzed. Global CS was − 19.1% (interquartile range [IQR] − 20.9%, − 15.3% in patients and − 21.7% (IQR − 22.7%, − 21.3%) in controls ($p = 0.011$). Patients had a median global ECV of 32.3% (IQR 28.4%, 37.6%). A positive significant correlation between global ECV and CS ($\rho = 0.733$, $p = 0.025$) and a borderline significant correlation between septal ECV and septal CS ($\rho = 0.667$, $p = 0.050$) were found.
Conclusion In DM1 patients with preserved ejection fraction, CMR allowed to detect impaired contractility, correlated with ECV expansion, likely due to subclinical fibrosis. CMR-derived CS and ECV may have a role as imaging biomarkers of myocardial involvement in DM1 patients, with potential prognostic role.

Late gadolinium enhancement at the inferior ventricular insertion point in patients with tetralogy of Fallot

U. Barbaro[1], C. B. Monti[2], G. Guarnieri[2], M. Alì[2], F. Sardanelli[2], F. Secchi[2]; [1]Messina/IT, [2]Milan/IT

Purpose To measure and quantify myocardial Late Gadolinium Enhancement (LGE) at the inferior ventricular insertion point in patients with Tetralogy of Fallot (ToF) who underwent intervention and who had not.
Methods & Materials 48 patients out of which 23 males and 25 female aged between 16 and 33 with ToF underwent 1.5 T cardiovascular magnetic resonance (Siemens MAGNETOM Aera) for routine assessment of cardiac function and LGE, analyzed in the period from April 2014 to April 2019. Two groups were identified: the first one included 27 patients who underwent surgical replacement of the pulmonary valve and then they were subjected to CMR examination. The other group of 21 patients had no previous intervention. LGE quantification was carried by one researcher within 12 months of experience on cardiovascular imaging using a semi-automatic technique reproduced by the use of a dedicated software (Medis Suite MR). Statistical analysis was made with the Mann–Whitney U test, considering as significant a p value less than 0.05.
Results Right Ventricle end-diastolic volume (RV EDVi) and Right Ventricle Stroke Volume (RV SV) were 112 ml (90–125) and 102 ml (73–126) for patients treated and 79 ml (73–107) and 80 ml (63–91) for patients not treated with a significant reduction ($p = 0.028$ and 0.048 respectively). On the other hand no significant differences were found for the indices related Right Ventricle end-sistolic Volume (RV ESVi) and Right Ventricle Ejection Fraction (RV EF), that were respectively 46 ml (35–58) and 55% (52–64) for the first group and 40 ml (32–50) ($p = 0.201$) and 51% (46–61) ($p = 0.204$) for the second group.
Besides no significant differences were found in the quantification of LGE among the two groups: the median amount of LGE expressed in % was 2.4 (1.2–4.1) for the first group and 1.3 (0.4–2.4) for the second group ($p = 0.128$). The median amount of LGE expressed as the volume (g) was 1.9 (0.7–2.8) for the first group and 1.2 (0.3–1.9) for the second group ($p = 0.169$).
Conclusion In patients with ToF treated for pulmonary valve replacement a significant difference of RV EDVi volume and RV SV was found. Inferior ventricular insertion point LGE was present in both groups without a significant difference.

Value of subtraction coronary computed tomography angiography for calcified or stented segments

T. Deflandre[1], J. Djekic[1], D. Hansen[2], A. Nchimi Longang[3], O. Ghekiere[2]; [1]Liege/BE, [2]Hasselt/BE, [3]Luxembourg/LU

Purpose Calcification- or stent-related artifacts limit interpretability and accuracy of coronary computed tomography angiography (CCTA). These limitations could theoretically be limited by using subtraction CCTA (sCCTA). Therefore, the purpose of this study was to evaluate the diagnostic accuracy of sCCTA and the effect of patient-related factors on (s)CCTA image quality in calcified or stented coronary arteries, using invasive angiography (ICA) as the reference.
Methods & Materials We conducted a retrospective study including all consecutive patients who underwent both CCTA and ICA within a 3 months period, from June to December 2016. From the 24 patients (17 males, mean age 62 ± 7 SD) who matched these criteria, all segments with both a diameter > 1.5 mm and either calcifications ($n = 63$) or stents ($n = 11$) on CCTA were selected. Each segment was evaluated for the following artifacts using Likert scale (from 1 representing no artifact to 4 standing for severe artifacts): misregistration artifacts (sCCTA), motion artifacts, beam-hardening artifacts and blooming artifacts. Segments graded 3 and 4 were considered non-diagnostic. Regression models were used to determine patient- and examination-related factors for non-diagnostic segments. Stenoses were assessed as ≥ 50% diameter reduction or less, on CCTA, sCCTA and ICA.
Results On CCTA, 7/74 segments were non diagnostic because of the following artefact: Blooming ($n = 7$) and motion ($n = 1$). On sCCTA, 11/74 segments were non diagnostic, all because of misregistration ($n = 11$). One stent was non-diagnostic on CCTA due to Blooming and motion artifacts, while 5 stents were non-diagnostic on sCCTA. On regression analysis, factors determining non-diagnostic segments were the patient's heart rate, the coronary segment's diameter and circumferential extent of calcification (all $p < 0.05$). Of the diagnostic segments, the sensitivity, specificity and accuracy of CCTA versus sCCTA were respectively 58% (11/19) vs. 88% (14/16), 81% (39/48) vs. 89% (42/47) and 75% (50/67) vs. 89% (56/63).
Conclusion Compared to CCTA, sCCTA tends to increases the diagnostic accuracy for stenoses analysis in calcified and stented segments. The number of non-diagnostic segments in sCCTA increases as well, owing to misregistration artifacts.

Detection of myocardial scars with Late Iodine Enhancement cardiac Computed Tomography (LIE-CT): impact of experience in the clinical practice

D. Vignale[1], A. Esposito[1], G. Benedetti[2], A. Del Maschio[1], F. de Cobelli[1]; [1]Milan/IT, [2]London/UK

Purpose/Objectives Recent studies have shown that cardiac CT with Late Iodine Enhancement (LIE-CT) can be used to identify myocardial scars. However, to date no studies have clarified how reader's experience and scar aetiology affect the diagnostic performance of LIE-CT. LIE-CT diagnostic performance was assessed in consecutive unselected patients, according to reader's experience and scar pattern, using Late Gadolinium Enhancement MRI (LGE-MRI) as the reference standard.

Methods & Materials Thirty-three consecutive patients clinically referred for scar imaging and coronary tree assessment underwent LIE-CT and LGE-MRI. Two readers with difference experience in cardiac imaging (8 and 2 years) independently evaluated LIE-CT images to define patient-based and segment-based myocardial scar involvement, global scar burden, transmural scarring involvement and scar aetiology. LGE-MRI semiautomatically analised by two expert readers in consensus was used as standard of reference. In addition, Contrast-to-Noise Ratio (CNR) of myocardial scars was assessed on LIE-CT images and analysed according to scar pattern and scar aetiology.

Results The diagnostic performance of LIE-CT depended both on readers' experience and on scar aetiology. Scar burden showed a very good correlation between LIE-CT and LGE-MRI for the most experienced reader ($R = 0.949$, $p < 0.001$), while the correlation for the least experienced reader was good ($R = 0.794$, $p < 0.001$). The segmental agreement between LIE-CT and LGE-MRI was very good for most experienced reader ($K = 0.875$; $p < 0.001$) and good for least experienced reader ($K = 0.670$; $p < 0.001$). The most experienced reader showed higher diagnostic accuracy and sensitivity for the detection of LIE, in comparison to least experienced one, both in per-segment (Accuracy: 96% vs. 91%; Sensitivity: 84% vs. 59%) and per-patient (Accuracy: 94% vs. 85%; Sensitivity: 92% vs. 80%) analysis. Reader's experience did not impact on specificity, which was excellent (99% per-segment, 100% per-patient) regardless of readers' experience. Diagnostic accuracy was lower in patients with small scars (scar burden < 6%) with a non-ischemic pattern; this was explained by the lower CNR of non-ischemic scars in respect to ischemic scars [median 2.01 (IQR 1.07–2.85) vs. 4.46 (IQR 2.74–6.36), $p = 0.0070$].

Conclusion LIE-CT is an excellent alternative to LGE-MRI for the detection of myocardial scars and scar pattern definition, although readers experience impacts on LIE-CT sensitivity for small non-ischemic scars.

Feature tracking allows detection of diminishing wall motion disturbances in Tako Tsubo Cardiomyopathy

R. Brumberg, F. Hahn, S. Benz, M. C. Halfmann, C. Düber, K.-F. Kreitner, T. Emrich; Mainz/DE

Purpose Wall motion disturbances in Tako Tsubo cardiomyopathy (TTCM) are often rapidly decreasing in days between diagnosis via ventriculography and CMR imaging. The purpose of this retrospective study was to illuminate the diagnostic performance of cardiac magnetic resonance imaging feature tracking in fading wall motion abnormalitites in TTCM.

Methods & Materials We compared cardiac magnetic resonance imaging (CMR) and ventriculography of 41 consecutive patients with TTCM. TTCM-involved regions were defined as regions with wall motion disturbances in ventriculography. With a dedicated cardiovascular software (Circle CVI®, Calgary, Canada), left and right ventricular strain values from TTCM-involved and not involved region were analysed and recorded.

Results In the period between coronary angiography and CMR, the severity of wall motion abnormalities is regularly declining. Nevertheless, even in the presence of only mild wall motion disturbances, feature tracking parameters of the left ventricle could easily discriminated between TTCM-involved and non-involved segments (e.g.: Circumferential strain in TTCM-involved region: -14.0 ± 7.9 vs. TTCM-not-involed: -19.2 ± 4.4; $p < 0.0001$). Interestingly, right ventricular strain values did not differ between involved and non-involved segments (e.g. RV radial strain: $p = 0.069$).

Conclusion CMR feature tracking is a powerful tool for detection of fading left ventricular wall motion abnormalities in TTCM. Further research in larger cohorts is needed to establish the time relation between diminution of wall motion disturbance and feature tracking parameters.

Extracellular Volume Calculation in clinical routine—comparison between "true" and synthetic haematocrit values in patients with dilated cardiomyopathy

P. Locherer, F. Hahn, K.-F. Kreitner, C. Düber, T. Emrich; Mainz/DE

Purpose Extracellular volume (ECV) is a promising diagnostic and prognostic imaging biomarker. For optimal calculation, a prompt measurement of the haematocrit is needed. In daily routine, blood drawings in hospital are sometimes delayed from the time point of the CMR measurement and could therefore alternate the calculation of ECV. Haematocrit can be estimated by the change of the T1 relaxation time of the blood ("Synthetic haematocrit"). The purpose of this retrospective study was to evaluate the diagnostic performance of ECV-measurements using a synthetic haematocrit compared to ECV measurements with a "true" (laboratory) haematocrit in a population of dilated cardiomyopathy patients.

Methods & Materials In a first step, a regression formula using pre and post contrast T1 relaxation times for calculation of the synthetic haematocrit was obtained from a prospective study of 62 healthy volunteers with haematocrit measurement directly at the time point of MR imaging. Secondly, this regression formula was used to calculate ECV values in a cohort of 40 DCM patients. T1 Maps were post-processed with dedicated cardiovascular software (Circle CVI®, Calgary, Canada).

Results ECV calculated from synthetic and true haematocrit values differed significantly from each other (True ECV: 28.8 ± 4.3 vs. Synthetic ECV: 29.9 ± 5.1; $p = 0.006$), but showed a good correlation between each other ($r = 0.88$; $R^2 = 0.782$) (Figure).

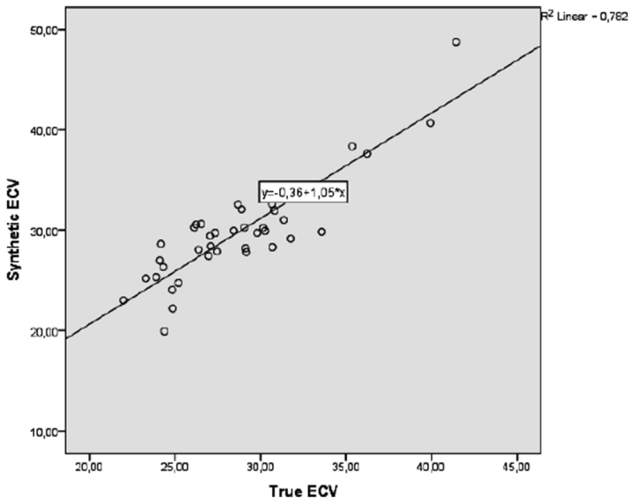

Conclusion ECV calculation using a synthetic haematocrit is a reliable tool to avoid diagnostic uncertainty in case of delay of blood drawings in everyday clinical routine.

Deep Learning for Fully Automatic 3D quantification of Body Composition

P. Moeskops, B. de Vos, W. B. Veldhuis, P. A. de Jong, I. Isgum, T. Leiner; Utrecht/NL

Purpose The amount and anatomical distribution of fat and muscle in different body compartments is an important prognostic factor in patients with cardiovascular disease. Although this information is routinely contained in many types of CT scans it is hard to quantify in daily clinical routine because manual segmentation is time-consuming, especially in 3D. The purpose of this study is to investigate the use of a deep learning-based method for automatic segmentation of subcutaneous fat, visceral fat and psoas muscle.

Methods & Materials The feasibility of fully automated body composition measurement was studied using a dataset of 20 CT scans of the abdomen (in-plane resolution 0.63–0.75 mm, slice thickness 5.0 mm, slice increment 5.0 mm). Trained observers defined the reference standard by manual annotation of subcutaneous fat, visceral fat and psoas muscle in all slices that contain the psoas muscle. Images from 10 patients were used to train a dilated convolutional neural network with a receptive field of 131 × 131 voxels to distinguish between the three tissue classes. Voxels were assigned to the class with the highest probability. Data from the remaining 10 patients were used to evaluate the performance of the method. Segmentation performance was evaluated with Dice coefficients between the manual and automatic segmentations. Additionally, linear correlation coefficients (Pearson's r) were computed between the manual and automatic segmentation volumes.

Results On average, segmentation of a full scan was performed in about 15 s. The average Dice coefficients over 10 test scans were 0.89 ± 0.022 for subcutaneous fat, 0.92 ± 0.042 for visceral fat, and 0.76 ± 0.052 for psoas muscle. At the L3 time-consuming level, the average Dice coefficients were 0.92 ± 0.019 for subcutaneous fat, 0.93 ± 0.048 for visceral fat, and 0.87 ± 0.035 for psoas muscle. Pearson's r between the manual and automatic volumes were 0.996 for subcutaneous fat, 0.997 for visceral fat, and 0.941 for psoas muscle.

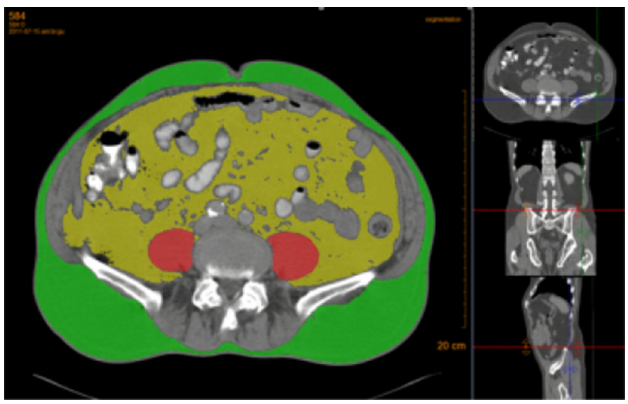

Conclusion The results of this feasibility study show that accurate fully automatic segmentation of subcutaneous fat, visceral fat and psoas muscle from abdominal CT is feasible without human input. Our work may facilitate automatic extraction of markers of body composition in clinical routine."